

Non-invasive Label-free Cytometry Based on Laser Light Scattering Technique

by

Yu Wan

A thesis submitted in partial fulfillment of the requirements for the degree of

Master of Science

in

Photonics and Plasmas

Department of Electrical and Computer Engineering
University of Alberta

© Yu Wan, 2018

Abstract

A non-invasive label-free cytometry technique has been developed and advanced. This laser light scattering technique, alternative to the conventional fluorescent-activated flow cytometry (FACS) using biomarkers, identifies a micro scale particle or biological cell based on its two-dimensional scattered laser light patterns. Patterns have been obtained in three directions: forward, side and backward, and two different wavelengths (green and red) illumination. In this thesis, the label-free cytometry technique was first used to study different sizes of spherical and non-spherical beads, and then non-treated and staurosporine-treated SH-SY5Y cells. The experimental results from the spherical beads were compared to Mie theory. To analyze the patterns from the cells, pattern classification and recognition based on angle distribution method and finding local maximum method have been applied. Preliminary experiment with a capillary tube as well as particles scattering in a droplet which could help the design of practical cytometers have been carried out.

Acknowledgements

I would first like to thank my supervisor Dr. Ying Yin Tsui for the support and guidance of my master project, not only in research studies but also in the way of thinking and solving problems.

I would also like to thank my co-supervisor Dr. Wojciech Rozmus for the precious contributions provided for my project. Furthermore, I would like to thank Dr. Manisha Gupta for providing a safe lab environment for me to carry on my experiment and arranging my oral exam as a chair. Moreover, I would like to thank Chunhua Dong and Graig Garen from Dr. Michael Woodside group for preparing me cell samples.

I would like to thank to my landlord and my lovely roommates for taking care of my life. I no longer feel lonely with you guys since I came to Edmonton.

I would also like to thank to my friends, no matter we know each other in badminton court, or running for Marathon, or even in the university. Optimism, helpfulness and determination I've seen from my friends motivating me for pursuing a healthier body and a more optimistic attitude.

Finally, I must express my very profound gratitude to my parents and grandparents for providing me with unfailing support and continuous encouragement throughout my years of study and through the process of researching and writing this thesis. This accomplishment would not have been possible without them.

Contents

1. Cytometric technology and its application on biological cells	1
1.1. Current cytometric technology	1
1.2. Measurements of current flow cytometry	3
1.3. Study of biological cells.....	6
1.4. Previous light scattering studies of cells.....	8
1.5. Outline.....	10
2. Background of light scattering technique.....	11
2.1. Light scattering studies of single dielectric particles	11
2.2. Mie scattering theory	12
2.3. FDTD simulation of light scattering from dielectric particles	16
3. Experimental setup for laser light scattering and studies of homogenous spherical and non-spherical particles.....	18
3.1. Introduction	18
3.2. Experimental setup description of label-free cytometer.....	19
3.3. Experimental setup alignment	21
3.4. Experimental and Mie scattering results for spherical polystyrene microbeads ...	24
3.5. Fast Fourier transform (FFT) analysis of experiment results with spherical microbeads.....	32
3.6. Experimental results for non-spherical polystyrene latex particles	33
4. Laser light scattering studies for biological cells and scattering pattern analysis.....	36
4.1. Introduction	36
4.2. Sample preparation and experimental procedure	37
4.3. Microscopic image of non-treated and staurosporine-treated SH-SY5Y neuroblastoma cells.....	38
4.4. Experimental scattering pattern of non-treated and staurosporine-treated SH-SY5Y neuroblastoma cells.....	40
4.5. Pattern classification of scattering data	43
4.5.1. Angle distribution method — a method distinguishes non-fringe from fringe pattern	43
4.5.2. Finding local maximum — a method of analyzing non-fringe pattern	50

4.6.	Some explanations for fringe and non-fringe pattern based on FDTD modelling.	62
4.7.	Other findings of label-free cytometer light scattering technique.....	64
4.8.	Finding fraction of non-treated and staurosporine-treated SH-SY5Y cells.....	65
4.9.	Experiments with a capillary tube.....	68
5.	Conclusion and future work.....	71
5.1.	Summary of non-invasive label-free cytometry.....	71
5.2.	Future work.....	73
	Bibliography.....	74
	Appendices.....	82
A.1	Matlab code for angle distribution method.....	82
A.2	Matlab code for finding local maximum method.....	84
A.3	SEM and TEM imaging.....	90
A.4	Flow chart of collecting data from CCD camera until data analysis.....	94
A.5	Preparation procedure of non-treated and treated SH-SY5Y.....	95

List of Tables

Figure 1.1: Schematic diagram of five basic components in flow cytometry.	2
Figure 1.2: Schematic diagram of a microscope-based label-free microfluidic light scattering cytometer.....	2
Figure 1.3: Illustration of how a Fluorescence-activated Cell Sorting (FACS) performing the cell sorting. Image was copied from [12]	4
Figure 1.4: Diagram of forward, side and backward light scattering of one single particle.....	4
Figure 1.5: Models of prokaryotic and eukaryotic cells [20]	6
Figure 2.1: Interaction between incident wave and particle.	12
Figure 2.2: Validation of FDTD simulation results with Mie simulation results.	17
Figure 3.1: Schematic diagram of experimental setup for the forward and side light scattering.	20
Figure 3.2: Schematic diagram of experimental set up for the backward light scattering.....	20
Figure 3.3: A single mode fiber is locked in a vertically placed fiber chuck which is suspended by a height adjustable mount.	22
Figure 3.4: Optical fiber image on forward direction CCD camera (a) and side direction CCD camera (b). Defocused optical fiber image on forward direction camera (a') and side direction camera (b').....	22
Figure 3.5: Resolution test of experimental system with a resolution test target.	24
Figure 3.6: (a): Illustration for the two-dimensional scattering of a single homogeneous particle captured by CCD camera. (b): Microscopic image of 6 μm spherical bead in the forward CCD camera.	25
Figure 3.7: Light scattering pattern for 10 μm and 15 μm spherical bead with red laser illumination. A-A'': Forward, side and backward scattering of 10 μm bead. B-B'': Forward, side and backward scattering of 15 μm bead.	26
Figure 3.8: Light scattering pattern for 10 μm and 15 μm spherical bead with green laser illumination. C-C'': Forward, side and backward scattering of 10 μm bead. D-D'': Forward, side and backward scattering of 15 μm bead.	26
Figure 3.9: Spectrum comparison between Mieplot and experimental results for 10 μm spherical bead with red laser illumination in three directions.....	27
Figure 3.10: Scattering pattern from experiment of spherical microbeads. A and A' are obtained from 4 μm diameter bead in the forward direction and side direction respectively, while B and B' are the pattern captured from 6 μm spherical bead under the same direction.	29
Figure 3.11: Layout of Mieplot with a diameter of 6 μm spherical particle.....	30
Figure 3.12: 1D FFT result of 4 μm , 6 μm , 10 μm and 15 μm spherical bead. Frequency and amplitude are normalized by dividing the length of each data.	32
Figure 3.13: Microscopic images for non-spherical polystyrene latex particles. 4.0 μm \times 6.0 μm peanut-like (left), 9 \times 10.5 μm pear-like (right).....	34

Figure 3.14: A-D are the light scattering patterns for $4.0 \mu\text{m} \times 6.0 \mu\text{m}$ non-spherical bead in the forward direction, while A'-D' are the light scattering patterns for $4.0 \mu\text{m} \times 6.0 \mu\text{m}$ non-spherical bead in the side direction.	34
Figure 3.15: A-D are the light scattering patterns for the $9 \times 10.5 \mu\text{m}$ non-spherical bead in the forward direction, while A'-D' are the light scattering patterns for the $9 \times 10.5 \mu\text{m}$ non-spherical bead in the side direction.	35
Figure 4.1: Microscopic image of non-treated SH-SY5Y neuroblastoma cells (a) and staurosporine-treated SH-SY5Y neuroblastoma cells (b).	38
Figure 4.2: SEM imaging of non-treated SH-SY5Y neuroblastoma cells (a) and staurosporine-treated SH-SY5Y neuroblastoma cells (b); TEM imaging of non-treated SH-SY5Y neuroblastoma cells (b); TEM imaging of non-treated SH-SY5Y neuroblastoma cells (c) and staurosporine-treated SH-SY5Y neuroblastoma cells (d).	39
Figure 4.3: Experimental light scattering pattern in three directions (forward, side and backward) with red laser illumination in staurosporine-treated SH-SY5Y.	41
Figure 4.4: Experimental light scattering pattern in three directions (forward, side and backward) with red laser illumination in non-treated SH-SY5Y.	41
Figure 4.5: Experimental light scattering pattern in three directions (forward, side and backward) with green laser illumination in staurosporine-treated SH-SY5Y.	41
Figure 4.6: Experimental light scattering pattern in three directions (forward, side and backward) with green laser illumination in non-treated SH-SY5Y.	42
Figure 4.7: Angle distribution of three different types of original and rotated pattern. A and A' are typical fringe pattern and fringe pattern after rotation. B, B' and C, C' are two typical non-fringe patterns and their patterns after rotation. Right-hand side are the angle distribution spectrums to the corresponding left-hand side scattering pattern.	45
Figure 4.8: Absolute difference between original and rotated pattern collected in the forward direction with red laser illumination.	48
Figure 4.9: A is the percentage comparison of "dead" cell group with red laser in all three directions; B is the percentage comparison of "live" cell group with red laser in all three directions; C is the percentage of "dead" cell with green laser in all three directions; D is the percentage comparison of "live" cell with green laser in all three directions.	49
Figure 4.10: Original image and Gaussian smoothed image in grey scale and the corresponding 3D mesh plot.	51
Figure 4.11: Full width at half maximum (FWHM) approximation of each local peak. Cross area is approximated based on a diamond area (left side). Flow chart of scanning for half maximum in four directions (right side).	52
Figure 4.12: Calculated local cross area (red diamond) with corresponding local maximum (green circle).	53
Figure 4.13: Speckle analysis in the forward direction based on finding local maximum method. (A) is the comparison between two groups with green laser illumination. (B) is the comparison between two groups with red laser illumination.	54

Figure 4.14: Speckle analysis in the side direction based on finding local maximum method. (A) is the comparison between two groups with green laser illumination. (B) is the comparison between two groups with red laser illumination.	55
Figure 4.15: Speckle analysis in the backward direction based on finding local maximum method. (E) is the comparison between two groups with green laser illumination. (F) is the comparison between two groups with red laser illumination.	56
Figure 4.16: Speckle analysis based on finding local maximum method for “dead” group. (A) is the comparison between two different illumination sources in the forward direction. (B) is the comparison between two different illumination sources in the side direction. (C) is the comparison between two different illumination sources in the backward direction.	57
Figure 4.17: Speckle analysis based on finding local maximum method for “live” group. (D) is the comparison between two different illumination sources in the forward direction. (E) is the comparison between two different illumination sources in the side direction. (F) is the comparison between two different illumination sources in the backward direction.	58
Figure 4.18: Speckle analysis based on finding local maximum method for “dead” cell group. (A) is the comparison between two different collecting times in the forward direction. (B) is the comparison between two different collecting times in the side direction.	59
Figure 4.19: Speckle analysis based on finding local maximum method for “live” cell group. (C) is the comparison between two different collecting times in the forward direction. (D) is the comparison between two different collecting times in the side direction.	60
Figure 4.20: Simulated forward 2D scattered light patterns with various size ration of nucleus and cytoplasm.	62
Figure 4.21: The simulated 2D scattered light patterns with different mitochondria distributions.	63
Figure 4.22: Upper eight scattering patters are captured from non-treated SH-SY5Y cells with red laser illumination in the forward and side directions, respectively; Lower eight scattering patterns are captured from staurosporine-treated SH-SY5Y cells with red laser illumination in the forward and side directions, respectively.	64
Figure 4.23: One single staurosporine-treated SH-SY5Y cell tracking on the side direction with red laser illumination.	65
Figure 4.24: (A) is all data collected from both “dead” and “live” group in the forward direction with red laser illumination; (B) is the light scattering data from mixed solution in the forward direction with red laser illumination (cells received in 2018).	66
Figure 4.25: Non-fringe light scattering pattern of “dead” group cells at different time analysis (cells received in 2017).	67
Figure 4.26: Schematic diagram of 2D light scattering static cytometer.	69
Figure 4.27: Image of 6 μm spherical bead (A) and its corresponding light scattering pattern (B).	69
Figure 4.28: Mieplot spectrum of a diameter of 6 μm spherical bead.	70
Figure 7. 0.1: SEM imaging of non-treated SH-SY5Y neuroblastoma cells.	90

Figure 7. 0.2: SEM imaging of staurosporine-treated SH-SY5Y neuroblastoma cells.	91
Figure 7.0.3: TEM imaging of non-treated SH-SY5Y neuroblastoma cells.....	92
Figure 7.0.4: TEM imaging of staurosporine-treated SH-SY5Y neuroblastoma cells.	93
Figure 7. 0.5: Flow chart of procedure after data collected from CCD camera.	94
Figure 7. 0.6: A is an example of good frame after filtered by intensity, B is an example of useless frame after filtered by intensity.	95

1. Cytometric technology and its application on biological cells

1.1. Current cytometric technology

Cytometer is an instrument of measuring characterizations of cells, such as cell size, cell number, cell morphology and other chemical and biological features inside the cell. One of the cytometric devices called flow cytometry is a powerful technique for the analysis of multiple parameters of individual cells within heterogeneous population. It performs its analysis by passing thousands of cells per second through a laser beam and collect the scattering light or fluorescent light from each cell as it passes through. Flow cytometer includes five fundamental parts: the fluidic system, which manipulates the mixed sample into a stream of single particles that can be interrogated individually by the detection system; the lasers, which are illumination sources for scatter and fluoresce; the optics, which gather light and direct light; the detectors, which receive the light from optics; the electronics and computer system, which converts optical signal into electronic signal and performs analysis. The data gathered from detectors can be analyzed statistically by flow cytometry software and further study the characteristics of cells. The schematic diagram of flow cytometry is demonstrated in Figure 1.1. Flow cytometry has been widely used in cell counting, cell sorting, biomarker detection and protein engineering [1] [2] [3] .

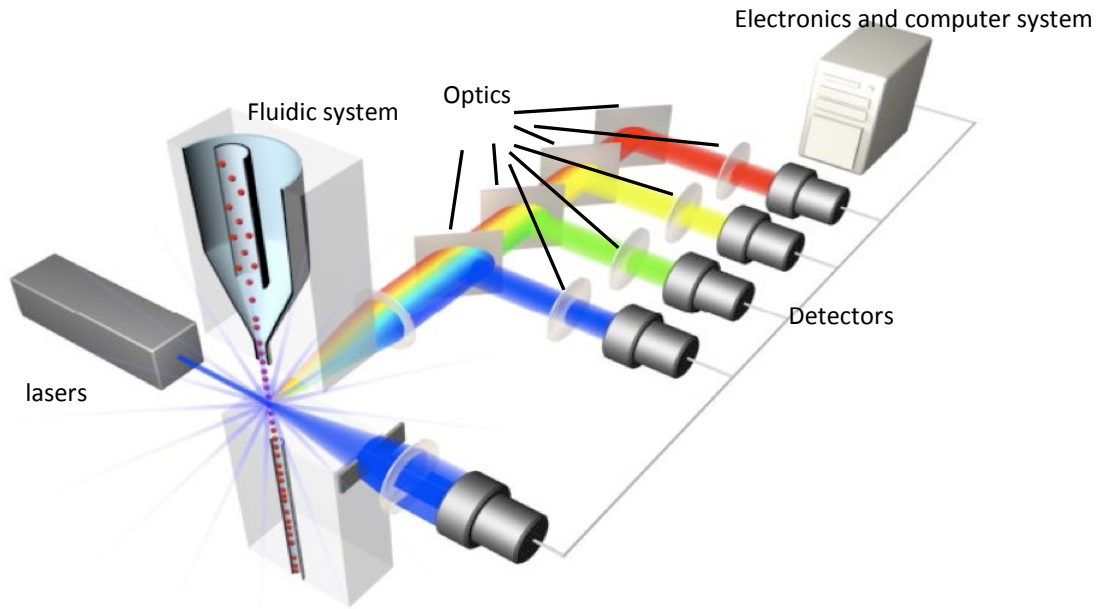


Figure 1.1: Schematic diagram of five basic components in flow cytometry.

Microfluidic cytometry is another cytometric technology which is known by its miniaturized, economic features comparing with conventional flow cytometry technique. Technique including optical stretching, shear flow, or capillary-like microchannel and microfluidic-based systems enables the analysis of single cell which can be applied for biological study and clinical diagnosis.

Figure 1.2 shows a microfluidic cytometry manufactured by Su et al. [4].

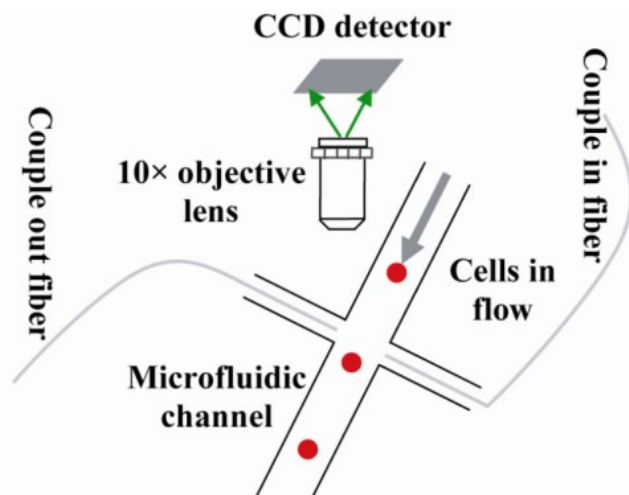


Figure 1.2: Schematic diagram of a microscope-based label-free microfluidic light scattering cytometer.

Successful measurements have done by microfluidic cytometry on single cell analysis, such as leukemic cells [5] , hematopoietic stem cells [6] and blood cells [7] .

1.2. Measurements of current flow cytometry

To characterize cells [8] [9] and diagnose diseases [10] [11] ,conventional flow cytometry measures the fluorescence signal from labelled cells. The Fluorescence-activated Cell Sorting (FACS) technique sorts cells based on fluorescent characteristics of each labelled cell. In FACS, cells stained with fluorophore-conjugated antibodies can be separated from one to another depending on which fluorophore they have been stained with. Individual cells are first illuminated by a laser and leaves the nozzle tip in a single droplet. The drop is given a positive or negative charge, depending on the fluorescence signal inside the cell. Deflection plates attract or repel the cells and these cells are going into corresponding collection tubes, which finishes the cell sorting. Figure 1.3 illustrates how a FACS sorting cell system.

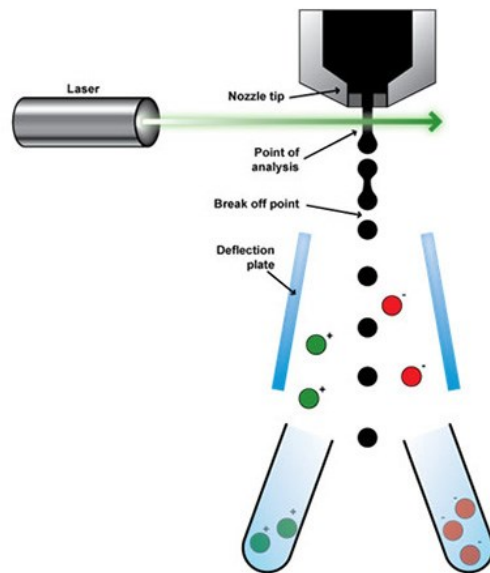


Figure 1.3: Illustration of how a Fluorescence-activated Cell Sorting (FACS) performing the cell sorting. Image was copied from [12].

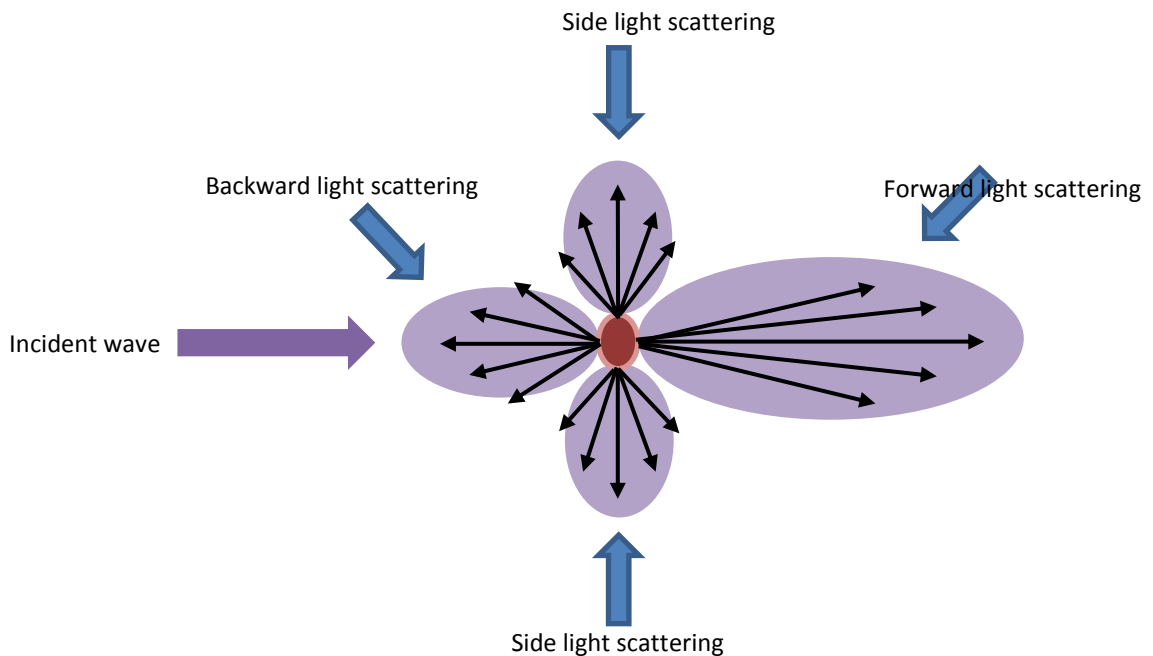


Figure 1.4: Diagram of forward, side and backward light scattering of one single particle.

However, due to the time-consuming process of labelling cells and the potential of damage cell from labelling dyes, developing a flow cytometry without labeling attracts more and more

attention. Agnarsson developed a label-free imaging method of the size of vesicles based on the evanescent light-scattering signals [13] . However, this method still need fluorescence signal involved. Vibrational microscopy based on infrared absorption and Raman scattering [14] [15] is another label-free technology by studying characteristic frequencies of different bonds. However, spatial resolution has been limited because of long infrared wavelengths. Spontaneous Raman scattering microscopy has the higher spatial resolution but lower imaging speed and is insensitive [16] . Coherent anti-Stokes Raman scattering (CARS) microscopy has higher sensitivity but is more difficult to interpret the spectrum because spontaneous Raman scattering involved [17] [18] . Stimulated Raman scattering (SRS) is another vibrational imaging technique which has a significant greater sensitivity than spontaneous Raman microscopy, and is easier to interpret the chemical contrast comparing with CARS [19] .

In this project, a non-invasive label-free cytometer based on laser light scattering technique has been introduced. Scattering patterns illuminated with two different wavelengths in three directions (forward, side and backward), as shown in Figure 1.4, will be discussed in detail in Chapter 3.

1.3. Study of biological cells

All cells have three fundamental structures in common: (i) cell membrane, which separate inside of the cell from outer environment; (ii) cytoplasm, which is a jelly-like fluid containing all organelles are located; (iii) DNA, which is the genetic material of the cell. Cells can be categorized into two groups: eukaryotic cells, which usually are plant and animal cells with a nucleus and membrane-enclosed organelles; prokaryotic cells, which are unicellular organisms without a nucleus or membrane-enclosed organelles. These two types of cells are illustrated in Figure 1.5.

Prokaryotic vs Eukaryotic Cells

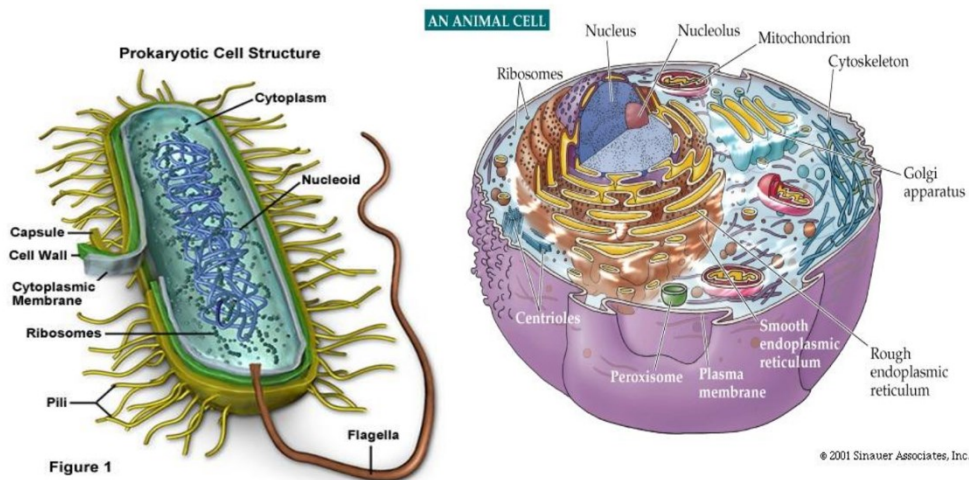


Figure 1.5: Models of prokaryotic and eukaryotic cells [20] .

When incident light interacts with a cell, the majority of light transmit through the cell without being affected, while rest of them interact with inner structures of the cell such as nucleus. As a result, studying the size of the cell and its inner structure, and the distribution of organelles as well as the corresponding refractive index will help us to understand how light behaves inside the cell

and transmits across the membrane. However, organelles with the size much smaller than incident wavelength cannot be resolved by imaging.

Cell component	Size (diameter)	Refractive index	Volume ratio
Cytoplasm	10~30 μm	1.38	50~80%
Nucleus	3~10 μm	1.39	5~10%
Mitochondrion	0.3~0.7 μm	1.42	5~15%
Lysosome	0.2~0.5 μm	1.3785	1~10% (including other organelles)

Table 1.1: Size, refractive index and volume ratio of different organelles in a eukaryotic cell.

According to Table 1.1, sizes of cytoplasm (10~30 μm [57]) and nucleus (3~10 μm) are much greater than mitochondrion (0.3~0.7 μm) and lysosome (0.2~0.5 μm [21]). Besides, cytoplasm, nucleus and mitochondrion are greater in refractive index (1.38 [57] , 1.39 [22] and 1.42 [23] , respectively) and volume ratio comparing with lysosome (refractive index is 1.3785 [58] , and volume ratio is 1~10% [56]) and other organelles in an eukaryotic cell. As a result, cytoplasm, nucleus and mitochondrion scatter more light comparing with other organelles such as lysosome.

1.4. Previous light scattering studies of cells

Multiple types of cell have been studied using label-free cytometry technique in our group [4] [6] [23] [24] [25] [26] [26] . Table 1.2 describes the brief work done by previous students and myself.

Student	Light scattering system	Forward light scattering detection	Side light scattering detection	Backward light scattering	Multiwavelength illumination	Cells type
Xuantao Su	Integrated microfluidic waveguide cytometer	No	Yes	No	No	Yeast, human Raji cells
Debbie Feng Shan Ha	Microfluidic chip with flow control system	No	Yes	No	No	CD34+, NC-37, HL-60, KG-1a, E. coli DH5 α
Hesam Shahin	Label-free flow cytometry with cuvette	Yes	Yes	No	No	HSC, VSELs

Wendy Yu Wan	Label-free flow cytometry with cuvette	Yes	Yes	No	Yes	SH- SY5Y
-----------------	---	-----	-----	----	-----	-------------

Table 1.2: Brief description about previous students' work and my work.

Experimental 2D light scattering patterns from yeast and human Raji cells have been obtained by Xuantao Su et al [24] used an integrated microfluidic optical waveguide cytometer. FDTD simulations [4] [6] [45] such as side scattering indicates that small angle scattered light determines cell size while large angle scattered light determines the mitochondria distribution inside the cell. Fourier spectrum analysis of experimental side scattering data reveals that highest dominant frequency contributes to cell size while lower frequency results from mitochondria distribution. Experimental scattering pattern in the side direction for normal cell lines CD34+, leukemic cell lines NC-37, HL-60, and KG-1a, as well as E. coli DH5 α have been successfully obtained [26] . A customized flow control system embedded with the microfluidic system allows the control ability of pressure and speed of flow within the channel has been developed [26] . Hematopoietic Stem Cells (HSC) and Very Small Embryonic Like Stem Cells (VSELs) have been studied by Shahin et al. 2D experimental light scattering pattern can be obtained in two directions. Good agreements between calculated 2D scattered light patterns based on FDTD simulation and patterns obtained experimentally give us a better understanding of physical background of cells.

1.5. Outline

In this thesis, the laser light scattering based non-invasive label-free cytometry technique has been advanced to include patterns in backward scattering as well as illumination in two wavelengths in red and green. This chapter briefly introduces current flow cytometric technique and biological cells, as well as previous efforts of our group for this label-free cytometry technique. Chapter 2 describes the background of light scattering and fundamentals of Mie theory. FDTD simulation and other algorithm for light scattering studies have also been discussed. Chapter 3 describes the label-free cytometer system and experimental results of spherical and non-spherical micro scale beads. Experimental results have been compared with Mieplot [36] results. Chapter 4 presents the experimental light scattering pattern obtained from non-treated and staurosporine-treated SH-SY5Y neuroblastoma cells. Two methods which can be called “angle distribution method” and “finding local maximum method” have been proposed for pattern classification and recognition. Chapter 5 summarizes the work done by this project and provides some recommendations for the future work.

2. Background of light scattering technique

2.1. Light scattering studies of single dielectric particles

Light scattering occurs when the dielectric particles are illuminated by the light. The electromagnetic wave interacts with the electric charges inside the particle and cause oscillatory motion. The oscillated electric charges radiate electromagnetic energy in all directions which is called scattering. In addition to reradiated electromagnetic energy, the excited charges may transform part of incident electromagnetic energy into other forms such as kinetic energy and thermal energy, which leads to absorption of the wave energy. A combination of scattering and absorption is called extinction, which is usually expressed by extinction coefficient μ_t . The relationship between extinction coefficient, scattering coefficient μ_s and absorption coefficient μ_a is:

$$\mu_t = \mu_s + \mu_a \quad 2.1$$

Different ways of scattering have been studied and used in scientific research as well as commercial applications. Elastic scattering and inelastic scattering are the two forms of electromagnetic scattering. Rayleigh scattering [27] [28] [29] and Mie scattering [30] are two major elastic scattering while inelastic scattering includes Brillouin scattering[31] and Raman scattering [32].

2.2. Mie scattering theory

Mie scattering theory has a wide application in current research of scattering electromagnetic waves by dielectric spherical particles with any radius. The dielectric sphere is made of homogeneous and isotropic material. The important work done by Mie in 1908, led to a general analytical solution for optical light scattering by a homogeneous sphere of any size in a homogeneous medium based on the electromagnetic theory of light [32] , and the Mie solution involves dielectric particle size and wavelength.

Figure 2.1 is an illustration of interaction between light and single dielectric sphere. Coordinate will be used in the discussion below. Incident wave is x-polarized with propagation in the z-direction which is expressed as follows:

$$\vec{E}_{inc} = E_0 e^{i\beta_0 z} \hat{x} \quad 2.2$$

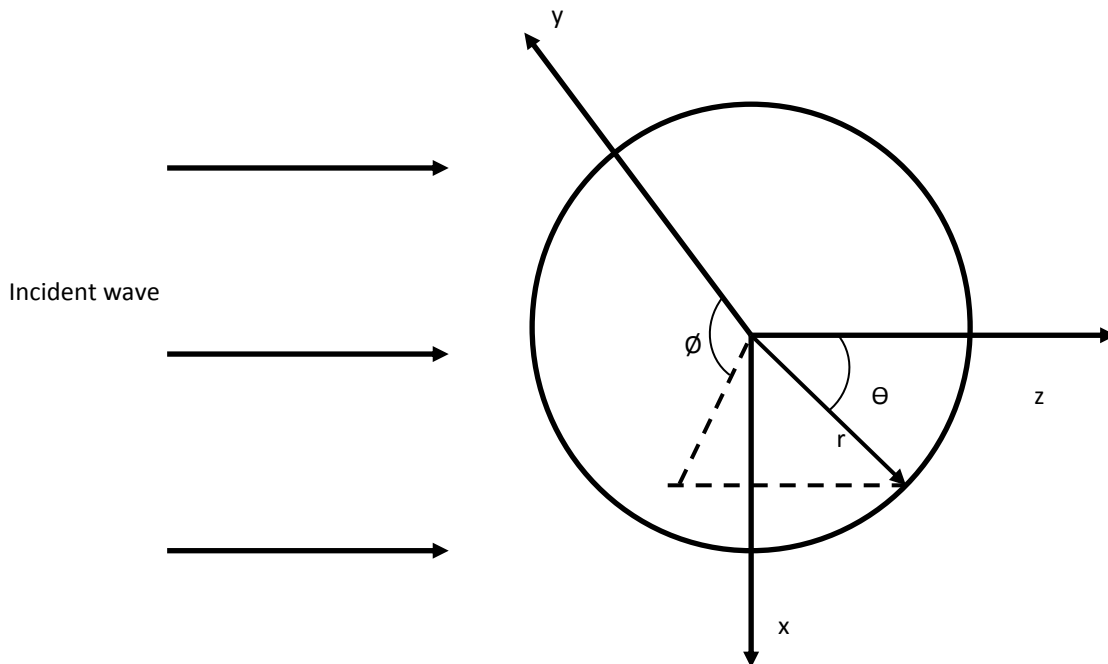


Figure 2.1: Interaction between incident wave and particle.

For a better understanding of Mie theory, we need to know how wave behaves in the medium and I start with Maxwell's equations with a single frequency electromagnetic wave.

$$\nabla \times \vec{E} = i\omega\mu\vec{H} \quad 2.3$$

$$\nabla \times \vec{H} = -i\omega\epsilon\vec{E} \quad 2.4$$

By taking curl of equation 2.3 and 2.4 and applying vector identity resulting in the time-independent wave equation

$$\nabla^2 \vec{E} + k_m^2 \vec{E} = 0 \quad 2.5$$

$$\nabla^2 \vec{H} + k_m^2 \vec{H} = 0 \quad 2.6$$

where $k_m^2 = \omega^2 \epsilon_m \mu$ is the wave vector in the medium and ϵ_m is the permittivity in the medium. Our next step is deriving the vector solutions of wave equation. Assume Ψ to be the solution of the scalar function

$$\nabla^2 \Psi + k_m^2 \Psi = 0 \quad 2.7$$

In spherical coordinate system, equation 2.7 can be rewrite as a function of r , θ and ϕ :

$$\frac{1}{r^2} \frac{\partial}{\partial r} \left(r^2 \frac{\partial \Psi}{\partial r} \right) + \frac{1}{r^2 \sin \theta} \frac{\partial}{\partial \theta} \left(\sin \theta \frac{\partial \Psi}{\partial \theta} \right) + \frac{1}{r^2 \sin^2 \theta} \frac{\partial^2 \Psi}{\partial \phi^2} + k_m^2 \Psi = 0 \quad 2.8$$

Solution can be written as the form of

$$\Psi(r, \theta, \phi) = R(r)\Theta(\theta)\Phi(\phi) \quad 2.9$$

By applying separation of variables, three solutions can be obtained in equation 2.10-2.12.

$$\Phi = e^{\pm im\phi} \quad 2.10$$

$$\Theta = P_l^m(\eta) = \frac{(1-\eta^2)^{\frac{m}{2}} d^{l+m} (\eta^2-1)^l}{2^{l!} d(\eta)^{l+m}} \quad 2.11$$

$$R = \sqrt{\frac{2}{\pi}} Z_l(p) \quad 2.12$$

Where $\eta = \cos\theta$, $p = k_m r$, and $Z_l(p)$ represents the radial spherical Bessel $j_l(p)$ and first order Hankel functions $h_l(p)$.

As a result, the full description of the scalar solution can be written as

$$\Psi_{l,m}(r, \theta, \phi) = \sqrt{\frac{2}{\pi}} Z_l(k_m r) P_l^m e^{im\phi} \quad 2.13$$

Mie scattering coefficients a_l, b_l , and coefficients of an internal field c_l, d_l can be determined by boundary conditions. Mie theory requires that the permittivity and the permeability are isotropic and constant in the region where electromagnetic wave propagates. When the wave crosses the boundary of a particle which is embedded in medium, the tangential components of \hat{E} and \hat{H} are continuous across the boundary

$$[\hat{E}_{inc} + \hat{E}_{scat} - \hat{E}_{int}] \times \hat{r} = 0 \quad 2.14$$

$$[\hat{H}_{inc} + \hat{H}_{scat} - \hat{H}_{int}] \times \hat{r} = 0 \quad 2.15$$

Where \hat{E}_{inc} and \hat{H}_{inc} are incident fields, \hat{E}_{scat} and \hat{H}_{scat} are scattered fields, \hat{E}_{int} and \hat{H}_{int} are internal fields, and \hat{r} is the unit vector perpendicular to the boundary surface. Therefore,

$$E_{inc,\theta} + E_{scat,\theta} = E_{int,\theta} \quad H_{inc,\theta} + H_{scat,\theta} = H_{int,\theta} \quad 2.16$$

$$E_{inc,\emptyset} + E_{scat,\emptyset} = E_{int,\emptyset} \qquad H_{inc,\emptyset} + H_{scat,\emptyset} = H_{int,\emptyset} \qquad 2.17$$

The scattered and internal fields can be expressed as:

$$\vec{E}_{scat} = \frac{k_m}{\omega^2 \epsilon_m \mu} \sum [A_{l,m} a_l \vec{M}_{l,m} + B_{l,m} b_l \vec{N}_{l,m}] \qquad 2.18$$

$$\vec{H}_{scat} = -\frac{ik_m}{\omega \mu} \sum [A_{l,m} a_l \vec{N}_{l,m} + B_{l,m} b_l \vec{M}_{l,m}] \qquad 2.19$$

$$\vec{E}_{int} = \frac{k_m}{\omega^2 \epsilon_m \mu} \sum [A_{l,m} c_l \vec{M}_{l,m} + B_{l,m} d_l \vec{N}_{l,m}] \qquad 2.20$$

$$\vec{H}_{int} = -\frac{ik_m}{\omega \mu} \sum [A_{l,m} c_l \vec{N}_{l,m} + B_{l,m} d_l \vec{M}_{l,m}] \qquad 2.21$$

$\vec{M}_{l,m}$ and $\vec{N}_{l,m}$ are time-independent vector solution of electrical and magnetic field which expressed as:

$$\vec{M}_{l,m} = \nabla \times \vec{r} \psi_{l,m}, \quad \vec{N}_{l,m} = \frac{1}{k_m} \nabla \times \vec{M}_{l,m} \qquad 2.22$$

The Mie scattering coefficient a_l , b_l , c_l and d_l are obtained as

$$a_l = \frac{N^2 j_l(N\chi) [\chi j_l(\chi)]' - j_l(\chi) [N\chi j_l(N\chi)]'}{N^2 j_l(N\chi) [\chi h_l(\chi)]' - h_l(\chi) [N\chi j_l(N\chi)]'} \qquad 2.23$$

$$b_l = \frac{j_l(N\chi) [\chi j_l(\chi)]' - j_l(\chi) [N\chi j_l(N\chi)]'}{j_l(N\chi) [\chi h_l(\chi)]' - h_l(\chi) [N\chi j_l(N\chi)]'} \qquad 2.24$$

$$c_l = \frac{j_l(\chi) [\chi h_l(\chi)]' - h_l(\chi) [\chi j_l(\chi)]'}{j_l(N\chi) [\chi h_l(\chi)]' - h_l(\chi) [N\chi j_l(N\chi)]'} \qquad 2.25$$

$$d_l = \frac{N j_l(\chi) [\chi h_l(\chi)]' - N h_l(\chi) [\chi j_l(\chi)]'}{N^2 j_l(N\chi) [\chi h_l(\chi)]' - h_l(\chi) [N\chi j_l(N\chi)]'} \qquad 2.25$$

Where j_l and h_l denote the spherical Bessel function of the first kind and spherical Hankel function of the first kind, respectively. χ denotes the spherical Bessel functions of second kind. N^2 is associated with relative refractive index of the sphere ($n_{rel} = \frac{n_s}{n_b} = \frac{1}{N^2}$).

The denominators of a_l and d_l , b_l , and c_l are the same. When one of these dominators is very small, the corresponding normal mode will dominate the scatter field. This dominant mode is strongly depending on the size of the sphere, refractive index of the sphere and the surrounding medium as well as the incident wavelength. More details can be found from works of Bohren and Huffman [34] and Wang and Wu [35] .

In this project, Mie scattering calculation was carried out by using a public software named Mieplot [36] , whose calculation is based on work from Bohren and Huffman [34] . Calculated scattering results are presented and discussed in Chapter 3.

2.3. FDTD simulation of light scattering from dielectric particles

Previous students have done a lot of work on modelling particles with different inner structures as well as their light scattering patterns based on Finite-Difference Time-Domain (FDTD) method. Detailed explanation of FDTD light scattering simulation was introduced in Su's and Shahin's theses [25] [26] . The fundamental of FDTD method is solving electric and magnetic fields in time and space by using the coupled Maxwell's curl equations. The scattering patterns are computed based on total-field/scattered-field (TF/SF) technique [37] [38] . Stability and absorbing boundary conditions [38] [39] [40] [41] [24] have been taken into consideration to allow FDTD calculation in all time steps. Near-to far-field transformation is applied to allow the calculation obtaining scattering patterns not only in the near field but also in the far field. The numerical results from

FDTD have been validated with Mie theory results. As shown in Figure 2.2, which was done by Shahin et al. [25] , good agreements can be achieved by a diameter of 6 μm spherical polystyrene bead with a refractive index of 1.59 in Phosphate Buffered Saline (PBS) medium with a refractive index of 1.334. Both methods show the fact that light scattering is strongly depending on the angular distribution since the number of peaks and the intensity at two different angle distribution range are different, which is also be observed and verified in [42] . More examples of comparison between calculated FDTD results and Mie theory results can be found in Su’s thesis.

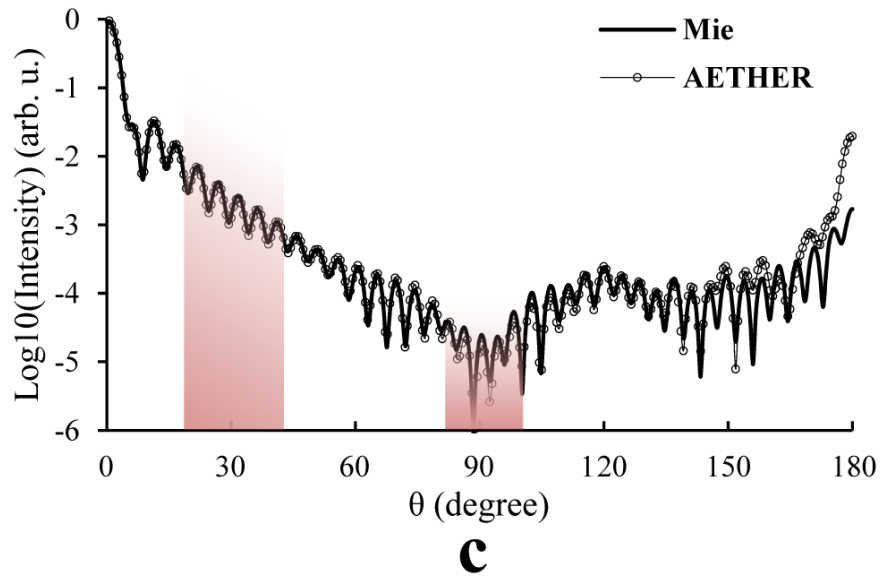


Figure 2.2: Validation of FDTD simulation results with Mie simulation results.

Other algorithm such as Discrete Source method (DSM), which is a well-known method for the analysis of light scattering [39] [40] has been calculated by Helden [41] , who realized the light scattering of a micrometer-sized spherical particle in an evanescent light field.

3. Experimental setup for laser light scattering and studies of homogenous spherical and non-spherical particles

3.1. Introduction

Laser light scattering studies of characterizing or identifying particles in micro or sub-micro scale and biological cells have been addressed an increasing number of attention recently. Flow cytometers developed by our group are able to analyze characterizations of biological cells based on laser light scattering technique especially in forward direction scattering and side direction scattering. In this thesis, I improved and advanced the label-free cytometer system based on Hesam's system by adding a backward scattering detection system and one more wavelength illumination. Two-dimensional scattering pattern of spherical microbeads and non-spherical microbeads, as well as biological cells can be captured simultaneously in forward, side and backward directions. Better alignment of the system makes it easier to capture the scattering pattern from one single particle at the same time on both forward and side directions. Alignment improvement will be described in detail in the following sections.

3.2. Experimental setup description of label-free cytometer

Figure 3.1 shows a schematic diagram of the experimental setup for collecting scattered patterns from beads and cells. The key components of the system include an illumination source (0.5-1.0 mW red helium neon laser, model: 05-LLR-811, wavelength at 632.8 nm, random polarization), another illumination source (340 mW, 532 nm green DPSS laser system, model: LRS-532-TM-200-5, vertical polarized), a plano-convex lens ($f = 5$ cm) which is used to create a small focal volume, a sample holder which carries sample solution (with a dimension length: 2.5 cm, width: 3.8 cm, height: 4 cm) called “cuvette”, detection system which includes a lens tube (17 cm in the forward direction, and 16 cm in the side direction) with a microscope objective on one side and a CCD camera (Chameleon USB 2.0, CMLN-13S2C-CS) on the other side. Two three-dimensional translation stages are connected to the detection system to adjust the distance and height from the imaging plane. All scattering patterns from both directions are generated on two CCD cameras and transmitted and saved into a laptop through a USB. The optical axis is 16.5 cm above the lab table. The detection system contains a microscope objective for collecting scattering light from sample in each direction. Especially, a long working distance microscope objective (Mitutoyo Plan Apo Infinity Corrected Long WD Objective, 10/0.28) is used in the forward direction about 30 degrees from the laser axis. Another microscope objective (Leitz Wetzlar, 10/0.25, 170/-) is used to collect side scattering light. For backward scattering measurement, a similar setup as forward scattering is used as shown in Figure 3.2.

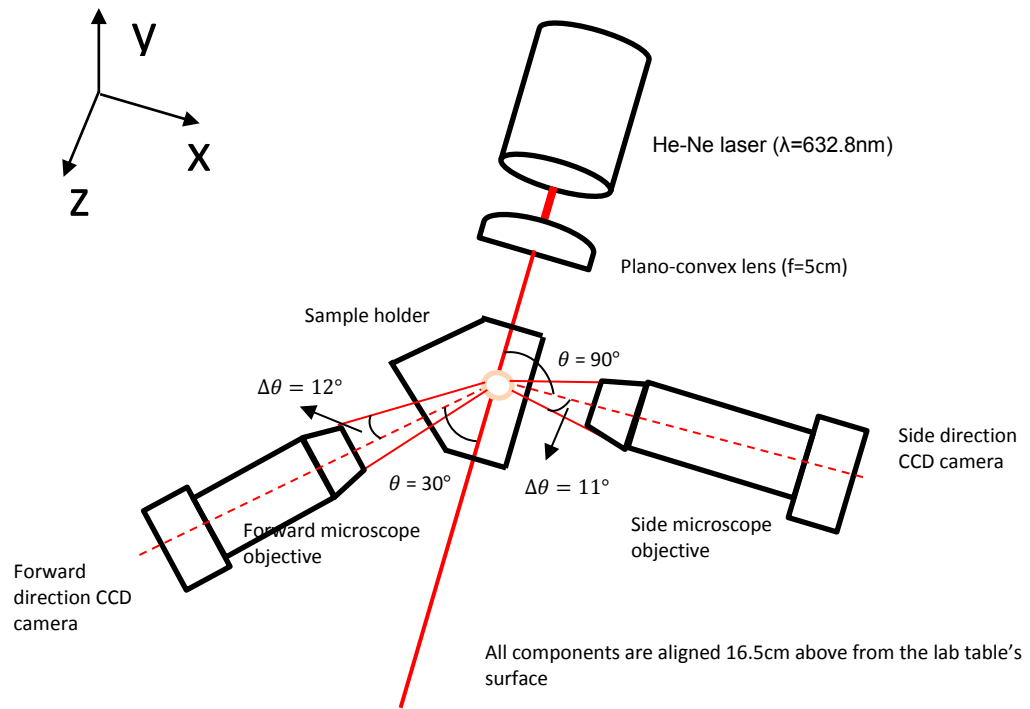


Figure 3.1: Schematic diagram of experimental setup for the forward and side light scattering.

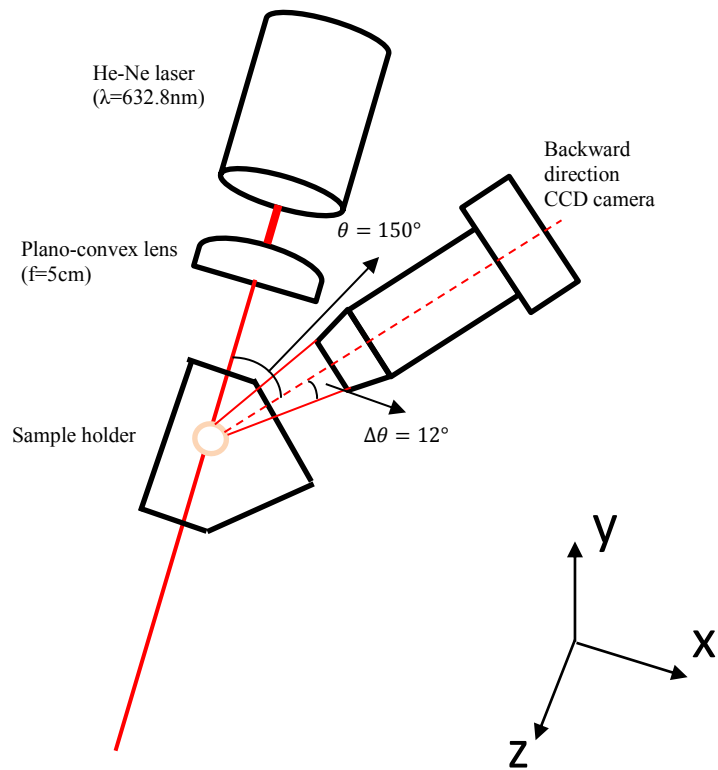


Figure 3.2: Schematic diagram of experimental set up for the backward light scattering.

Observation angle range in three directions depends on microscope objective and the refractive index of medium ($n = 1.332$) that light travels. Based on definition of numerical aperture shown in equation 3.1, the observation angle range can be calculated. Observation range angle in the forward direction is described in detail and other two observation angle ranges are shown in Table 3.1.

$$NA = n \sin \theta \quad 3.1$$

The long working distance objective with $NA = 0.28$, which resulting a covering angle $\theta \cong 12^\circ$. Since the objective is 30° away from incoming laser, the observation angle range is therefore between 18° and 42° .

Direction	Observation angle range
Forward	$[18^\circ, 42^\circ]$
Side	$[79^\circ, 101^\circ]$
Backward	$[138^\circ, 162^\circ]$

Table 3.1: Observation angle range in three different directions.

3.3. Experimental setup alignment

In order to make a better alignment of the system, a multimode fiber (62.5/125) is used to aid the alignment of the optical system. The fiber is suspended on a rod whose height is adjustable, as shown in Figure 3.3.

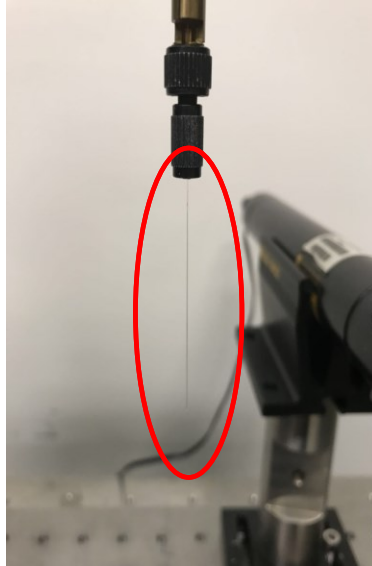


Figure 3.3: A single mode fiber is locked in a vertically placed fiber chuck which is suspended by a height adjustable mount.

After turning on the laser for about half an hour for the output power stabilization and turning off the room light, the fiber is gently lowering down until its end intersects with laser beam. Adjust the motion systems until the fiber images appear on the center of both CCD cameras screens as shown in Figure 3.4.

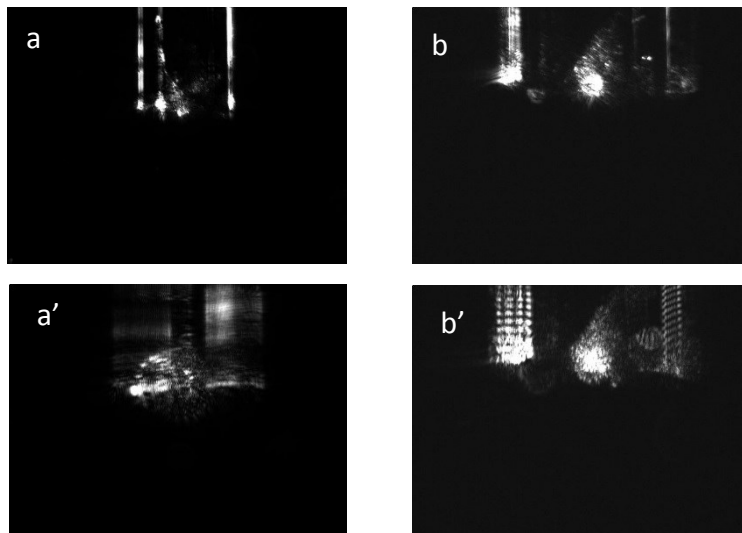


Figure 3.4: Optical fiber image on forward direction CCD camera (a) and side direction CCD camera (b). Defocused optical fiber image on forward direction camera (a') and side direction camera (b').

The two CCD cameras are connected to the laptop with USB 2.0. FlyCapture Viewer is used to view and save images from cameras. All the parameters are pre-settled as shown in Table 3.2.

	Forward CCD camera (CMLN-13S2M-CS, mono)	Side CCD camera (CMLN-13S2M-CS, mono)
Brightness	0%	6.2%
Exposure (eV)	0.015	2.214
Gain (dB)	0	24
Framerate (fps)	30	30
Resolution/pixel format	640×480/Y16	640×480/Y16

Table 3.2: Parameter settings on the two CCD cameras.

The experimental system resolution can be calculated as:

$$\text{Optical resolution} \cong 1.22 \frac{\lambda}{NA} \quad 3.1$$

Based on the NA provided above, resolution in the forward is approximate to 2.76 μm and side resolution is around 3.09 μm . it is also examined by a resolution test target (NBS 1952 Resolution Test Target, 3'' \times 1''). The smallest resolution is 80 lp/mm which give a line width of 6.3 μm as it clearly displays in Figure 3.5, which is captured by the forward detection system. It confirms that our experimental setup can detect a particle with a diameter larger than 6 μm .



Figure 3.5: Resolution test of experimental system with a resolution test target.

3.4. Experimental and Mie scattering results for spherical polystyrene microbeads

The plastic microsphere used is polystyrene latex beads with a high concentration around 10^7 particles/ml [43]. In order to make a proper concentration for single scattering measurement, dilution is required and phosphate-buffered saline (PBS) is used as liquid medium for bead sample. The refractive index of polystyrene latex beads and PBS is 1.587 and 1.332 at a wavelength of 632.8 nm, respectively, while the refractive index beads and PBS is 1.598 and 1.332 at a wavelength of 532 nm [44]. Spherical polystyrene microbeads with different diameters of 4 μm , 6 μm , 10 μm and 15 μm have been used in this project. The dilution step of 6 μm bead is described as follows.

The original concentration of 6 μm diameter microbead is 2×10^7 particles/ml. A volume of 20 ml PBS is drawn out with a pipette. Based on the dilution equation:

$$C_1V_1 = C_2V_2 \quad 3.2$$

Where C_1 and V_1 are the original sample concentration and original sample volume, C_2 and V_2 are the diluted concentration and diluted volume. When taking a volume of $3 \mu\text{l}$ from original sample with a different pipette, we can make a diluted concentration of $C_2 = \frac{C_1 V_1}{V_2} = (2 \times 10^7 \text{ particles/ml} \times 3 \times 10^{-3} \text{ ml}) / 20 \text{ ml} = 3000 \text{ particles/ml}$. Each dilution step is the similar and is targeted for all cases with a concentration around 3000 particles/ml.

For a single particle illuminated by a laser beam, the scattered light will propagate in space as shown in Figure 3.6 (a). The scattered light from a homogenous particle with a fixed angle Θ with regard to incident laser beam can form a cone, and the fringe pattern can be constructed at the intersection plane between the cone and CCD camera plane.

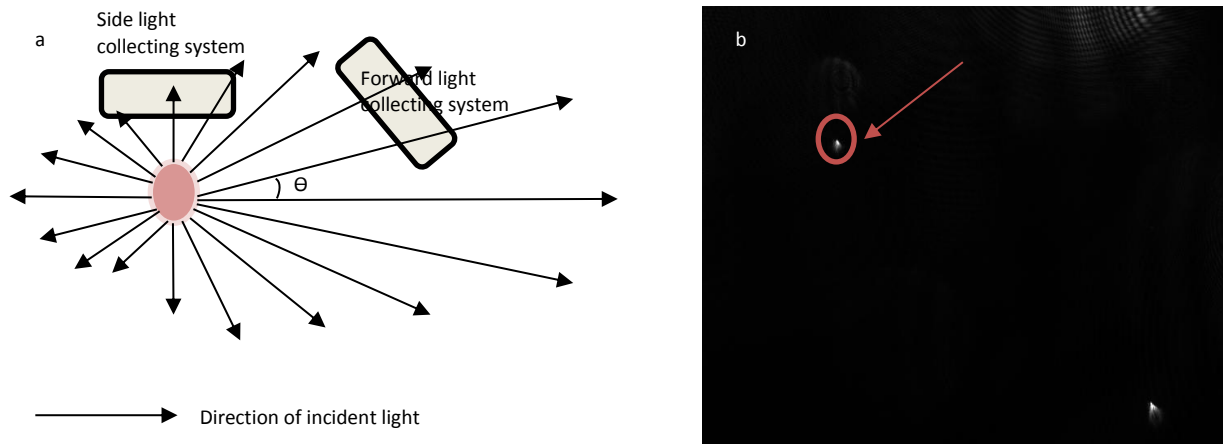


Figure 3.6: (a): Illustration for the two-dimensional scattering of a single homogeneous particle captured by CCD camera. (b): Microscopic image of $6 \mu\text{m}$ spherical bead in the forward CCD camera.

When the homogenous spherical bead is observed at the focal plane, a bright spot is captured by CCD camera as shown in Figure 3.6 (b). Since the spherical beads are in a solution and flowing freely in PBS due to molecular dynamics, bead images and scattering patterns can be observed at the same time depending on the position of beads with respect to the focal plane.

When the bead is not at focal plane, either further away or closer to the focal plane, which is defined as defocused state, two-dimensional scattering pattern can be captured with a diameter of

10 μm and 15 μm spherical bead in three observation angle range (forward, side and backward direction). Besides, light scattering pattern with different wavelengths have also been collected as shown in Figure 3.7 and Figure 3.8 with z-axis as the laser propagation direction.

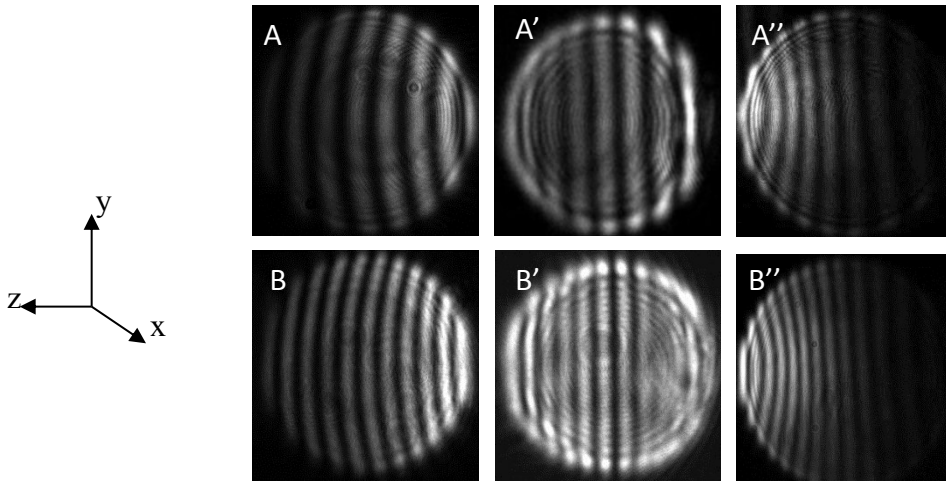


Figure 3.7: Light scattering pattern for 10 μm and 15 μm spherical bead with red laser illumination. A-A'': Forward, side and backward scattering of 10 μm bead. B-B'': Forward, side and backward scattering of 15 μm bead.

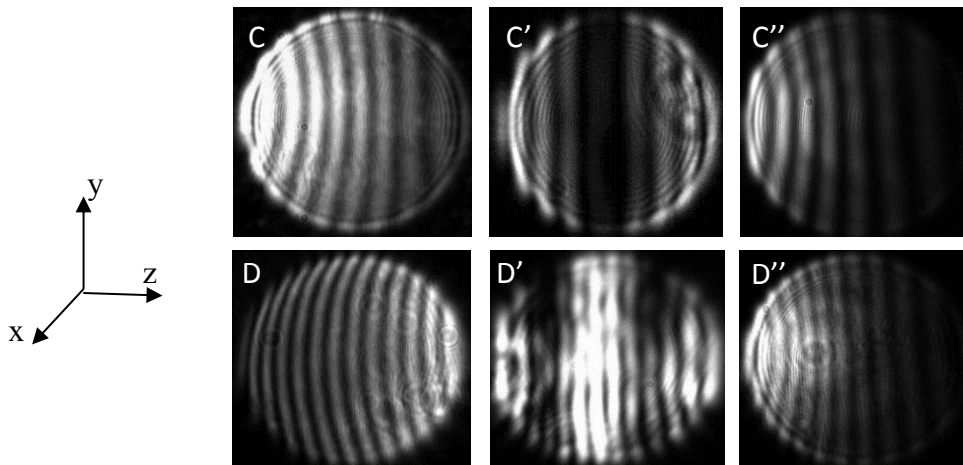


Figure 3.8: Light scattering pattern for 10 μm and 15 μm spherical bead with green laser illumination. C-C'': Forward, side and backward scattering of 10 μm bead. D-D'': Forward, side and backward scattering of 15 μm bead.

According to Figure 3.7 and Figure 3.8, eight, nine and nine number of fringes can be observed in the forward, side and backward direction respectively from the diameter of 10 μm spherical bead with red laser illumination, while ten, nine and eight number of fringes are counted of the same

diameter spherical bead in three directions (forward, side and backward respectively) with green laser illumination. On the other hand, for a 15 μm diameter bead shows eleven, eleven and thirteen number of fringe in three directions (forward, side and backward respectively) with red laser illumination and thirteen, thirteen and twelve fringes in three directions (forward, side and backward respectively) with green laser illumination.

It is interesting to note that in the forward direction, the fringes are a little bit curved and not vertical any more. This is because the projection of waveform from spherical bead scattering wave onto the flat surface of CCD elements.

Figure 3.9 summarizes the comparison between experimental results and Mie theory results for a 10 μm diameter spherical bead with 632 nm wavelength illumination in three directions.

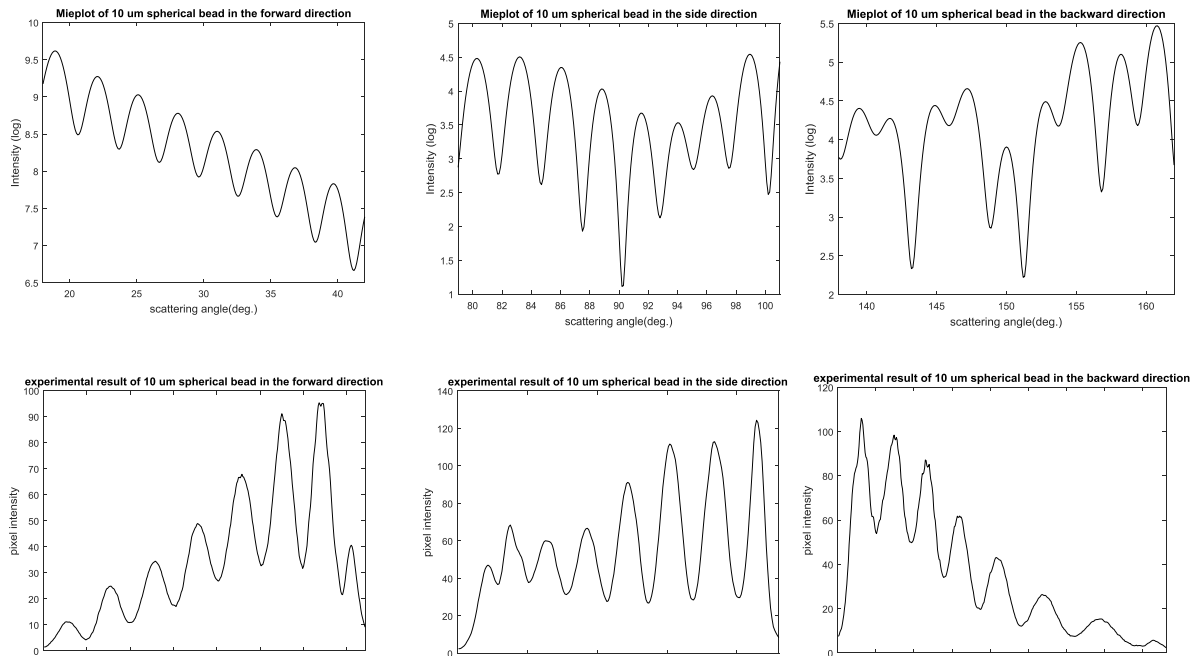


Figure 3.9: Spectrum comparison between Mieplot and experimental results for 10 μm spherical bead with red laser illumination in three directions.

According to Mieplot results, the number of peaks is eight in both forward and side directions, which matches the number of peaks from experiment results in the same direction. However, the

number of peaks is nine in the backward direction from Mieplot results while one number of peak less was obtained from experiment. The numbers of peaks for spherical beads with different diameters in three directions, and with two different wavelengths illumination as shown in Table 3.3 to Table 3.6.

	Forward	Side	Backward
Mieplot results	8	8	9
Experimental results	8	8	8

Table 3.3: Number of peaks comparison between Mieplot results and experimental results of a diameter of 10 μm bead with red laser illumination.

	Forward	Side	Backward
Mieplot results	10	8	10
Experimental results	10	9	9

Table 3.4: Number of peaks comparison between Mieplot results and experimental results of a diameter of 10 μm bead with green laser illumination.

	Forward	Side	Backward
Mieplot results	12	12	12
Experimental results	11	12	11

Table 3.5: Number of peaks comparison between Mieplot results and experimental results of a diameter of 15 μm bead with red laser illumination.

	Forward	Side	Backward
Mieplot results	15	13	14
Experimental results	13	13	14

Table 3.6: Number of peaks comparison between Mieplot results and experimental results of a diameter of 15 μm bead with green laser illumination.

All data generated from Mieplot and experiment have been imported to Matlab and saved as matrix for future use. In Figure 3.9, I averaged the counts along each column and made the plot of average intensity versus angle represented by horizontal pixel values in experimental results. Intensity are converted into log scale in Mieplot results. Scattering angle are calculated based on optical properties and geometry which is discussed in previous section. We are only interested in the number of peaks because the number of peaks carries the information of the size of the scattering particle.

In summary, comparison for the numbers of peaks observed and calculated has been carried out. Generally, more number of peaks are observed for a shorter wavelength illumination. Good agreement between Mieplot results and experimental results in terms of number of peaks, although slightly differences can be observed. Human counting error as well as the unclear fringe at the boundary on scattering pattern could be potential reasons for the slightly differences.

Experiments for micro sphere beads with diameters of 4 μm and 6 μm in both forward and side directions have also been carried out with red laser illumination, as shown in Figure 3.10.

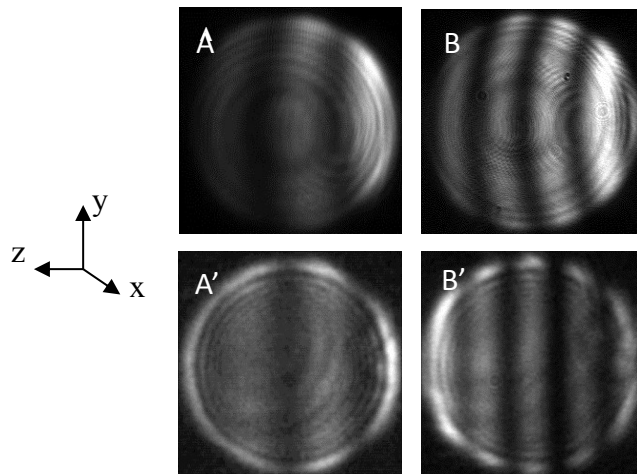


Figure 3.10: Scattering pattern from experiment of spherical microbeads. A and A' are obtained from 4 μm diameter bead in the forward direction and side direction respectively, while B and B' are the pattern captured from 6 μm spherical bead under the same direction.

Table 3.7 and Table 3.8 are the comparison between Mieplot and experimental results for 4 μm and 6 μm diameters spherical bead with red laser illumination. Good agreements can also be achieved in both forward and side directions.

	Forward	Side
Mieplot results	3	4
Experimental results	3	4

Table 3.7: Number of peaks comparison between Mieplot results and experimental results of a diameter of 4 μm bead with red laser illumination.

	Forward	Side
Mieplot results	5	5
Experimental results	4	5

Table 3.8: Number of peaks comparison between Mieplot results and experimental results of a diameter of 6 μm bead with red laser illumination.

It is worth to mention that when running Mieplot to obtain the Mie scattering from a sphere, proper parameters are needed to be chosen to approximate experimental conditions. Take diameter of 6

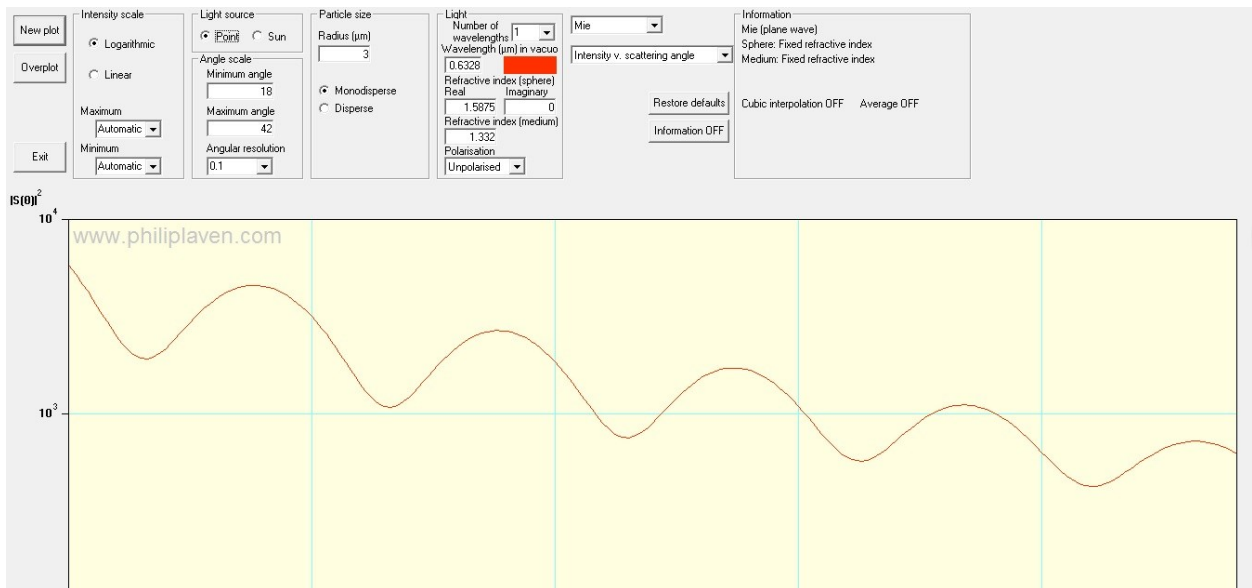


Figure 3.11: Layout of Mieplot with a diameter of 6 μm spherical particle.

μm spherical particle as an example. An unpolarized point light source with a wavelength of $0.6328 \mu\text{m}$ in vacuum is used. A fixed refractive index of sphere with 1.587 and the medium with 1.332 is adopted as discussed above. Angular resolution is set to be 0.1 rad. Scattering particle is considered as monodisperse [49] [50] . Angle scale is set to between 18 degrees and 42 degrees as is discussed before in terms of forward direction. The layout of the Mieplot of $6 \mu\text{m}$ spherical particle is shown as Figure 3.11.

Good agreements between Mieplot results and experimental results give confidence on the experiment set up which will be used for the study of biological cells in Chapter 4 of this thesis.

3.5. Fast Fourier transform (FFT) analysis of experiment results with spherical microbeads

One-dimensional Fast Fourier Transform (1D FFT) is applied to the experimental scattering pattern for the diameter of 4 μm , 6 μm , 10 μm and 15 μm spherical beads. Data from experimental light scattering pattern in the side direction with red laser illumination for these four different diameter spherical beads discussed in previous sections have been directly used for the input of FFT. Figure 3.12 shows the FFT result of four different diameters spherical beads.

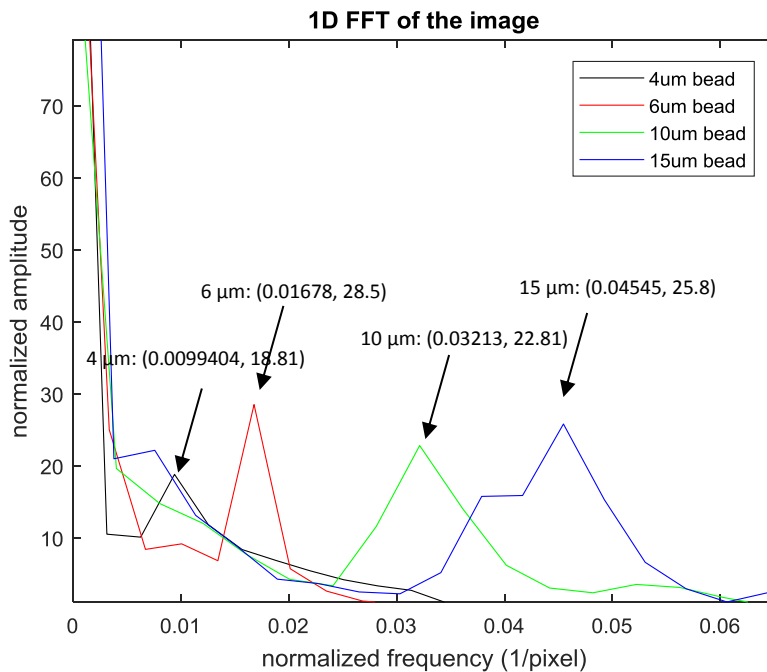


Figure 3.12: 1D FFT result of 4 μm , 6 μm , 10 μm and 15 μm spherical bead. Frequency and amplitude are normalized by dividing the length of each data.

Based on the 1D FFT result, we can calculate the actual periodicity of the fringe pattern and therefore figure out the number of fringe in the scattering pattern. Take a diameter of 4 μm spherical bead for example. A' in Figure 3.10 is imported into Matlab with function "imread" and saved as a matrix with a length of $N_1 = 319$ pixels. Based on the normalized frequency calculated by 1D FFT in Figure 3.12, the actual frequency of 4 μm spherical bead is the multiplication of length of the image and the normalized frequency, which give a value of 3 cycles. The length of

each image (A', B' in Figure 3.10, A', B' in Figure 3.7) and corresponding normalized frequency are shown in Table 3.9. It is clear to observe that the normalized frequency will increase as the size of the spherical bead becomes larger, and it has been also verified in [24] [25] .

	Length of input image (pixels)	Normalized frequency (1/pixel)
4 μm	319	3
6 μm	298	5
10 μm	249	8
15 μm	264	12

Table 3.9: Length of each saved image in Matlab and corresponding calculated normalized frequency after 1D FFT.

One of the applications of 1D FFT is that the actual size of pattern or particle with unknown size can be calculated based on the calculated frequency.

3.6. Experimental results for non-spherical polystyrene latex particles

In general, biological cells are non-spherical and inhomogeneous. Three basic categories based on their morphology can be identified for most mammalian cells: fibroblast-like cells, epithelial-like cells and lymphoblast-like cells. To learn the behavior of scattered light patterns for non-spherical dielectric objects, non-spherical polystyrene latex particles (Magsphere, USA) have been tested in this project. Microscopic image of two different size of non-spherical particles are shown in Figure 3.13.

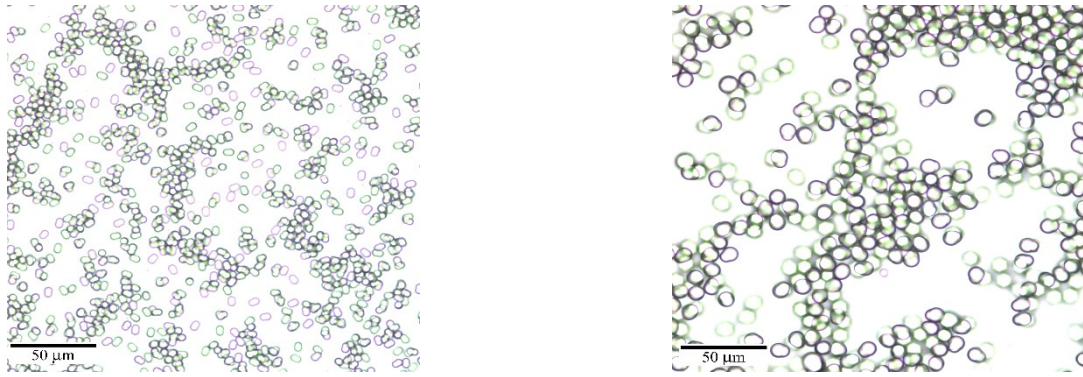


Figure 3.13: Microscopic images for non-spherical polystyrene latex particles. $4.0 \mu\text{m} \times 6.0 \mu\text{m}$ peanut-like (left), $9 \times 10.5 \mu\text{m}$ pear-like (right).

The aspect ratio is well defined according to manufactory. The two different sizes used in the experiment are $4.0 \times 6.0 \mu\text{m}$ and $9 \times 10.5 \mu\text{m}$. The light scattering results for both cases in two directions are shown in Figure 3.14 and Figure 3.15.

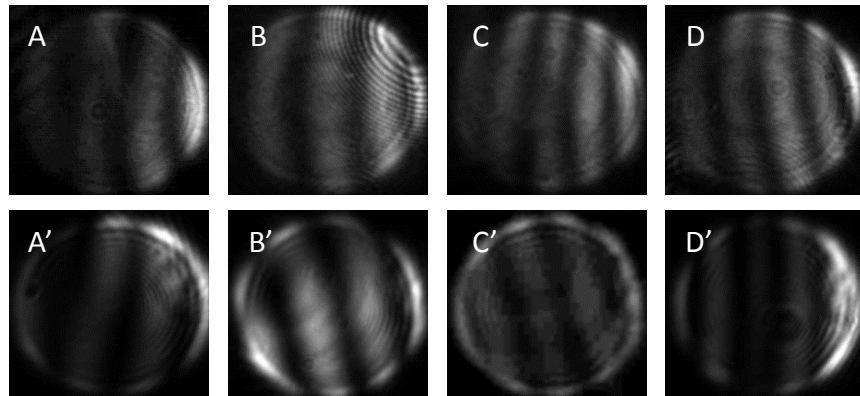


Figure 3.14: A-D are the light scattering patterns for $4.0 \mu\text{m} \times 6.0 \mu\text{m}$ non-spherical bead in the forward direction, while A'-D' are the light scattering patterns for $4.0 \mu\text{m} \times 6.0 \mu\text{m}$ non-spherical bead in the side direction.

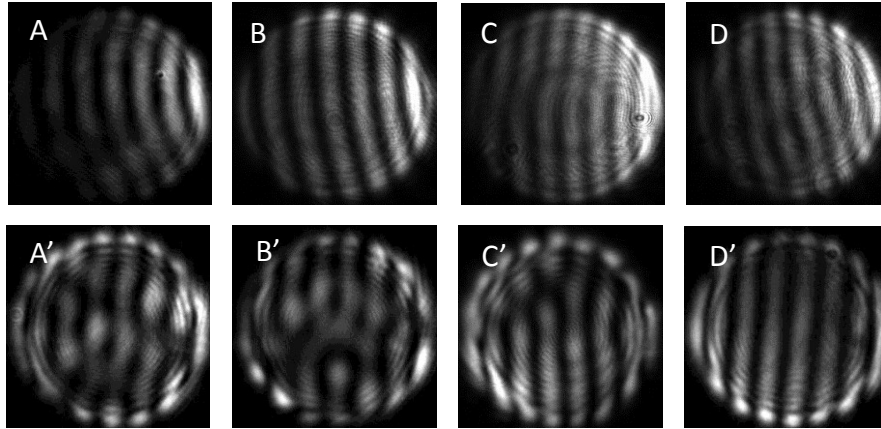


Figure 3.15: A-D are the light scattering patterns for the $9 \times 10.5 \mu\text{m}$ non-spherical bead in the forward direction, while A'-D' are the light scattering patterns for the $9 \times 10.5 \mu\text{m}$ non-spherical bead in the side direction.

According to the experimental light scattering patterns for two different size non-spherical beads, different number of fringes are obtained on both directions. Three to five number of fringes can be observed in forward and side directions for $4.0 \times 6.0 \mu\text{m}$ non-spherical bead, while seven to eight number of fringes can be observed on both directions for $9 \times 10.5 \mu\text{m}$ non-spherical bead. Based on the light scattering results for $4 \mu\text{m}$ and $6 \mu\text{m}$ spherical bead discussed in last section, which shows three number of fringes in the forward direction and four number of fringes in the side direction for $4 \mu\text{m}$ spherical bead and four number of fringes in the forward direction and five number of fringes in the side direction for $6 \mu\text{m}$ spherical bead, the $4.0 \times 6.0 \mu\text{m}$ non-spherical bead can be considered as a combination of $4 \mu\text{m}$ and $6 \mu\text{m}$ spherical bead. The number of fringes captured by the CCD camera depending on which aspect radius becomes dominant in the observation region. Likely, seven to eight number of fringes obtained for $9 \times 10.5 \mu\text{m}$ non-spherical bead on both directions can be considered as a combination as $9 \mu\text{m}$ and $10.5 \mu\text{m}$ spherical bead.

In summary, scattering pattern of non-spherical polystyrene latex bead varies in the number of fringes at different scattering angles. Number of fringes depends on the two-axis length of the non-spherical polystyrene latex.

4. Laser light scattering studies for biological cells and scattering pattern analysis

4.1. Introduction

Light scattering technique have been widely applied in many biological cells, such as human blood cells, undifferentiated embryonic cells and even cancer cells. In our label-free cytometry project, different types of biological cells have been studied in the past. Different methods such as Mie simulation [32] , finite-difference time-domain (FDTD) [38] have been developed for analyzing cell morphology and inner-structure. In this project, non-treated and staurosporine-treated SH-SY5Y neuroblastoma cell has been used. SH-SY5Y was first reported to be derived from SK-N-SH cell line, which was cloned from a bone marrow biopsy [51] , originating from a four-year-old female. SH-SY5Y neuroblastoma cells can be transiently transfected by Alpha-synuclein (α -syn), which is a soluble protein and treated as a pathological feature of sporadic and familial forms of Parkinson's disease (PD) [52] . Therefore, SH-SY5Y neuroblastoma cells is widely used in scientific research for disease and medical study.

In this project, two different wavelengths laser (red laser: 632.8 nm, green laser: 532 nm) were used to illuminate cells. Three different angle range (which are called as forward, side and backward direction respectively) of single cells have been detected. Experimental two-dimensional light scattering patterns in three directions with two different wavelengths haven been obtained. Pattern recognition and image analysis have been implemented to characterize and classify the experimental scattering patterns from both non-treated and staurosporine-treated SH-SY5Y neuroblastoma cells.

4.2. Sample preparation and experimental procedure

Both non-treated and staurosporine-treated SH-SY5Y neuroblastoma cells were prepared by Dr. Chunhua Dong and research technician Craig Garen from Dr. Michael Woodside's group (Department of Biochemistry, University of Alberta). They culture the cells with growth medium based on product sheet SH-SY5Y (ATCC®CRL-2266™). Sample from non-treated SH-SY5Y neuroblastoma cells defines as cells without extra process before fixing it, while sample from staurosporine-treated SH-SY5Y neuroblastoma cells means adding staurosporine into cultured cells before fixing it. Staurosporine is a type of toxic chemical medium to SH-SY5Y. More detailed information can be found in Appendix. As a result, two groups of SH-SY5Y cells are prepared for laser light scattering experiment.

The original sample with a high concentration reaching around 10^6 to 10^7 cells/ml. Dilution of sample is needed before injecting it to the sample holder. Same phosphate-buffered saline (PBS) is used for dilution. The concentration of diluted cell sample is usually around 3000 cells/ml. I just switch sample to cells and observe and record data like what I did to the light scattering experiment of homogenous bead.

4.3. Microscopic image of non-treated and staurosporine-treated SH-SY5Y neuroblastoma cells

Before performing the light scattering experiment of both groups of cells, microscopic images of both groups have been taken. Figure 4.1 shows the optical microscopic image of both group of cells respectively. Both images were taken by a 40× microscope objective (0.25, ZEISS, N-ACHROPLAN) from Department of Biological Sciences, with the help of Arlene Oatway.

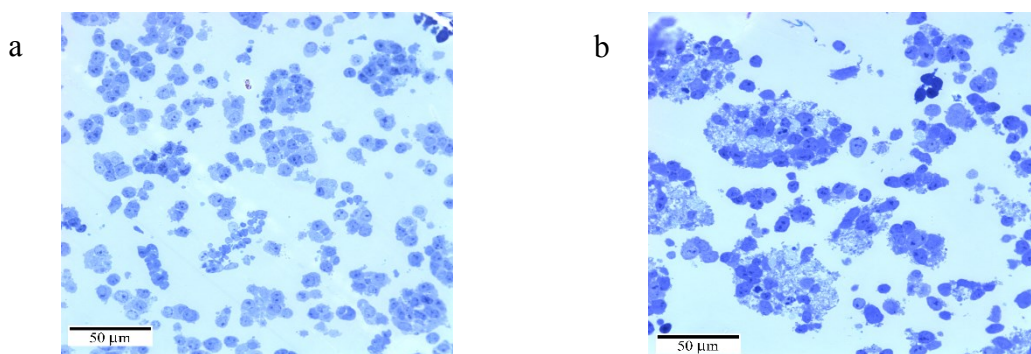


Figure 4.1: Microscopic image of non-treated SH-SY5Y neuroblastoma cells (a) and staurosporine-treated SH-SY5Y neuroblastoma cells (b).

Both sample were taken from sections which used for Transmission Electron Microscopy (TEM) (more detailed description will be given below) and blue dyes was dropped on sections for a better observation. Comparing (a) with (b) in Figure 4.1, non-treated SH-SY5Y neuroblastoma cells appear to be more homogenous than staurosporine-treated SH-SY5Y neuroblastoma cells.

To obtain higher resolution images of these cells, Scanning Electron Microscopy (SEM) and Transmission Electron Microscopy (TEM) has been used and their images are shown in Figure 4.2. More SEM and TEM images can be found in Appendix A.3.

Before taking TEM/SEM images, sample preparation is required. Same sample preparation procedure is used for both TEM/SEM imaging. Centrifuging, chemical removal, dehydrating as well as ethanol wash are the common sample preparing steps for SEM/TEM imaging. Metal coating is required for SEM imaging while BEEM capsules preparation and sectioning are required for TEM imaging. All the sample preparation procedure was undertaken with the help of Arlene Oatway.

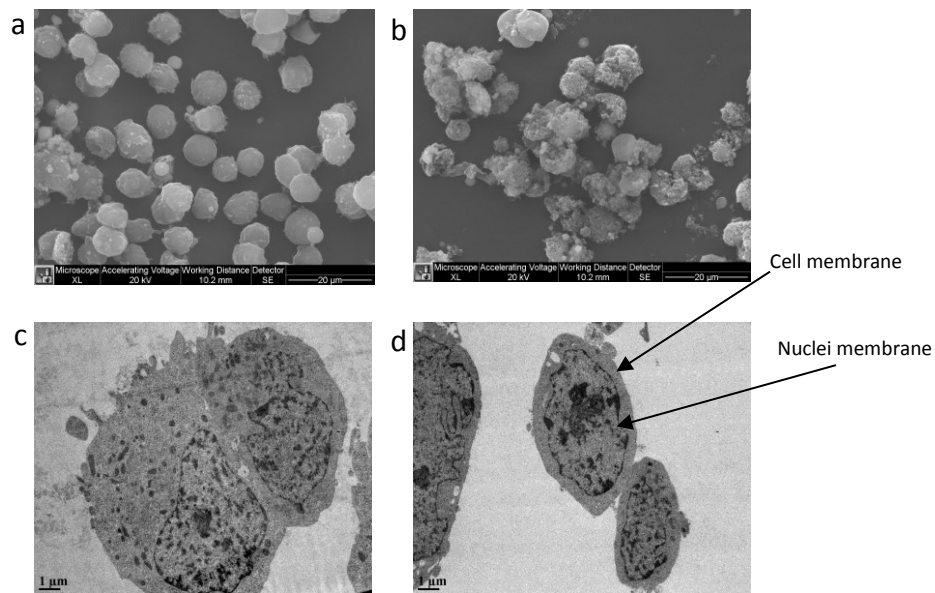


Figure 4.2: SEM imaging of non-treated SH-SY5Y neuroblastoma cells (a) and staurosporine-treated SH-SY5Y neuroblastoma cells (b); TEM imaging of non-treated SH-SY5Y neuroblastoma cells (c) and staurosporine-treated SH-SY5Y neuroblastoma cells (d).

According to SEM imaging in Figure 4.2 (a), non-treated SH-SY5Y neuroblastoma cells have an average diameter of 6 μm . Majority of the cells are spherical-like shape although some of the non-treated cells have different size of bubbles on the surface ranging from hundreds of nanometers to a few micrometers (average diameter size can be seen as 1 μm), which resulting from cell apoptosis [53] [54] [55], which cell is undergoing a process that cell kills itself and leads to cell death at the end. Cell apoptosis happens at any stage when growing cells, which results in size difference.

According to [53] [55] , membrane of apoptotic SH-SY5Y cells is blebbing and chromatin is accumulated beneath nuclear membrane while nuclear becomes condensed. Besides, mitochondria are swollen and formed many vacuoles while other organelle structure is unclear or disappear. Membrane disappears, and cell is not in shape any more from staurosporine-treated SH-SY5Y as shown in Figure 4.2 (b). Staurosporine-treated procedure is different from apoptosis which cells dies because of external factors that can be called necrosis. Furthermore, with a section image of both type of cells from TEM imaging shown in Figure 4.2 (c) and (d), the former has more mitochondria comparing with the latter. Besides, other organelle disappears, and the membrane of nuclei becomes denser from staurosporine-treated SH-SY5Y neuroblastoma cells.

4.4. Experimental scattering pattern of non-treated and staurosporine-treated SH-SY5Y neuroblastoma cells

According to the microscopic images from both group of cells, the morphology of non-treated SH-SY5Y is spherical-like and more homogeneous comparing with the morphology of staurosporine-treated SH-SY5Y, which cell shrinks and changes its shape. The difference between two group of cells is quite clear and easily to distinguish from one to the other based on images.

Figure 4.3 shows experimental light scattering patterns obtained from staurosporine-treated SH-SY5Y with red laser. Z direction represents the laser direction. The patterns from forward, side and backward direction are shown in the first, second and third rows respectively. Non-treated SH-SY5Y patterns with red laser are shown in Figure 4.4. Treated and non-treated SH-SY5Y patterns with green laser are shown in Figure 4.5 and Figure 4.6 respectively.

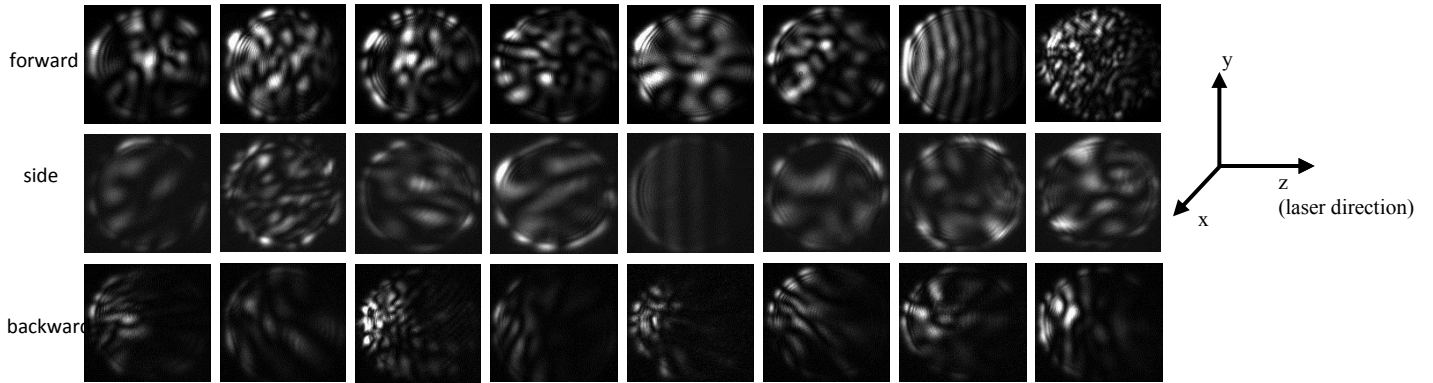


Figure 4.3: Experimental light scattering pattern in three directions (forward, side and backward) with red laser illumination in staurosporine-treated SH-SY5Y.

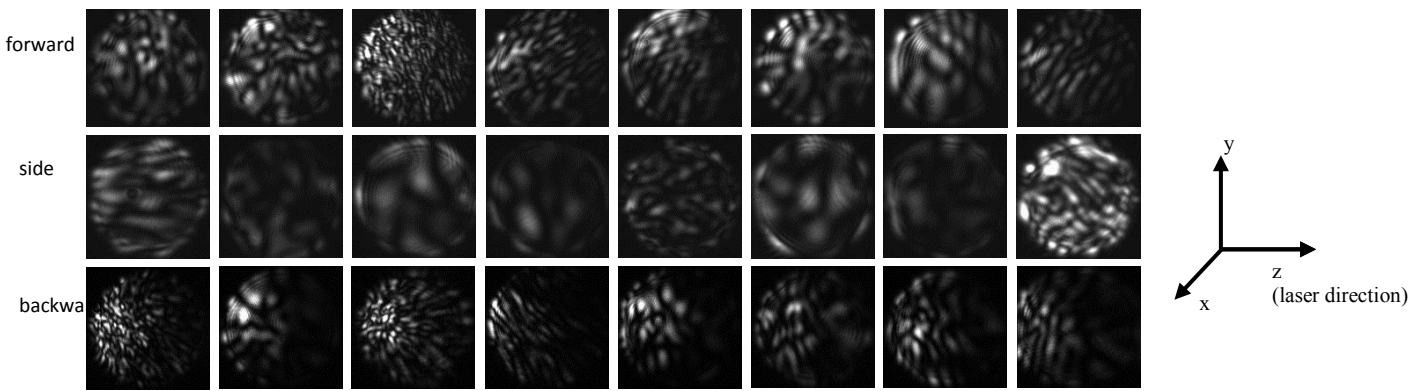


Figure 4.4: Experimental light scattering pattern in three directions (forward, side and backward) with red laser illumination in non-treated SH-SY5Y.

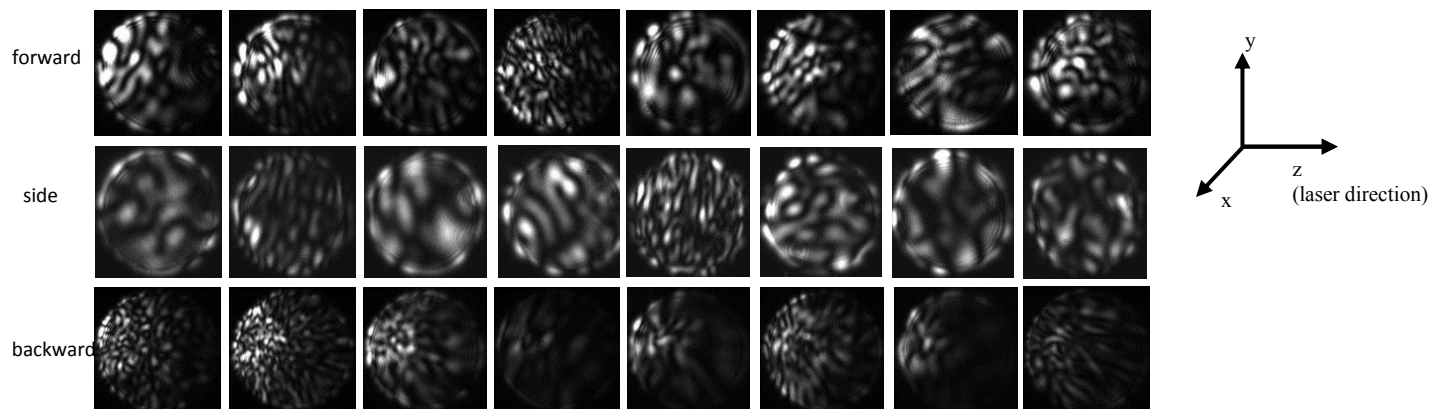


Figure 4.5: Experimental light scattering pattern in three directions (forward, side and backward) with green laser illumination in staurosporine-treated SH-SY5Y.

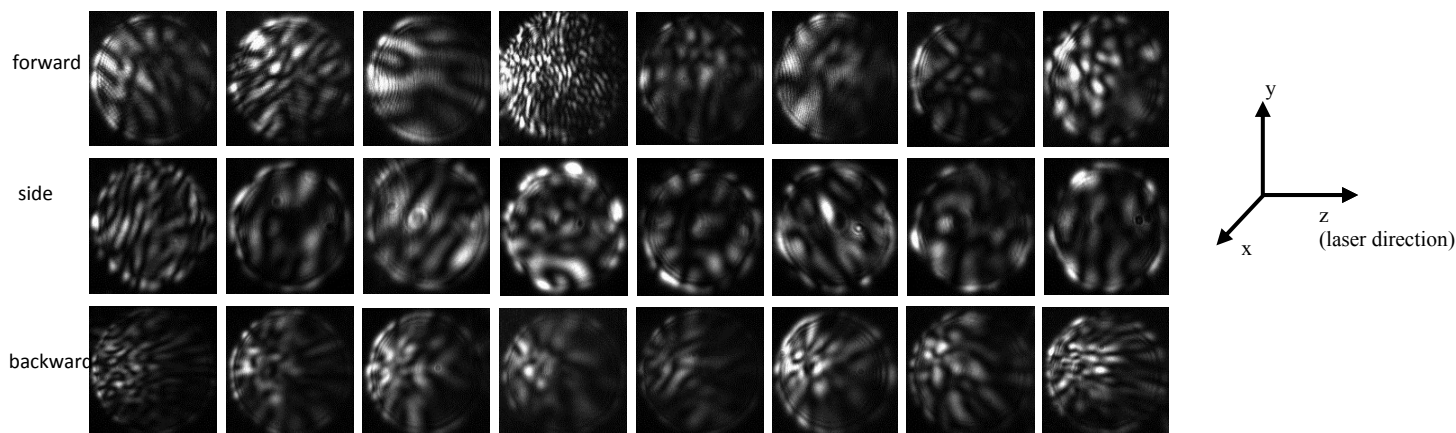


Figure 4.6: Experimental light scattering pattern in three directions (forward, side and backward) with green laser illumination in non-treated SH-SY5Y.

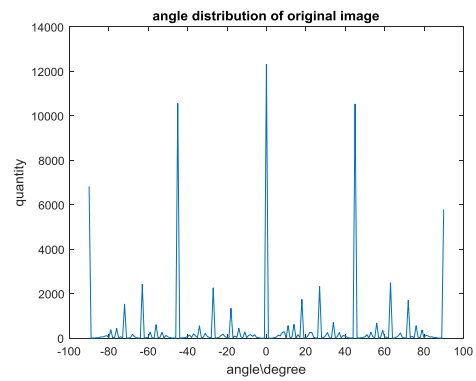
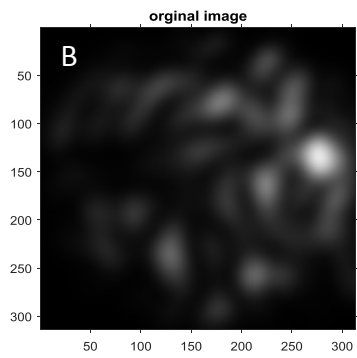
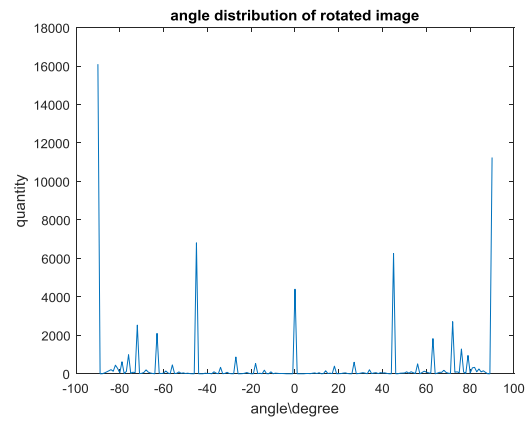
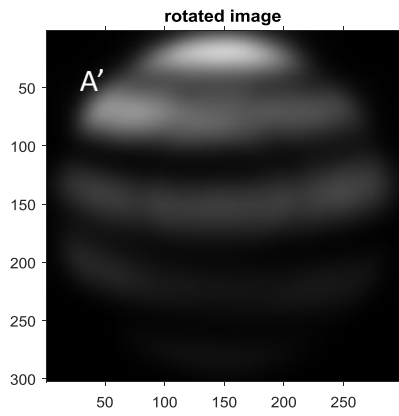
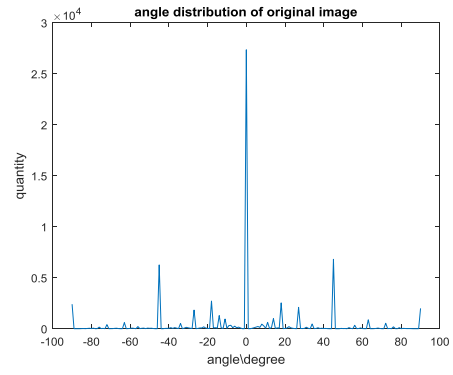
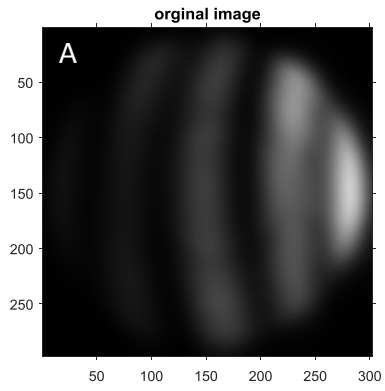
In general, light scattering patterns are brighter with green laser illumination, one reason is because the output power of green laser is higher than red laser (measured output power from green laser directly is 340 mW, and measured output power after a neutral density filter OD2 is 1.15mW, while measured output power from red laser is 0.9 mW). The other reason could be the light scattering cross-section is larger for green illumination than red illumination and the CCD camera is more sensitive for green light than red light. Fringe and non-fringe patterns can be observed in non-treated and staurosporine-treated SH-SY5Y with two different wavelengths in three directions which resulting in a technique separating non-fringe patterns from fringe patterns. Contents described in section 4.4 are approaches to distinguishing and characterizing light scattering patterns.

4.5. Pattern classification of scattering data

4.5.1. Angle distribution method — a method distinguishes non-fringe from fringe pattern

The first step to process the light scattering patterns is classifying them into two groups: fringe and non-fringe pattern. Since the fact that fringe pattern reflects a particle with a spherical shape and the number of fringe reflects the size of the particle based on Mie theory, characterizations of cells with fringe pattern can be analyzed. On the other hand, non-fringe pattern can be analyzed by finding local maximum, which will be discussed in 4.4.2.

From visual inspection, fringe patterns are long strips across the whole pattern which are easy to be distinguished from non-fringe patterns. Angle distribution method is an effective way to differentiate fringe pattern from non-fringe pattern. In this method, the gradients in x-direction (dX) and y-direction (dY) for each experimental scattering pattern has been calculated and the slope ($\frac{dY}{dX}$) can be further calculated. The number of each tilt angle falling between -90 degrees and 90 degrees for each scattering pattern has been counted. The angle distribution of each pattern can be obtained. At the same time, each original scattering pattern is counterclockwise rotated by 90 degrees and after applying the same method, the angle distribution of rotated pattern can be obtained. The angle distribution of original image and rotated image are illustrated in Figure 4.7.



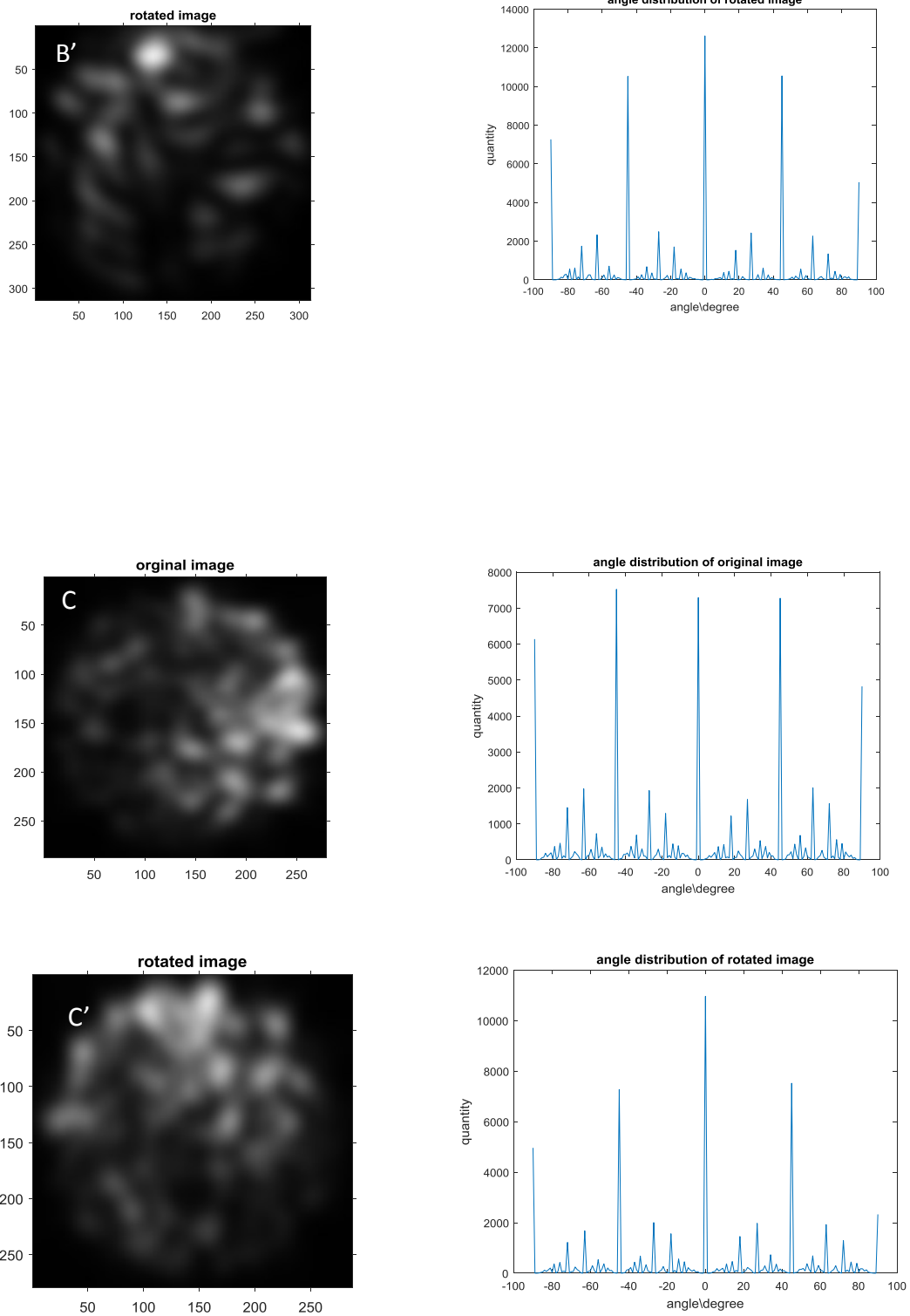


Figure 4.7: Angle distribution of three different types of original and rotated pattern. A and A' are typical fringe pattern and fringe pattern after rotation. B , B' and C , C' are two typical non-fringe patterns and their patterns after rotation. Right-hand side are the angle distribution spectrums to the corresponding left-hand side scattering pattern.

In Figure 4.7, most angles for each pattern are located at five angles: -90 degrees, -45 degrees, 0 degrees, 45 degrees and 90 degrees. The dominant peak of vertical fringe pattern is located at 0 degrees after rotation the dominant peaks are at 90 and -90 degrees. For mostly homogenous pattern, the dominant peak would remain at those five dominant peaks (-90 degrees, -45 degrees, 0 degrees, 45 degrees and 90 degrees). As a result, summation of absolute values of the difference of angle quantities between original pattern and rotated pattern at each angle is more significant for fringe pattern than non-fringe pattern. For example, the difference between A and A' is 77080, which is the summation of the whole angle range difference of original and rotated pattern, while the difference between B and B', C and C' is 8906 and 13162, respectively, which is much smaller than the difference between A and A'.

In this thesis, quantities of experimental light scattering pattern collected from all three directions (forward, side and backward) in both non-treated and staurosporine-treated SH-SY5Y groups with two different laser illuminations have been shown in Table 4.1. Each data has been calculated and obtained a difference. The absolute difference in absolute value between original and rotated pattern collected in the forward direction under red laser illumination can be observed as bar graph shown in Figure 4.8. A threshold is chosen by examining the scattering patterns between 35000 and 50000 which was suspected to be the region where the fringe and non-fringe patterns were overlapping. After inspecting scattering patterns in these region, a value of 47128 was chosen to be the threshold value to separate between fringe and non-fringe patterns.

Wavelength	Direction	Staurosporine- treated SH-SY5Y	Non-treated SH-SY5Y
Red laser	Forward (Nov. 28, 2017)	74	59
	Side (Nov. 28, 2017)	45	21
	Backward (Dec. 6, 2017)	42	29
Green laser	Forward (Dec. 1, 2017)	62	67
	Side (Dec. 1, 2017)	50	53
	Backward (Dec. 6, 2017)	30	52

Table 4.1: Quantities of collected experimental scattering pattern from all three directions in two cell sample groups with two different wavelengths.

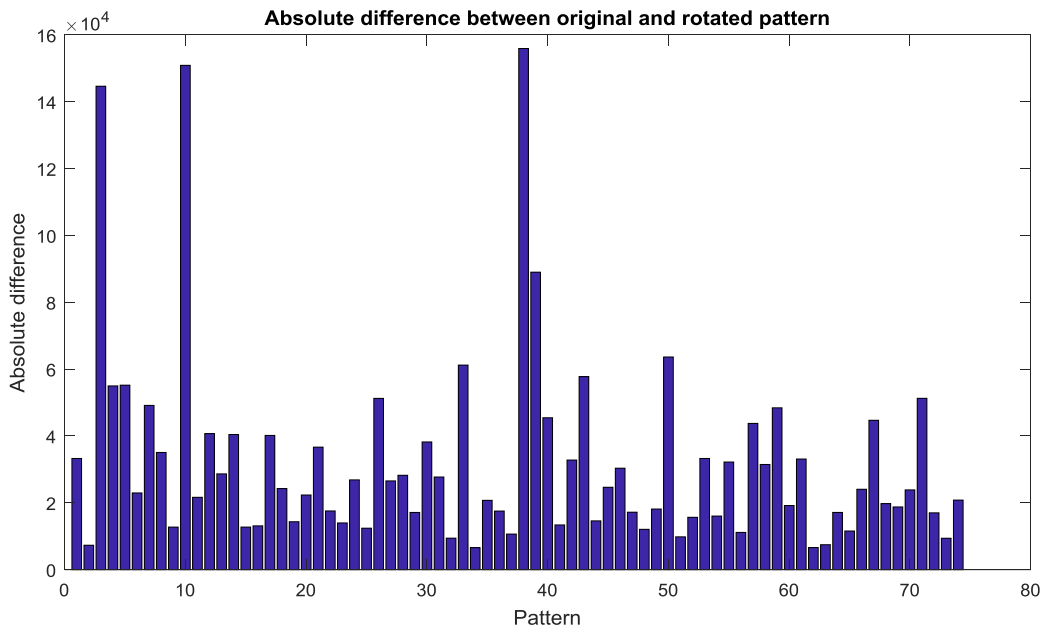


Figure 4.8: Absolute difference between original and rotated pattern collected in the forward direction with red laser illumination.

Based on angle distribution method, percentage of fringe and non-fringe pattern can be calculated, and the percentage bar graph for each group are illustrated in Figure 4.9. Four graphs displayed are percentage comparison of fringe and non-fringe pattern with two different wavelengths in three directions for both groups of cells. To simplify, staurosporine-treated SH-SY5Y is so called “dead” group, while non-treated SH-SY5Y is so called “live” cell group. I will use those abbreviation for the following figure illustration. The dates noted inside the table are the collecting dates for each group of data. Moreover, those data were collected from cell sample received at the beginning of year 2017 for further analysis from section 4.5.1 to in Figure 4.17 section 4.5.2.

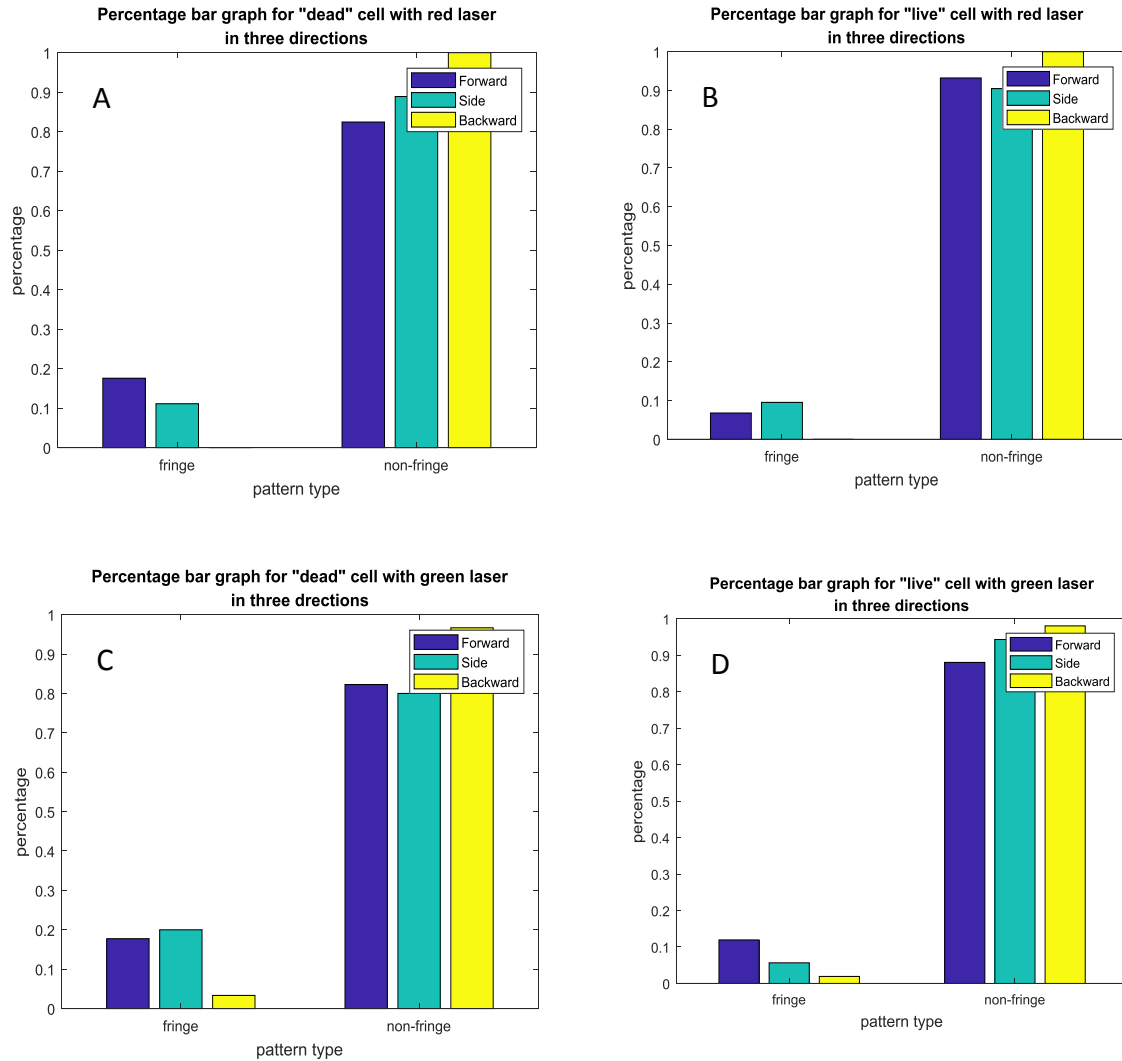


Figure 4.9: A is the percentage comparison of “dead” cell group with red laser in all three directions; B is the percentage comparison of “live” cell group with red laser in all three directions; C is the percentage of “dead” cell with green laser in all three directions; D is the percentage comparison of “live” cell with green laser in all three directions.

According to Figure 4.9, it is clear to see that fringe pattern only takes very small portion in each situation. Particularly, backward scattering only captures non-fringe pattern with red laser. In addition, non-fringe pattern always becomes the dominant pattern in backward direction comparing with other two directions scattering.

Angle distribution is used to distinguish fringe pattern from non-fringe pattern. Small portion of fringe pattern among all cases indicates that the shape of both non-treated and staurosporine-

treated SH-SY5Y mostly are non-spherical and heterogeneous. Next, a method called finding local maximum is used to characterize and analyze the non-fringe pattern

4.5.2. Finding local maximum — a method of analyzing non-fringe pattern

Non-fringe pattern is characterized by many bright spots which in most cases are isolated from other neighbor spots in the scattering pattern. Thus, a finding local maximum method is used to characterize the speckle pattern in non-treated and staurosporine-treated SH-SY5Y with two different wavelengths in three directions.

The scattering pattern experimentally obtained was firstly smoothed by a Gaussian smoothing filter, which behaves as a low pass filter. High frequency which generated by optical system is considered as systematic noise and is unable to avoid during the experiment. The three-dimensional (3D) mesh plot of original image and the Gaussian smoothed image are shown in Figure 4.10. Each peak is associated with a 3D Gaussian distribution. Gaussian smoothing is required to get rid of the high frequency fluctuations to avoid getting unwanted local maxima which would contaminate the result.

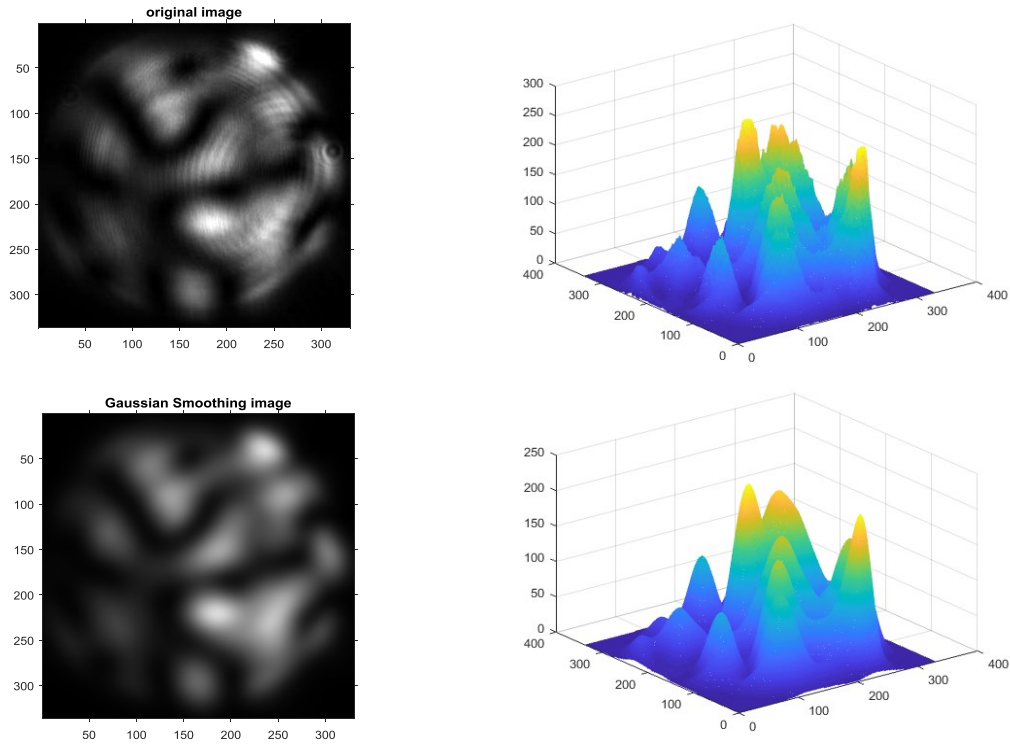


Figure 4.10: Original image and Gaussian smoothed image in grey scale and the corresponding 3D mesh plot.

After smoothing the image, local maximum can be obtained by Matlab function “imregionalmax”, which is a Matlab build-in function returns the binary image with identified regional maxima in original image, and pixels set to 1 identify regional maxima while other pixels are set to 0. It uses 8-connected neighborhoods for 2-D images for finding local maxima. The number of local maxima decides the number of spots in the pattern. The location and pixel intensity of each local maximum has been recorded and saved by Matlab function “bwlablel” and “find”. Afterwards, taking each local maximum as s starting point, keep scanning into four different directions (leftward, rightwards, upwards and downwards) until meeting the half maximum point. The scanning length in horizontal and vertical directions are considered as two diagonals, and the scanning area can be calculated and is approximated as the full width at half maximum (FWHM) of each local Gaussian distribution. Scanning area is colored with blue in Figure 4.11 (left side), which is also called cross area of local Gaussian distribution. The scanning process is illustrated as Figure 4.11(right side),

which shows in detail how the code calculates each local cross area, and the full code is also attached in the Appendix. After obtaining all cross area for each the pattern, average cross area of each non-fringe pattern can be calculated by dividing number of spots in this pattern.

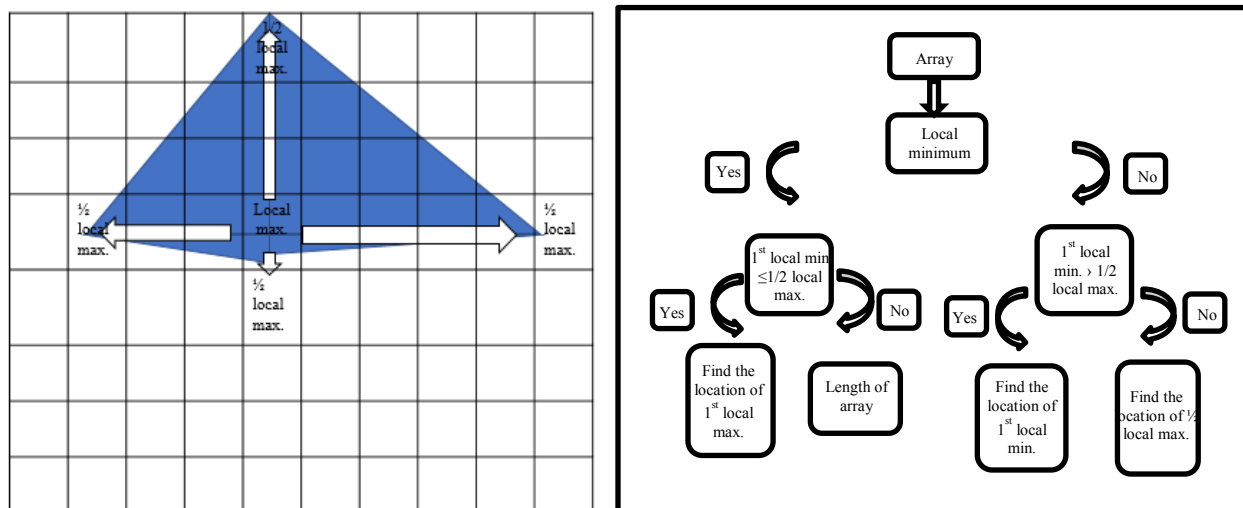


Figure 4.11: Full width at half maximum (FWHM) approximation of each local peak. Cross area is approximated based on a diamond area (left side). Flow chart of scanning for half maximum in four directions (right side).

In order to have a better understanding of how the local cross area calculates, Figure 4.12 demonstrates all the calculated local cross area (red diamond) and each local maximum (green circle). Each local maximum and its corresponding calculated local cross area has been labelled with red and green, respectively. A is one scattering pattern from staurosporine-treated SH-SY5Y cell group with red laser illumination and observed in the forward direction. B is one scattering pattern from staurosporine-treated SH-SY5Y cell group with red laser group illumination in the side direction. C is one scattering pattern from staurosporine-treated SH-SY5Y cell group with red laser illumination and captured in the backward direction.

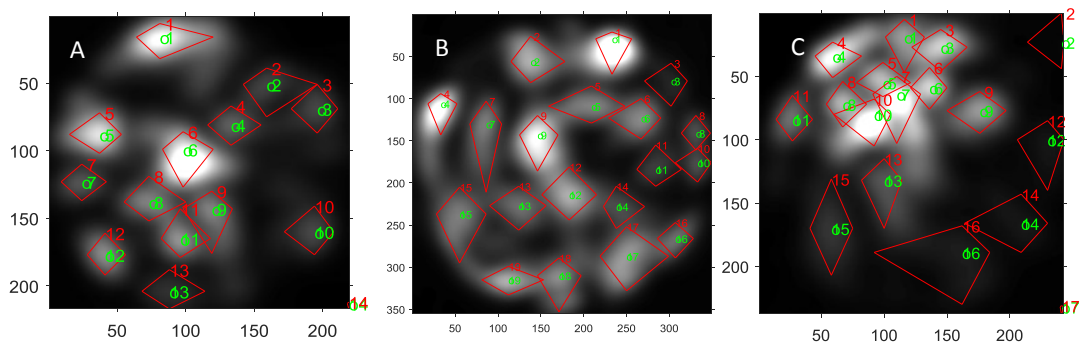


Figure 4.12: Calculated local cross area (red diamond) with corresponding local maximum (green circle).

All the non-fringe patterns obtained from experiment are analyzed by the finding local maximum method. The non-fringe pattern analysis of both group of cells are shown from Figure 4.13 to Figure 4.15. The x-axis shows the number of spots for each pattern, and y-axis represents the average cross area in pixels for each pattern. Each circle represents one scattering pattern. The blue color represents staurosporine-treated SH-SY5Y (illustrated as “dead”) while red color represents non-treated SH-SY5Y (“live”).

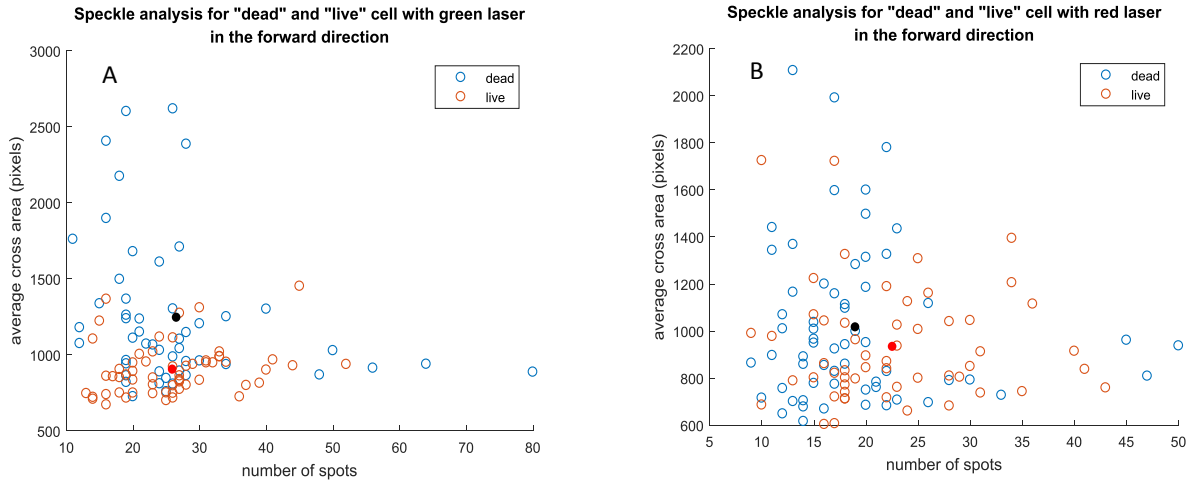


Figure 4.13: Speckle analysis in the forward direction based on finding local maximum method. (A) is the comparison between two groups with green laser illumination. (B) is the comparison between two groups with red laser illumination.

According to Figure 4.13 (A), the mean and standard deviation of “dead” group is $(27, 1244) \pm (13, 481.5)$, while the mean and standard deviation of “live” group is $(26, 902.5) \pm (9, 169.6)$. In Figure 4.13 (B), the mean and standard deviation of “dead” group is $(19, 1016) \pm (8, 333.7)$, while the mean and the standard deviation of “live” group is $(23, 932.9) \pm (8, 242.6)$. Based on finding local maximum method, average cross area from “dead” group is larger than average cross area from “live” group in the forward direction with green laser illumination. However, scattering patterns are unable to distinguish one with each other with a longer wavelength illumination in the forward direction.

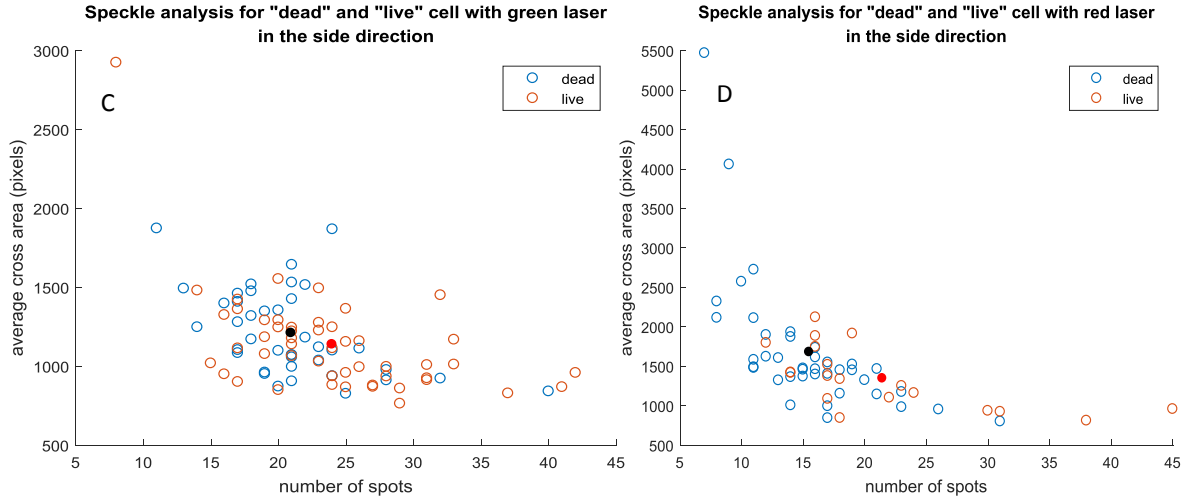


Figure 4.14: Speckle analysis in the side direction based on finding local maximum method. (A) is the comparison between two groups with green laser illumination. (B) is the comparison between two groups with red laser illumination.

According to Figure 4.14 (C), the mean and standard deviation of “dead” group is $(21, 1211) \pm (5, 271.5)$, while the mean and standard deviation of “live” group is $(24, 1139) \pm (7, 326.8)$. In Figure 4.14 (D), the mean and standard deviation of “dead” group is $(15, 1681) \pm (5, 848.8)$, while the mean and the standard deviation of “live” group is $(21, 1348) \pm (9, 396)$. Based on the finding local maximum method, average cross area does not show large difference between two groups in the side direction with two different wavelengths illumination. However, number of spots appear to be more for “live” group than “dead” group in the side direction with either red laser or green laser illumination.

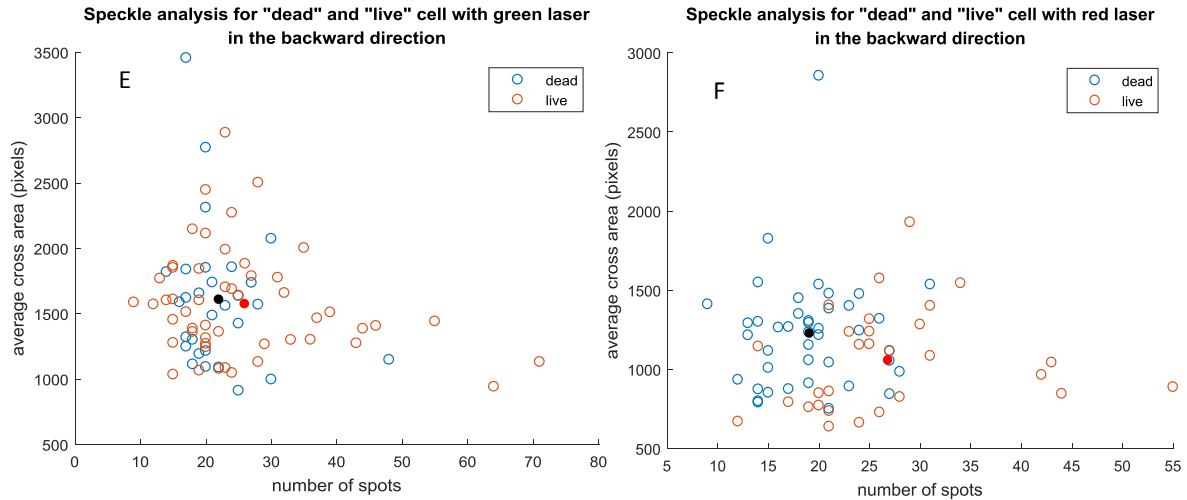


Figure 4.15: Speckle analysis in the backward direction based on finding local maximum method. (E) is the comparison between two groups with green laser illumination. (F) is the comparison between two groups with red laser illumination.

According to Figure 4.15 (E), the mean and standard deviation of “dead” group is $(22, 1607) \pm (6, 543.5)$, while the mean and standard deviation of “live” group is $(26, 1573) \pm (13, 409)$. In Figure 4.15 (F), the mean and standard deviation of “dead” group is $(19, 1226) \pm (5, 358.7)$, while the mean and the standard deviation of “live” group is $(27, 1056) \pm (9, 320.1)$. Based on finding local maximum method, no large difference shown for the scattering patterns from the two groups with green wavelength illumination in the backward direction. However, much larger differences between two groups are observed with red laser illumination. Larger average cross area but less number of spots can be observed in “dead” group, while smaller average cross area but more number of spots can be observed in the “live” group.

Effect of green versus red illumination for “dead” and “live” groups are summarized in Figure 4.16 and Figure 4.17 respectively.

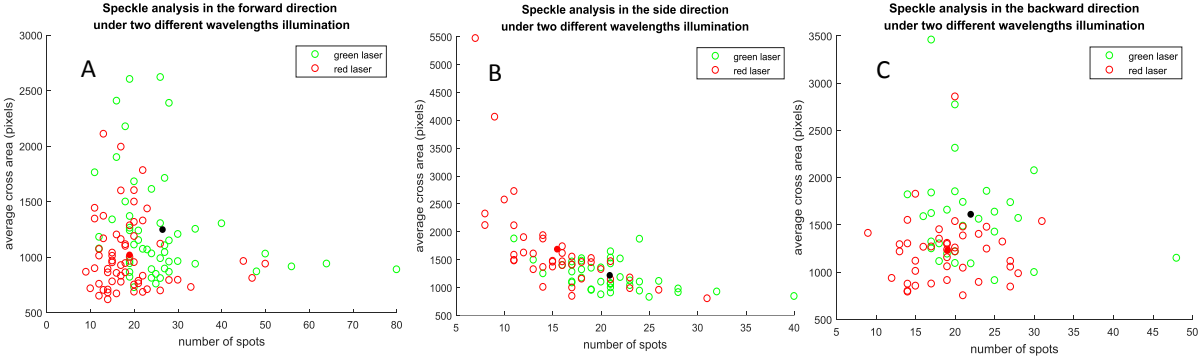


Figure 4.16: Speckle analysis based on finding local maximum method for “dead” group. (A) is the comparison between two different illumination sources in the forward direction. (B) is the comparison between two different illumination sources in the side direction. (C) is the comparison between two different illumination sources in the backward direction.

According to Figure 4.16 (A), the mean and standard deviation from green laser source in the forward direction is $(27, 1244) \pm (13, 481.5)$, while the mean and standard deviation from red laser source in the forward direction is $(19, 1016) \pm (8, 333.7)$. In Figure 4.16 (B), the mean and standard deviation from green laser source in the side direction is $(21, 1211) \pm (5, 271.5)$, while the mean and the standard deviation from red laser source in the side direction is $(15, 1681) \pm (5, 848.8)$. In Figure 4.16 (C), the mean and standard deviation from green laser source in the backward direction is $(23, 1607) \pm (6, 543.5)$, while the mean and the standard deviation from red laser source in the backward direction is $(19, 1226) \pm (5, 358.7)$. Based on finding local maximum method, more number of spots can be observed under green laser illumination in “dead” group than illuminated by red laser source. Average cross area is smaller in the forward and backward direction but slightly larger in the side direction with red laser source compared with green laser illumination.

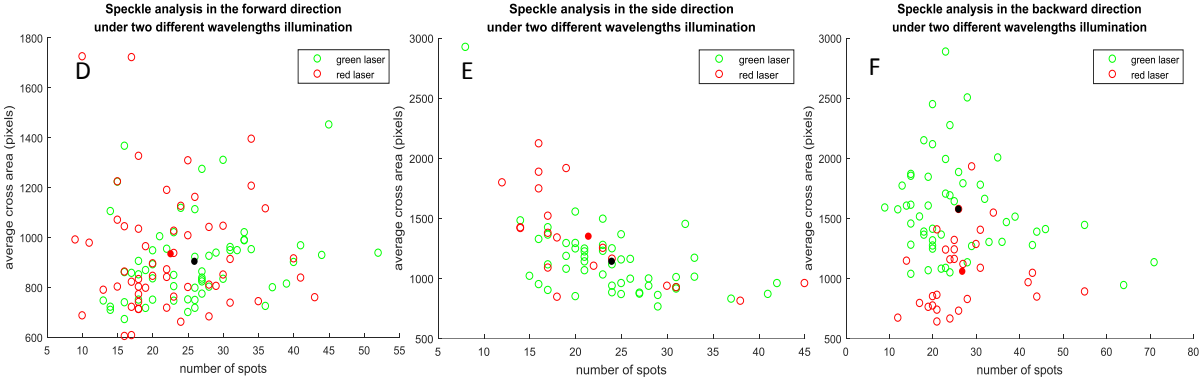


Figure 4.17: Speckle analysis based on finding local maximum method for “live” group. (D) is the comparison between two different illumination sources in the forward direction. (E) is the comparison between two different illumination sources in the side direction. (F) is the comparison between two different illumination sources in the backward direction.

According to Figure 4.17 (D), the mean and standard deviation from green laser source in the forward direction is $(26, 902.5) \pm (8, 169.6)$, while the mean and standard deviation from red laser source in the forward direction is $(22, 932.9) \pm (8, 242.6)$. In Figure 4.17 (E), the mean and standard deviation from green laser source in the side direction is $(24, 1139) \pm (7, 326.8)$, while the mean and the standard deviation from red laser source in the side direction is $(21, 1348) \pm (9, 396)$. In Figure 4.17 (F), the mean and standard deviation from green laser source in the backward direction is $(26, 1573) \pm (13, 409.1)$, while the mean and the standard deviation from red laser source in the backward direction is $(27, 1056) \pm (9, 320.1)$. Based on finding local maximum method, more number of spots can be observed in “live” cell group in both forward and side directions under green laser illumination compared with the red laser source, which is consistent with calculated results from “dead” group. Average cross area is larger under green laser illumination in the backward direction than with red laser source, while is smaller with green laser source in the side direction than red laser illumination. Same phenomenon can be observed from “dead” group.

Speckle analysis of the same group in the same direction with same laser source but observed at different times has also been conducted and results are shown in Figure 4.18 and Figure 4.19. Data 1 represents the scattering pattern obtained on May. 26, 2017, and data 2 represents the scattering pattern collected on Nov. 28, 2017. All data were obtained with red laser illumination.

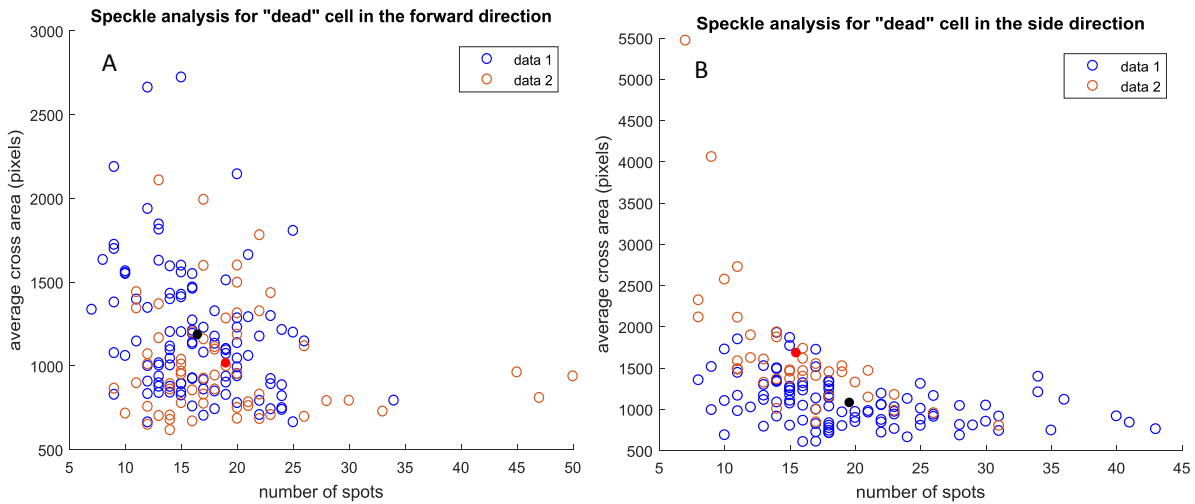


Figure 4.18: Speckle analysis based on finding local maximum method for “dead” cell group. (A) is the comparison between two different collecting times in the forward direction. (B) is the comparison between two different collecting times in the side direction.

According to Figure 4.18 (A), the mean and standard deviation for data collected on May. 26, 2017 is $(16, 1185) \pm (5, 393.3)$, while the mean and the standard deviation for data obtained on Nov. 28, 2017 is $(19, 1016) \pm (8, 333.7)$. In Figure 4.19 (B), the mean and standard deviation for data collected on May. 26, 2017 is $(20, 1077) \pm (7, 294.7)$, while the mean and standard deviation for data obtained on Nov. 28, 2017 is $(15, 1681) \pm (5, 848.8)$. Based on finding local maximum method, difference occurs in the side direction from same “dead” group cell that earlier obtained scattering pattern has more number of spots, but smaller average cross area compared with data collected later.

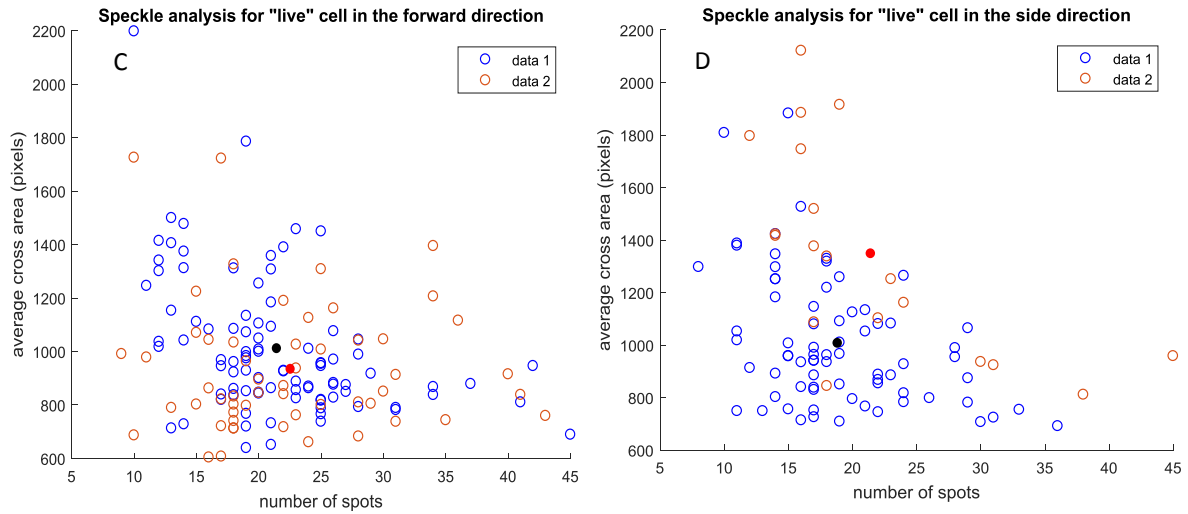


Figure 4.19: Speckle analysis based on finding local maximum method for “live” cell group. (C) is the comparison between two different collecting times in the forward direction. (D) is the comparison between two different collecting times in the side direction.

According to Figure 4.19 (C), the mean and standard deviation for data collected on May. 26, 2017 is $(21, 1010) \pm (7, 258.2)$, while the mean and the standard deviation for data obtained on Nov. 28, 2017 is $(23, 932.9) \pm (8, 242.6)$. In Figure 4.19 (D), the mean and standard deviation for data collected on May. 26, 2017 is $(19, 1007) \pm (6, 249.5)$, while the mean and standard deviation for data obtained on Nov. 28, 2017 is $(21, 1348) \pm (9, 396)$. Based on finding local maximum method, difference also occurs in the side direction that average cross area is smaller from data obtained on May. 26, 2017 than data collected on later time.

In summary, based on finding local maximum method, by analyzing speckle pattern obtained from experiment, larger average cross area but less number of spots can be observed from “dead” cell group in all three directions compared with data from “live” cell group. More number of spots can be obtained with green illumination than red illumination in all three directions from same cell groups. Scattering patterns have been observed to change slightly at different collecting times in the side direction while not much difference observed in the forward direction. The summary table

of absolute difference between mean value of treated and non-treated groups is shown in Table 4.2.

	Green laser			Red laser		
Direction	Forward	Side	Backward	Forward	Side	Backward
# of spots difference	1	3	4	4	6	8
Ave. cross area difference	341.5	72	34	83.1	333	170

Table 4.2: Summary of absolute difference in mean value between treated and non-treated cells

4.6. Some explanations for fringe and non-fringe pattern based on FDTD modelling

The effects of nucleus, mitochondria and cytoplasm on two-dimensional scattered light patterns from a single cell on both forward and side directions have already been investigated by Hesam [6] based on FDTD simulations. The numerical results indicate solo nucleus, solo cytoplasm and the combination of nucleus and cytoplasm generate fringe pattern in the forward direction. In addition, various ratio of nucleus and cytoplasm size will generate different number of fringes on two-dimensional scattered light pattern. The simulated results are illustrated in Figure 4.20. The modelled nucleus has a radius of $5\ \mu\text{m}$, and both nucleus and cytoplasm are considered to be spherical. The refractive index of nucleus and cytoplasm are 1.39 and 1.35 respectively.

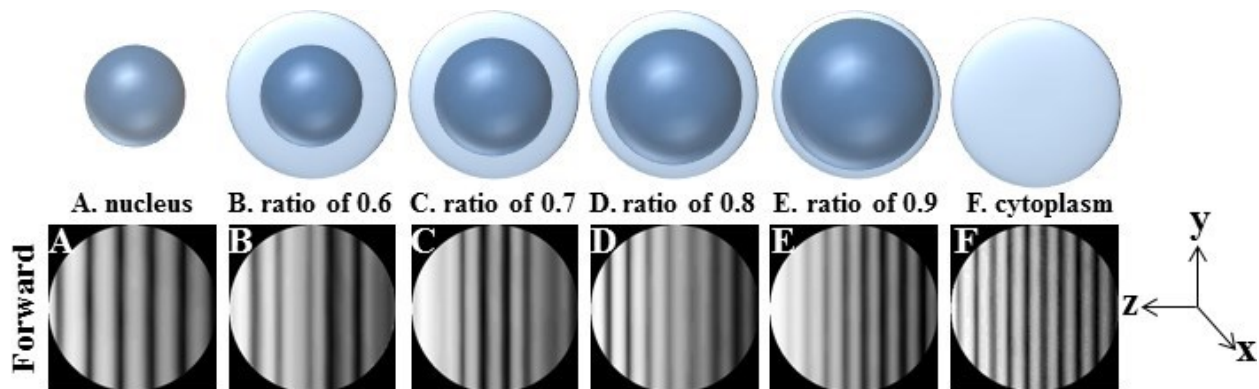


Figure 4.20: Simulated forward 2D scattered light patterns with various size ratios of nucleus and cytoplasm.

The side 2D scattered light patterns vary on with each other when the mitochondria distribution changes while the forward scattered light patterns do not have much changes. Furthermore, speckle pattern occurs on the side scattered light patterns. Figure 4.21 shows the simulated 2D scattered light patterns with various mitochondria distribution. The model is assumed that the nucleus has a radius of $2\ \mu\text{m}$ with refractive index of 1.39, the cytoplasm has a radius of $3.3\ \mu\text{m}$ with refractive index of 1.35, and eighty mitochondria with $0.25\ \mu\text{m}$ radius and a refractive index of 1.42. Good

agreement has been achieved between calculated scattered light patterns and the experimental scattered light patterns of UCB HSCs.

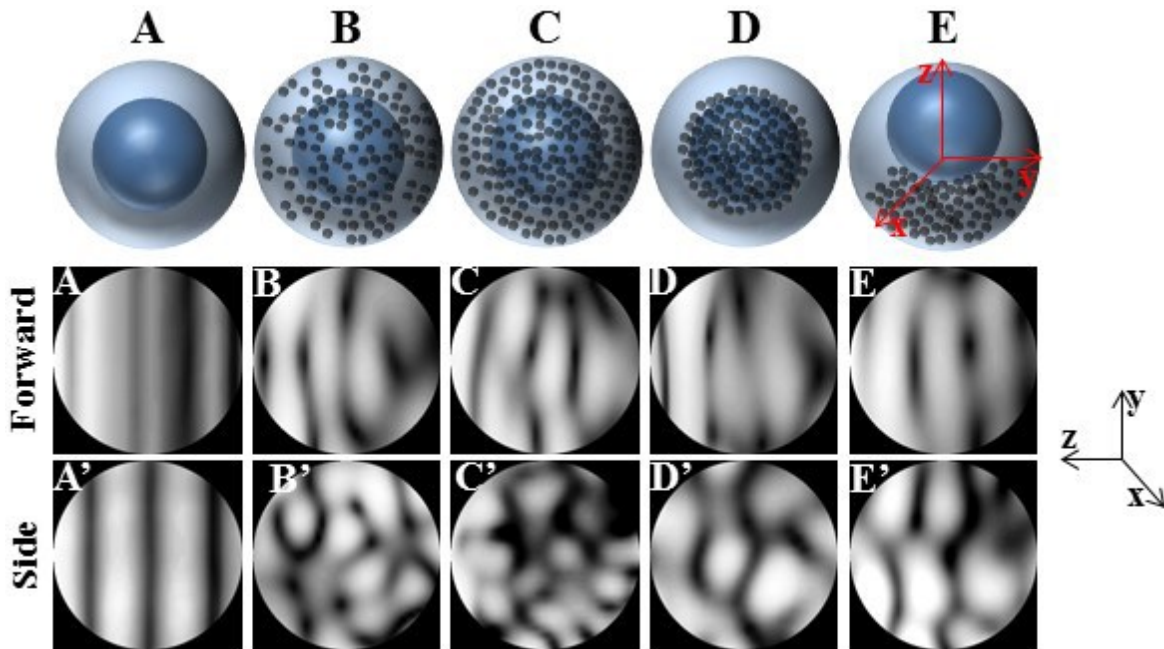


Figure 4.21: The simulated 2D scattered light patterns with different mitochondria distributions.

Based on the simulated results from Hesam, mitochondria distribution creates the bright spots on the scattered light pattern which is called “speckle” pattern. However, based on the SEM imaging displays in Figure 4.2, bubbles on the surface could also scatter light and make contributions to the scattering patterns, which could explain the speckle pattern obtained from both forward and side directions from Figure 4.3 to Figure 4.6.

4.7. Other findings of label-free cytometer light scattering technique

In our non-invasive label-free cytometer experiment, light scattering pattern of one single cell can be captured simultaneously in both forward and side directions. Figure 4.22 shows light scattering patterns captured by forward and side CCD camera at the same time for four non-treated SH-SY5Y cells and four staurosporine-treated SH-SY5Y cells.

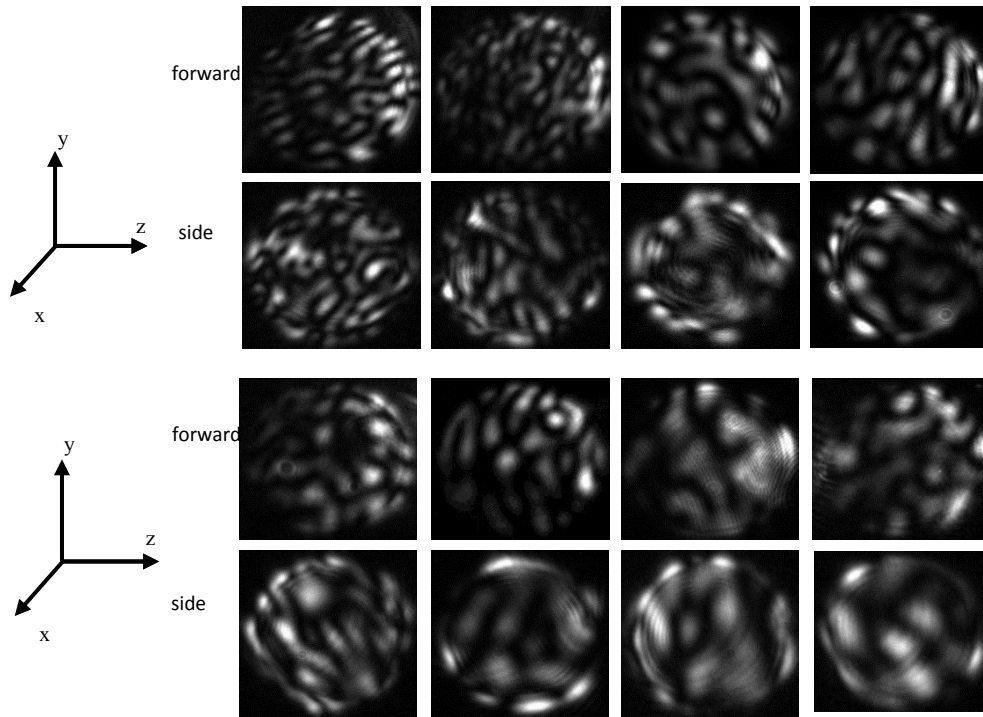


Figure 4.22: Upper eight scattering patterns are captured from non-treated SH-SY5Y cells with red laser illumination in the forward and side directions, respectively; Lower eight scattering patterns are captured from staurosporine-treated SH-SY5Y cells with red laser illumination in the forward and side directions, respectively.

Ability to capture the scattering pattern for one single cell in both forward and side directions simultaneously can give us more information to study single cell. The ability to keep track on one single cell when it goes through the observation region could also be obtained in this light

scattering experiment. Figure 4.23 shows one single staurosporine-treated SH-SY5Y cell's scattering pattern collected when it is moving across the camera.

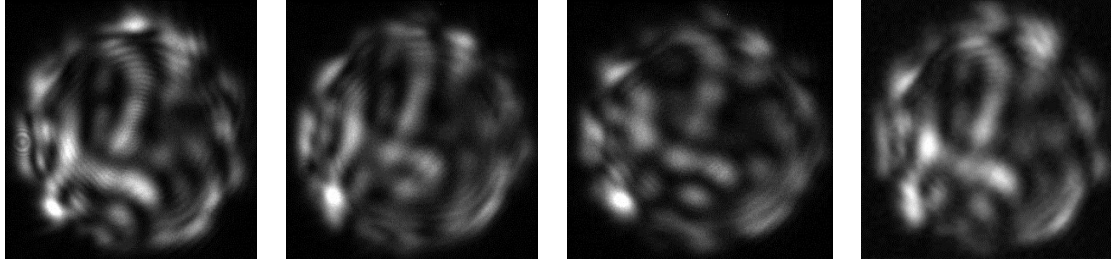


Figure 4.23: One single staurosporine-treated SH-SY5Y cell tracking on the side direction with red laser illumination.

4.8. Finding fraction of non-treated and staurosporine-treated SH-SY5Y cells

One practical application for our label-free technique is to determine the fraction of “live” or “dead” cells in a sample. Figure 4.24 (A) shows the data collected on Mar. 17, 2018 with newly arrived cell sample in 2018. The mean and standard deviation of number of spots and average cross area for “dead” group is $(23, 892.3) \pm (7, 251.2)$, and the mean and the standard deviation of number of spots and average cross area for “live” group is $(26, 806.6) \pm (7, 226.4)$. A distinguishable difference in quantities for “dead” and “live” group when the number of spots is greater than 25, where 9 out of 31 (0.2903) in “dead” group and 22 out of 38 (0.5789) in “live” group. A mixed sample with approximate proportion between “dead” and “live” group (1:4) was made and used for light scattering experiment. Analysis for non-fringe pattern from mixed group based on finding local maximum method has been made as shown in Figure 4.24 (B). 27 scattering patterns was collected from mixed solution and 17 scattering patterns have number of spots greater than 25. The predicted value for 27 captured scattering patterns with number of spots exceeding 25 for “dead” to “live” group with a ratio of 1 to 4 would be $0.2903 \times \frac{1}{5} \times 27 + 0.5789 \times \frac{4}{5} \times 27$

= 15, which is significantly less than the observed value. A deviation of 12% between predicted value and experiment value can be observed ($\frac{17-15}{17} \times 100\% = 12\%$). A summary table of deviation percent between predicted value and experiment value at different number of spots range is shown in **Error! Reference source not found.**

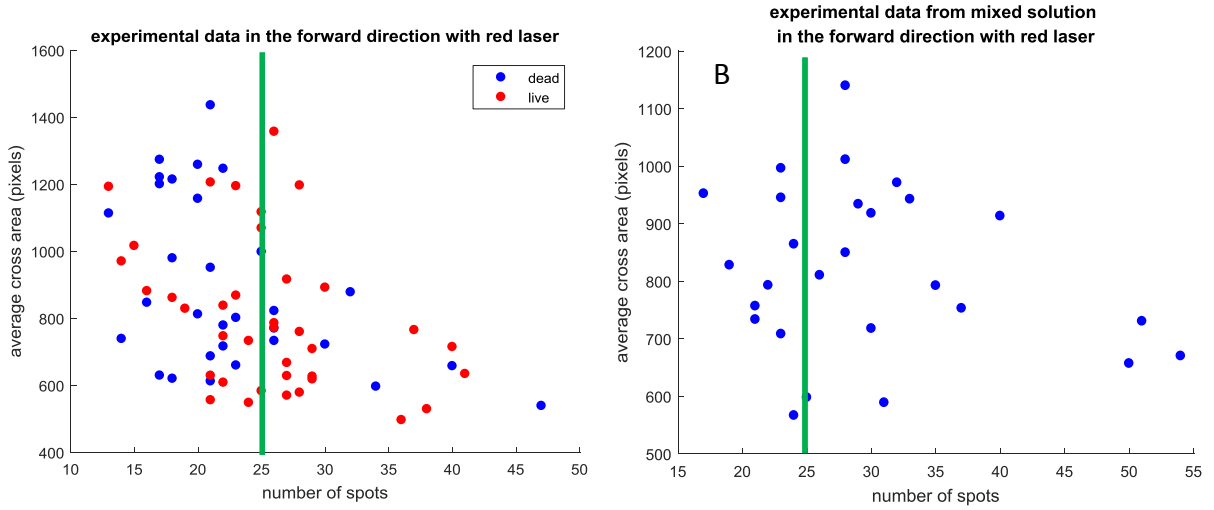


Figure 4.24: (A) is all data collected from both “dead” and “live” group in the forward direction with red laser illumination; (B) is the light scattering data from mixed solution in the forward direction with red laser illumination (cells received in 2018).

Spot number range	≥ 22	≥ 23	≥ 24	≥ 25	≥ 26	≥ 27	≥ 28	≥ 29	≥ 30
P_{dead}	0.4516	0.3548	0.2903	0.2903	0.2581	0.1613	0.1613	0.1613	0.1613
P_{live}	0.7632	0.6842	0.6316	0.5789	0.5	0.4211	0.3158	0.2368	0.1579
N_{pred}	19	17	15	15	12	10	8	6	4
N_{actu}	23	22	19	17	16	15	15	12	11
Deviation	17.4%	22.8%	21%	11.8%	25%	33.3%	46.7%	50%	63.6%

Table 4.3: Summary of different deviations in different range of number of spots.

The minimum deviation according to Table 4.3 can be observed under the situation when the number of spots greater than 25. As a result, when number of spots greater than 25 can be considered as the optimal range for distinguishing treated and non-treated cells based on finding local maximum method.

Non-fringe analysis has also been performed from treated SH-SY5Y cells collected at different times throughout the year. A right-ward shift can be observed over time in Table 4.4 from data in Figure 4.25, which could result from cell aging. A major difference can be observed from data collected in Jan. 23, which could result from some contamination inside the solution.

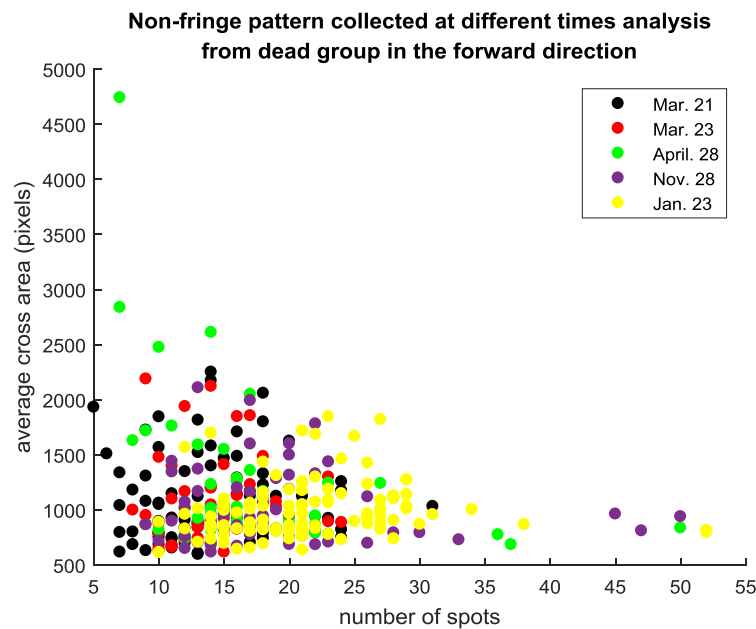


Figure 4.25: Non-fringe light scattering pattern of “dead” group cells at different time analysis (cells received in 2017).

Date	Mar. 21, 2017	Mar. 23, 2017	April. 28, 2017	Nov. 28, 2017	Jan. 23, 2018
Centroid	(14, 851.3)	(14, 797.1)	(18, 930.1)	(19, 739.9)	(22, 736.6)

Table 4.4: Centroid for each group of data in Figure. 4.25.

4.9. Experiments with a capillary tube

In practical cytometry technique, a flow system is typically used to move single cells through the interrogation region which allows a large number of single cells to be analyzed. Preliminary investigation has been carried out on a concept based on a rectangle capillary tube. A capillary tube is compatible with our multi-angle light scattering technique. A normal planar system such as microfluidic device could only collect side scattered light.

Schematic diagram of the 2D light scattering label-free static cytometer is illustrated in Figure 4.26. A 670-nm fiber-coupled laser is used for illuminating the system. A borosilicate square tubing (Model number: BST-080-14, Friedrich & Dimmock, inc.) which has an inner diameter of 0.8 mm is suspended horizontally in the x-axis and used to carry samples. A detection system including a normal microscope objective (Leitz Wetzlar, 10/0.25, 170/-) and a CCD camera (Chameleon USB 2.0, CMLN-13S2C-CS) is located above the capillary tube and collect side direction scattering light from the capillary tube.

Samples used for the label-free static cytometer are a diameter of 6 μm spherical bead. The diluted solution was first distilled by a syringe and then injected into the capillary tube with a slow injection speed by hand. Observation is achieved by adjusting the detection system to make the sample in the focusing and defocusing state.

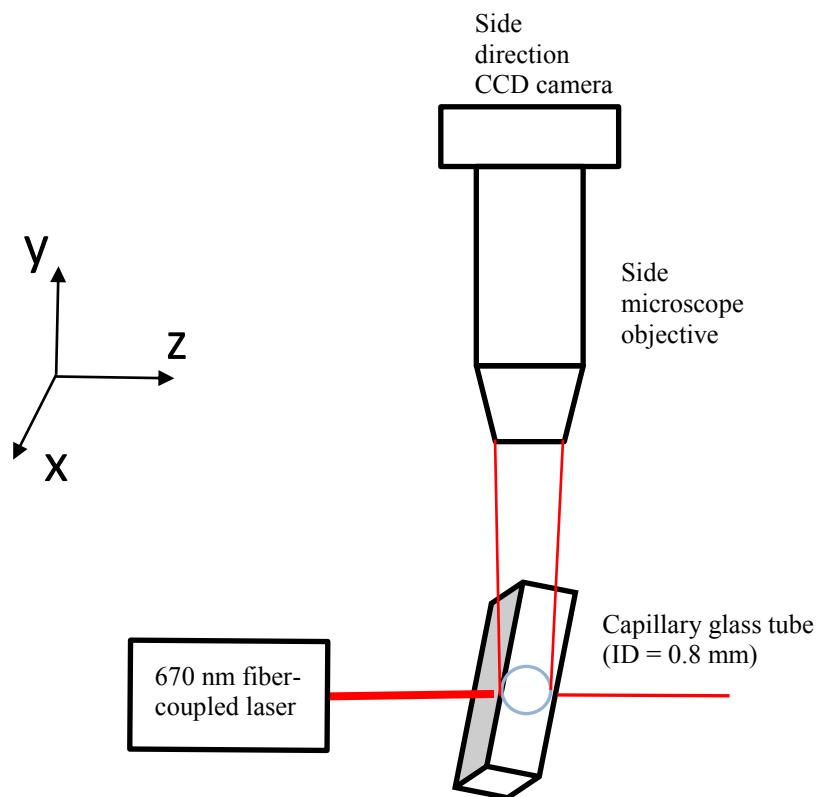


Figure 4.26: Schematic diagram of 2D light scattering static cytometer.

Image of the 6 μm spherical bead and its 2D light scattering pattern are obtained and illustrated in Figure 4.27. A bright dot is the image of a 6 μm spherical bead in focus as it shows in Figure 4.27 (A), and Figure 4.27 (B) is the corresponding light scattering pattern in defocus. Five number of fringes can be observed in the pattern. Good agreement is achieved with Mieplot results which shows five peaks in Figure 4.28.

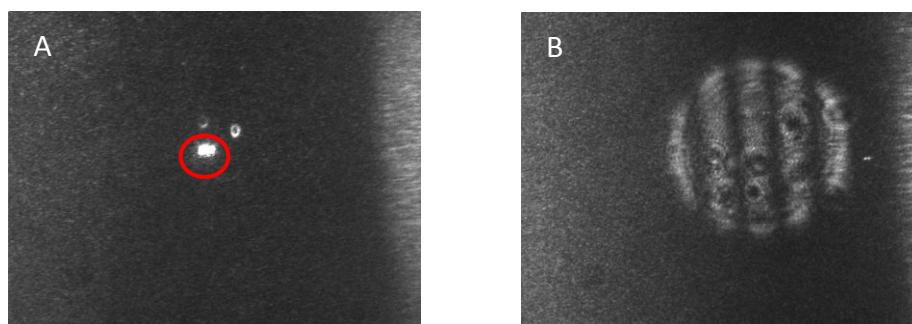


Figure 4.27: Image of 6 μm spherical bead (A) and its corresponding light scattering pattern (B).

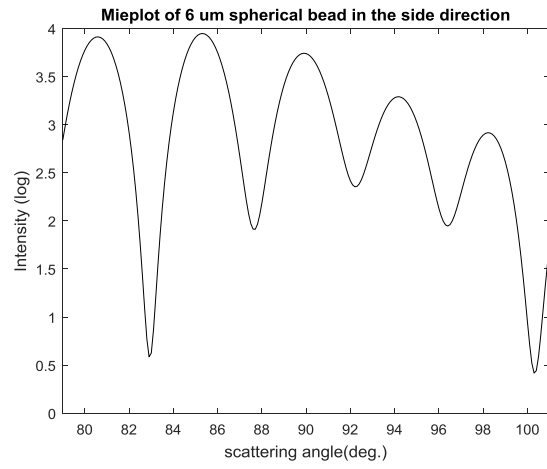


Figure 4.28: Mieplot spectrum of a diameter of 6 μm spherical bead.

5. Conclusion and future work

5.1. Summary of non-invasive label-free cytometry

This thesis describes a non-invasive label-free cytometry based on light scattering technique. Vertical fringe light scattering pattern of micro-scale particles can be obtained experimentally in three directions (forward, side and backward). Besides, light scattering experiment of same micro spherical particle but with different wavelengths illumination has been tested. Different light scattering pattern of same size of micro spherical beads can be obtained successfully. Good agreements between experimental results and calculated results based on Mieplot have been achieved for size of 4 μm , 6 μm , 10 μm and 15 μm micro spherical bead. FFT analysis of four different sizes micro spherical bead has been done and indicates an increased size of micro sphere resulting in a larger normalized frequency. In addition, light scattering pattern of non-spherical particles with the size of 4.0 \times 6.0 μm and 9 \times 10.5 μm can also be collected in both forward and side directions. Non-vertical and different number of fringes of scattering pattern can be observed from one single non-spherical bead.

Light scattering experiment for non-treated and staurosporine-treated SH-SY5Y cells have been implemented successfully. Light scattering patterns of two different cell groups with different wavelengths illumination have been captured in all three directions. Fringe and non-fringe pattern can be observed from both non-treated and staurosporine-treated SH-SY5Y cell groups. Angle distribution method has been proposed to distinguish fringe pattern from non-fringe pattern. Fringe pattern can only be observed in both forward and side directions from both cell groups with red laser source. According to percentage bar graph displayed in Chapter 4, fringe pattern only takes a small percent in overall data. As a result, finding local maximum method has been developed for

analyzing non-fringe pattern. Non-fringe pattern for different group of cells, non-fringe pattern for one group of cells but with different source illumination, as well as non-fringe pattern for one group of cells collected at different times have been analyzed based on finding local maximum technique. More number of spots but smaller average cross area can be observed in staurosporine-treated SH-SY5Y cell group compared with non-treated SH-SY5Y cell group. More number of spots can be obtained from one group of cells with green laser illumination than red laser source. Differences occurs in the side direction from one group of cells but collected at different times with red laser illumination. SEM images and TEM images as well as images under normal microscope objective have been taken for a better understanding of the morphology of non-treated and staurosporine-treated SH-SY5Y cells.

Light scattering pattern of one single SH-SY5Y cell can be captured in both forward and side directions simultaneously, which gives us one more perspective to study cells. In addition, tracking of one single SH-SY5Y cell can be achieved which helps us understand how a cell moving and spinning in solution.

Light scattering experiment with capillary tube and droplet has also been achieved. Light scattering pattern of 6 μm micro spherical bead can be captured and good agreements have been achieved between experiment and calculated Mieplot results. Preliminary experimental set-up has been working towards a commercial flow cytometer.

5.2. Future work

Multi-directional observation of micro scale particles with two different wavelengths illumination has been developed. Two-dimensional light scattering pattern for microsphere and non-spherical bead as well as a new type of cell (SH-SY5Y) have been successfully captured. However, more work still need to be done to improve our label-free cytometer. Further studies are recommended as follows:

- More statics is required to drop error from fraction of different types of cells down.
- Building a fully automation collection system instead of manually selection.
- Improving the accuracy of finding local maximum method.
- More analysis based on different criterion, such as average cross area.
- Carry out larger range of wavelengths illumination such as blue, UV or IR light source, and it is expected more wavelength difference could result in more different results.

Bibliography

- [1] Pol, E. V., Coumans, F. A., Grootemaat, A. E., Gardiner, C., Sargent, I. L., Harrison, P., . . . Nieuwland, R. (2014). Particle size distribution of exosomes and microvesicles determined by transmission electron microscopy, flow cytometry, nanoparticle tracking analysis, and resistive pulse sensing. *Journal of Thrombosis and Haemostasis*, 12(7), 1182-1192. doi:10.1111/jth.12602
- [2] Dorfman, D. M. (2017). *Clinical Flow Cytometry: State-of-the-Art and New Approaches*. *Clinics in Laboratory Medicine*, 37(4), Xiii-Xiv. doi:10.1016/j.cll.2017.09.001
- [3] Guidelines for the use of flow cytometry and cell sorting in immunological studies
- [4] Su, X., Kirkwood, S. E., Gupta, M., Marquez-Curtis, L., Qiu, Y., Janowska-Wieczorek, A., . . . Tsui, Y. Y. (2010). Microscope-based label-free microfluidic cytometry. *Optics Express*, 19(1), 387. doi:10.1364/oe.19.000387
- [5] Xie, L., Liu, Q., Shao, C., & Su, X. (2016). Differentiation of normal and leukemic cells by 2D light scattering label-free static cytometry. *Optics Express*, 24(19), 21700. doi:10.1364/oe.24.021700
- [6] Shahin, H., Gupta, M., Janowska-Wieczorek, A., Rozmus, W., & Tsui, Y. Y. (2016). Physical characterization of hematopoietic stem cells using multidirectional label-free light scatterings. *Optics Express*, 24(25), 28877. doi:10.1364/oe.24.028877
- [7] Rosenbluth, M. J., Lam, W. A., & Fletcher, D. A. (2008). Analyzing cell mechanics in hematologic diseases with microfluidic biophysical flow cytometry. *Lab on a Chip*, 8(7), 1062. doi:10.1039/b802931h
- [8] Dragovic, R., Collett, G., Hole, P., Ferguson, D., Redman, C., Sargent, I., & Tannetta, D. (2015). Isolation of syncytiotrophoblast microvesicles and exosomes and their

- characterisation by multicolour flow cytometry and fluorescence Nanoparticle Tracking Analysis. *Methods*, 87, 64-74. doi:10.1016/j.ymeth.2015.03.028
- [9] Pol, E. V., Coumans, F. A., Grootemaat, A. E., Gardiner, C., Sargent, I. L., Harrison, P., . . . Nieuwland, R. (2014). Particle size distribution of exosomes and microvesicles determined by transmission electron microscopy, flow cytometry, nanoparticle tracking analysis, and resistive pulse sensing. *Journal of Thrombosis and Haemostasis*, 12(7), 1182-1192. doi:10.1111/jth.12602
- [10] R. Paredes-Aguilera, L. Romero-Guzman, N. Lopez-Santiago, L. Burbano-Ceron, O. Camacho-Del Monte, and S. Nieto-Martinez, "Flow cytometric analysis of cell-surface and intracellular antigens in the diagnosis of acute leukemia," *Am. J. Hematol.* 68(2), 69–74 (2001)
- [11] K. Mrózek, G. Marcucci, P. Paschka, S. P. Whitman, and C. D. Bloomfield, "Clinical relevance of mutations and gene expression changes in adult acute myeloid leukemia with normal cytogenetics: are we ready for a prognostically prioritized molecular classification?" *Blood* 109(2), 431–448 (2007).
- [12] Fluorescence activated cell sorting of live cells. (2017, December 23). Retrieved December 22, 2017, from <http://www.abcam.com/protocols/fluorescence-activated-cell-sorting-of-live-cells>.
- [13] Agnarsson, B., Lundgren, A., Gunnarsson, A., Rabe, M., Kunze, A., Mapar, M., . . . Höök, F. (2015). Evanescent Light-Scattering Microscopy for Label-Free Interfacial Imaging: From Single Sub-100 nm Vesicles to Live Cells. *ACS Nano*, 9(12), 11849-11862. doi:10.1021/acsnano.5b04168

- [14] G. (1928). The optical analogue of the Compton effect. *Journal of the Franklin Institute*, 206(2), 273. doi:10.1016/s0016-0032(28)91542-2
- [15] Turrell, G., & Corset, J. (2003). *Raman microscopy: developments and applications*. San Diego, CA, London: Elsevier Academic Press.
- [16] CHENG, J. (2016). *COHERENT RAMAN SCATTERING MICROSCOPY*. Place of publication not identified: CRC Press.
- [17] Burkacky, O., & Zumbusch, A. (n.d.). Coherent Anti-Stokes Raman Scattering (CARS) Microscopy. *Biomedical Vibrational Spectroscopy*, 209-220. doi:10.1002/9780470283172.ch9
- [18] Fussell, A. (n.d.). Coherent anti-Stokes Raman scattering microscopy for pharmaceuticals. doi:10.3990/1.9789036536714
- [19] Ramachandran, P. V., Mutlu, A. S., & Wang, M. C. (2015). Label-Free Biomedical Imaging of Lipids by Stimulated Raman Scattering Microscopy. *Current Protocols in Molecular Biology*. doi:10.1002/0471142727.mb3003s109
- [20] Differences between Prokaryotes and Eukaryotes. (2013, March 31). Retrieved December 22, 2017, from <https://biocheganics.wordpress.com/2013/03/29/differences-between-prokaryotes-and-eukaryotes/>
- [21] G. M. Cooper and R. E. Hausman, *The cell: A molecular approach*, (AMS Press, Washington, 2004).
- [22] H. L. Liu, B. Beauvoit, M. Kimura, and B. Chance, "Dependence of tissue optical properties on solute-induced changes in refractive index and osmolarity," *J. Biomed. Opt.* 1, 200-211 (1996).

- [23] Shahin, H., Gupta, M., Janowska-Wieczorek, A., Rozmus, W., & Tsui, Y. Y. (2016). Physical characterization of hematopoietic stem cells using multidirectional label-free light scatterings. *Optics Express*, 24(25), 28877. doi:10.1364/oe.24.028877
- [24] Su, X. T. (2008). *Light Scattering in an Integrated Microfluidic Waveguide Cytometer*. PhD. Thesis, University of Alberta: Edmonton, AB.
- [25] Shahin, H. (2016). *Forward and Side Two Dimensional Scattered Light Patterns Studies of Single Cell for Label-Free Flow Cytometry*. MSc. Thesis, University of Alberta: Edmonton, AB.
- [26] Ha, D. F. S. (2013). *Development of Microfluidic Chips and a Customised Flow Control System for use in a Label-Free Cytometer*. MSc. Thesis, University of Alberta: Edmonton, AB.
- [27] Crispin, J. W., & Siegel, K. M. (1968). *Methods of radar cross-section analysis*. New York: Academic Press.
- [28] Thalman, R., Zarzana, K. J., Tolbert, M. A., & Volkamer, R. (2014). Rayleigh scattering cross-section measurements of nitrogen, argon, oxygen and air. *Journal of Quantitative Spectroscopy and Radiative Transfer*, 147, 171-177. doi:10.1016/j.jqsrt.2014.05.030
- [29] Liu, S., Yang, Z., Liu, Z., & Kong, L. (2006). Resonance Rayleigh-scattering method for the determination of proteins with gold nanoparticle probe. *Analytical Biochemistry*, 353(1), 108-116. doi:10.1016/j.ab.2006.03.012
- [30] Musa, A., & Paul, B. S. (2017). Prediction of electromagnetic wave attenuation in dust storms using Mie scattering. *2017 Ieee Africon*. doi:10.1109/africon.2017.8095550

- [31] Speziale, S., Marquardt, H., & Duffy, T. S. (n.d.). 14. Brillouin Scattering and its Application in Geosciences. *Spectroscopic Methods in Mineralogy and Material Sciences*. doi:10.1515/9781501510618.543
- [32] Guo, Z., Zhang, H., Lu, S., Wang, Z., Tang, S., Shao, J., . . . Chu, P. K. (2015). Phosphorene: From Black Phosphorus to Phosphorene: Basic Solvent Exfoliation, Evolution of Raman Scattering, and Applications to Ultrafast Photonics (*Adv. Funct. Mater.* 45/2015). *Advanced Functional Materials*, 25(45), 7100-7100. doi:10.1002/adfm.201570292
- [33] Mie, G. (1908). Beiträge zur Optik trüber Medien, speziell kolloidaler Metallösungen. *Annalen der Physik*, 330(3), 377-445. doi:10.1002/andp.19083300302
- [34] Bohren, C. F., & Huffman, D. R. (2009). *Absorption and scattering of light by small particles*. Weinheim: Wiley-VCH.
- [35] Wang, L. V., & Wu, H. (2007). *Biomedical optics: principles and imaging*. Hoboken: Wiley-Interscience.
- [36] Laven, P. (n.d.). Retrieved February 12, 2018, from <http://www.philiplaven.com/mieplot.htm#DownloadMiePlot>.
- [37] Mitra, R., & Pikel, U. (1995). A new look at the perfectly matched layer (PML) concept for the reflectionless absorption of electromagnetic waves. *IEEE Microwave and Guided Wave Letters*, 5(3), 84-86. doi:10.1109/75.366461
- [38] Navarro, C., & Samartin, A. (1987). A Transmitting Boundary in Time Domain for Soil-Structure Interaction Problems. *Transient/Dynamic Analysis and Constitutive Laws for Engineering Materials*, 135-142. doi:10.1007/978-94-009-3655-3_13

- [39] Doicu, A., Eremin, Y., & Wriedt, T. (2000). Discrete sources method in electromagnetic theory. *Acoustic and Electromagnetic Scattering Analysis Using Discrete Sources*, 203-239. doi:10.1016/b978-012219740-6/50010-1
- [40] A. Doicu, Y. Eremin, and T. Wriedt, *Acoustic and Electromagnetic Scattering Analysis using Discrete Sources* (Academic, 2000).
- [41] Helden, L., Eremina, E., Riefler, N., Hertlein, C., Bechinger, C., Eremin, Y., & Wriedt, T. (2006). Single-particle evanescent light scattering simulations for total internal reflection microscopy. *Applied Optics*, 45(28), 7299. doi:10.1364/ao.45.007299.
- [42] Luk'Yanchuk, B. S., Voshchinnikov, N. V., Paniagua-Domínguez, R., & Kuznetsov, A. I. (2015). Optimum Forward Light Scattering by Spherical and Spheroidal Dielectric Nanoparticles with High Refractive Index. *ACS Photonics*, 2(7), 993-999. doi:10.1021/acsp Photonics.5b00261
- [43] Home | Polysciences. (n.d.). Retrieved January 02, 2018, from <http://www.polysciences.com/>
- [44] RefractiveIndex.INFO. (n.d.). Retrieved January 02, 2018, from <https://refractiveindex.info/shelf=organic&book=polystyren&page=Sultanova>
- [45] Su, X., Liu, S., Qiao, X., Yang, Y., Song, K., & Kong, B. (2015). Pattern recognition cytometry for label-free cell classification by 2D light scattering measurements. *Optics Express*, 23(21), 27558. doi:10.1364/oe.23.027558
- [46] Lin, M., Qiao, X., Liu, Q., Shao, C., & Su, X. (2016). Light-sheet-based 2D light scattering cytometry for label-free characterization of senescent cells. *Biomedical Optics Express*, 7(12), 5170. doi:10.1364/boe.7.005170

- [47] Xie, L., Liu, Q., Shao, C., & Su, X. (2017). Automatic classification of acute and chronic myeloid leukemic cells with wide-angle label-free static cytometry. *Optics Express*, 25(23), 29365. doi:10.1364/oe.25.029365
- [48] Liu, S., Xie, L., Yang, Y., Qiao, X., Song, K., Kong, B., & Su, X. (2015). Label-free analysis of single and multiple cells with a 2D light scattering static cytometer. *Imaging, Manipulation, and Analysis of Biomolecules, Cells, and Tissues XIII*. doi:10.1117/12.2080519
- [49] Ottewill, R. H., & Shaw, J. N. (1966). Stability of monodisperse polystyrene latex dispersions of various sizes. *Discussions of the Faraday Society*, 42, 154. doi:10.1039/df9664200154
- [50] Konno, M., & Nagao, D. (2014). Monodisperse Polymer Particles. *Encyclopedia of Polymer Science and Technology*, 1-26. doi:10.1002/0471440264.pst617
- [51] Biedler, J. L., Helson, L. et al. Morphology and Growth, Tumorigenicity, and Cytogenetics of Human Neuroblastoma Cells in Continuous Culture, *Cancer Research*.1973;33:2643-2652
- [52] Perfeito, R., Lázaro, D. F., Outeiro, T. F., & Rego, A. C. (2014). Linking alpha-synuclein phosphorylation to reactive oxygen species formation and mitochondrial dysfunction in SH-SY5Y cells. *Molecular and Cellular Neuroscience*, 62, 51-59. doi:10.1016/j.mcn.2014.08.002
- [53] Feng, C., Luo, T., Zhang, S., Liu, K., Zhang, Y., Luo, Y., & Ge, P. (2016). Lycopene protects human SH-SY5Y neuroblastoma cells against hydrogen peroxide-induced death via inhibition of oxidative stress and mitochondria-associated apoptotic pathways. *Molecular Medicine Reports*, 13(5), 4205-4214. doi:10.3892/mmr.2016.5056

- [54] Tian, X., Hou, W., Bai, S., Fan, J., Tong, H., & Bai, Y. (2014). XAV939 promotes apoptosis in a neuroblastoma cell line via telomere shortening. *Oncology Reports*, 32(5), 1999-2006. doi:10.3892/or.2014.3460
- [55] Sanz, B., Calatayud, M. P., Torres, T. E., Fanarraga, M. L., Ibarra, M. R., & Goya, G. F. (2017). Magnetic hyperthermia enhances cell toxicity with respect to exogenous heating. *Biomaterials*, 114, 62-70. doi:10.1016/j.biomaterials.2016.11.008
- [56] B. Albertas, D. Bray, J. Levis, K. Raff, K. Roberts and J. D. Watson, *Molecular biology of the cell*, (Garland, New York, 1994).
- [57] J. Beuthan, O. Minet, J. Helfmann, M. Herrig and G. Muller, "The spatial variation of the refractive index in biological cells," *Physics in Medicine and Biology* 41, 369-382 (1996).
- [58] P. R. Pryor, B. M. Mullock, N. A. Bright, S. R. Gray and J. P. Luzio, "The role of intraorganellar Ca²⁺ in late endosome-lysosome heterotypic fusion and in the reformation of lysosomes from hybrid organelles," *Journal of Cell Biology* 149, 1053-1062 (2000).

Appendices

A.1 Matlab code for angle distribution method

```
I1=imread('D:\experiment results\2017\Oct. 11\live\F\high-
densed\fc2_save_2017-03-23-105410-20242-1.jpg');

if numel(size(I1)) == 3
    I1 = rgb2gray(I1);
end
I1 = imgaussfilt(I1,8);

[M N] = size(I1);
[FX,FY] = gradient(double(I1));
temp = [];
for r = 1:M
    for c = 1:N
        temp(r,c) = FY(r,c)/FX(r,c);
        %if FY(r,c) == 0 && FX(r,c) == 0
            %temp(r,c) = 1;
        %end
    end
end

theta = atan(temp)*180/pi;
thetal = [];
for i = 1:M
    for j = 1:N
        thetal(i,j) = round(theta(i,j));
    end
end
A = [-90:1:90]; B = zeros(1,length(A));
i = 1;
for k = -90:1:90
    B(1,i) = length(find(abs(thetal-k)<1));
    i = i+1;
end

Ir = rot90(I1);
%Ir = imrotate(I1,45); figure; imshow(Ir);
[M N] = size(Ir);
[FX,FY] = gradient(double(Ir));
temp = [];
for r = 1:M
    for c = 1:N
        temp(r,c) = FY(r,c)/FX(r,c);
        %if FY(r,c) == 0 && FX(r,c) == 0
            %    temp(r,c) = 1;
        %end
    end
end
```

```
theta = atan(temp)*180/pi;
thetal = [];
for i = 1:M
    for j = 1:N
        thetal(i,j) = round(theta(i,j));
    end
end
A = [-90:1:90]; Br = zeros(1,length(A));
i = 1;
for k = -90:1:90
    Br(1,i) = length(find(abs(thetal-k)<1));
    i = i+1;
end
diff = sum(abs(B-Br));
```

A.2 Matlab code for finding local maximum method

```
imag=imread('D:\experiment results\2017\Nov. 28(cell red
laser)\filter1\dead\S_1_speckle\15.bmp');
if numel(size(imag)) == 3
    imag = rgb2gray(imag);
end
Id = imgaussfilt(imag,8);% with standard deviation by sigma = 8
Id = imadjust(Id); %figure; imshow(Id);
I1 = imregionalmax(Id,4);
L1 = bwlabel(I1,8);
num = max(max(L1));
x = []; y = []; %X = []; Y = [];
for j = 1:num
    [x(j,:),y(j,:)] = find(L1 == j,1);
end
if find(x == 1) ~= 0
    k = find(x == 1);
    x(k) = [];
    y(k) = [];
end
if find(y == 1) ~= 0
    k = find(y == 1);
    y(k) = [];
    x(k) = [];
end
[M,N] = size(Id);
local_fwhm = [];
figure; imshow(Id');
for ind = 1:length(x)
    L = 0; R = 0; U = 0; D = 0;
    A1 = []; A2 = []; A3 = []; A4 = [];
    for j = 1:y(ind)
        A1(j) = Id(x(ind),j);
    end
    A1 = double(A1);
    if length(A1) < 3
        L = length(A1);
    else
        [pks,locs] = findpeaks(-A1);
        if isempty(pks)
            if min(A1) <= 1/2*double(Id(x(ind),y(ind)))
                c = y(ind);
                while Id(x(ind),c) >= 1/2*double(Id(x(ind),y(ind)))
                    L = L+1;
                    c = c-1;
                    if length(A1) - c ==length(A1)
                        break;
                    end
                end
            end
        else
            L = length(A1);
        end
    end
end
end
```

```

        temp1 = -pks(length(pks)); % make sure temp1 saves a local
max. which is nearest to Id(x(ind),y(ind));
        if temp1 > 1/2*double(Id(x(ind),y(ind)))
            c = y(ind);
            for j = 1:length(A1)
                L = L+1;
                c = c-1;
                if Id(x(ind),c) < Id(x(ind),c-1) && Id(x(ind),c) <=
Id(x(ind),c+1)
                    break;
                end
            end
            elseif temp1 == 1/2*double(Id(x(ind),y(ind)))
                c = y(ind);
                while Id(x(ind),c) >= 1/2*double(Id(x(ind),y(ind)))
                    L = L+1;
                    c = c-1;
                    if Id(x(ind),c) == 1/2*double(Id(x(ind),y(ind))) &&
Id(x(ind),c-1) ~= 1/2*double(Id(x(ind),y(ind)))
                        break;
                    end
                end
            else
                c = y(ind);
                for j = 1:length(A1)
                    L = L+1;
                    if Id(x(ind),c) >= 1/2*double(Id(x(ind),y(ind))) &&
Id(x(ind),c-1) < 1/2*double(Id(x(ind),y(ind)))
                        break;
                    end
                    c = c-1;
                end
            end
        end
        end
        for j = 1:(N-y(ind)+1)
            A2(j) = Id(x(ind),y(ind)+j-1);
        end
        A2 = double(A2);
        if length(A2) < 3
            R = length(A2);
        else
            [pks,locs] = findpeaks(-A2);
            if isempty(pks)
                if min(A2) <= 1/2*double(Id(x(ind),y(ind)))
                    c = y(ind);
                    while Id(x(ind),c) >= 1/2*double(Id(x(ind),y(ind)))
                        R = R+1;
                        c = c+1;
                        if c == length(A2)+y(ind)
                            break;
                        end
                    end
                else
                    R = length(A2);
                end
            else
                R = length(A2);
            end
        end
    end
end

```

```

temp2 = -pks(1);
if temp2 > 1/2*double(Id(x(ind),y(ind)))
    c = y(ind);
    for j = 1:length(A2)
        R = R+1;
        c = c+1;
        if Id(x(ind),c) <= Id(x(ind),c-1) && Id(x(ind),c) <
Id(x(ind),c+1)
            break;
        end
    end
elseif temp2 == 1/2*double(Id(x(ind),y(ind)))
    c = y(ind);
    while Id(x(ind),c) >= 1/2*double(Id(x(ind),y(ind)))
        R = R+1;
        c = c+1;
        if Id(x(ind),c) == 1/2*double(Id(x(ind),y(ind))) &&
Id(x(ind),c+1) ~= 1/2*double(Id(x(ind),y(ind)))
            break;
        end
    end
else
    c = y(ind);
    for j = 1:length(A2)
        R = R+1;
        c = c+1;
        if Id(x(ind),c) >= 1/2*double(Id(x(ind),y(ind))) &&
Id(x(ind),c+1) < 1/2*double(Id(x(ind),y(ind)))
            break;
        end
    end
end
end
for j = 1:x(ind)
    A3(j) = Id(j,y(ind));
end
A3 = double(A3);
if length(A3) < 3
    U = length(A3);
else
    [pks,locs] = findpeaks(-A3);
    if isempty(pks)
        if min(A3) <= 1/2*double(Id(x(ind),y(ind)))
            r = x(ind);
            while Id(r,y(ind)) >= 1/2*double(Id(x(ind),y(ind)))
                U = U+1;
                r = r-1;
                if length(A3) - r ==length(A3)
                    break;
                end
            end
        else
            U = length(A3);
        end
    else
        temp3 = -pks(length(pks));
    end
end

```

```

    if temp3 > 1/2*double(Id(x(ind),y(ind)))
        r = x(ind);
        for j = 1:length(A3)
            U = U+1;
            r = r-1;
            if Id(r,y(ind)) < Id(r-1,y(ind)) && Id(r,y(ind)) <=
Id(r+1,y(ind))
                break;
            end
        end
    elseif temp3 ==1/2*double(Id(x(ind),y(ind)))
        r = x(ind);
        while Id(r,y(ind)) >= 1/2*double(Id(x(ind),y(ind)))
            U = U+1;
            r = r-1;
            if Id(r,y(ind)) == 1/2*double(Id(x(ind),y(ind))) && Id(r-
1,y(ind)) ~= 1/2*double(Id(x(ind),y(ind)))
                break;
            end
        end
    else
        r = x(ind);
        for j = 1:length(A3)
            U = U+1;
            if Id(r,y(ind)) >= 1/2*double(Id(x(ind),y(ind))) && Id(r-
1,y(ind)) < 1/2*double(Id(x(ind),y(ind)))
                break;
            end
            r = r-1;
        end
    end
end
end
end
for j = 1:(M-x(ind)+1)
    A4(j) = Id(x(ind)+j-1,y(ind));
end
%if isempty(A4)
%    D = 0;
%end
A4 = double(A4);
if length(A4) < 3
    D = length(A4);
else
    [pks,locs] = findpeaks(-A4);
    if isempty(pks)
        if min(A4) <= 1/2*double(Id(x(ind),y(ind)))
            r = x(ind);
            while Id(r,y(ind)) >= 1/2*double(Id(x(ind),y(ind)))
                D = D+1;
                r = r+1;
                if r == length(A4) + x(ind)
                    break;
                end
            end
        else
            D = length(A4);
        end
    end
end
end

```

```

else
    temp4 = -pks(1);
    if temp4 > 1/2*double(Id(x(ind),y(ind)))
        r = x(ind);
        for j = 1:length(A4)
            D = D+1;
            r = r+1;
            if Id(r,y(ind)) <= Id(r-1,y(ind)) && Id(r,y(ind)) <
Id(r+1,y(ind))
                break;
            end
        end
    elseif temp4 == 1/2*double(Id(x(ind),y(ind)))
        r = x(ind);
        while Id(r,y(ind)) >= 1/2*double(Id(x(ind),y(ind)))
            D = D+1;
            r = r+1;
            if Id(r,y(ind)) == 1/2*double(Id(x(ind),y(ind))) &&
Id(r+1,y(ind)) ~= 1/2*double(Id(x(ind),y(ind)))
                break;
            end
        end
    else
        r = x(ind);
        for j = 1:length(A4)
            D = D+1;
            r = r+1;
            if Id(r,y(ind)) >= 1/2*double(Id(x(ind),y(ind))) &&
Id(r+1,y(ind)) < 1/2*double(Id(x(ind),y(ind)))
                break;
            end
        end
    end
end
end
end
end
local_fwhm(ind) = 1/2*(R+L)*(D+U);
text(x(ind),y(ind),'o','color','g');
%rectangle('Position',[x(ind)-U y(ind)+R L+R U+D],'EdgeColor','g');
%text(x(ind),y(ind)-L,'+', 'color','g');
%text(x(ind)-U,y(ind),'+', 'color','g');
%text(x(ind),y(ind)+R,'+', 'color','g');
%text(x(ind)+D,y(ind),'+', 'color','g');
hold on;
plot([x(ind) x(ind)-U],[y(ind)-L y(ind)],'r'); hold on; plot([x(ind)
x(ind)+D],[y(ind)-L y(ind)],'r');
hold on; plot([x(ind) x(ind)-U],[y(ind)+R y(ind)],'r'); hold on;
plot([x(ind) x(ind)+D],[y(ind)+R y(ind)],'r');
X(1,ind) = x(ind);
Y(1,ind) = y(ind)-L;
%w(1,ind) = L+R;
%h(1,ind) = D+U;

end

labels = cellstr(num2str([1:length(x)]));
dx = 0.1; dy = 0.1;

```

```
text(x+dx,y+dy,labels,'Color','green');  
labels = cellstr(num2str([1:length(X)]));  
dx = 0.1; dy = 0.1;  
text(X+dx,Y+dy,labels,'Color','red');
```

A.3 SEM and TEM imaging

Figure 7. 0.1 shows the SEM imaging of non-treated SH-SY5Y neuroblastoma cells. Figure 7. 0.2 shows the SEM imaging of staurosporine-treated SH-SY5Y neuroblastoma cells.

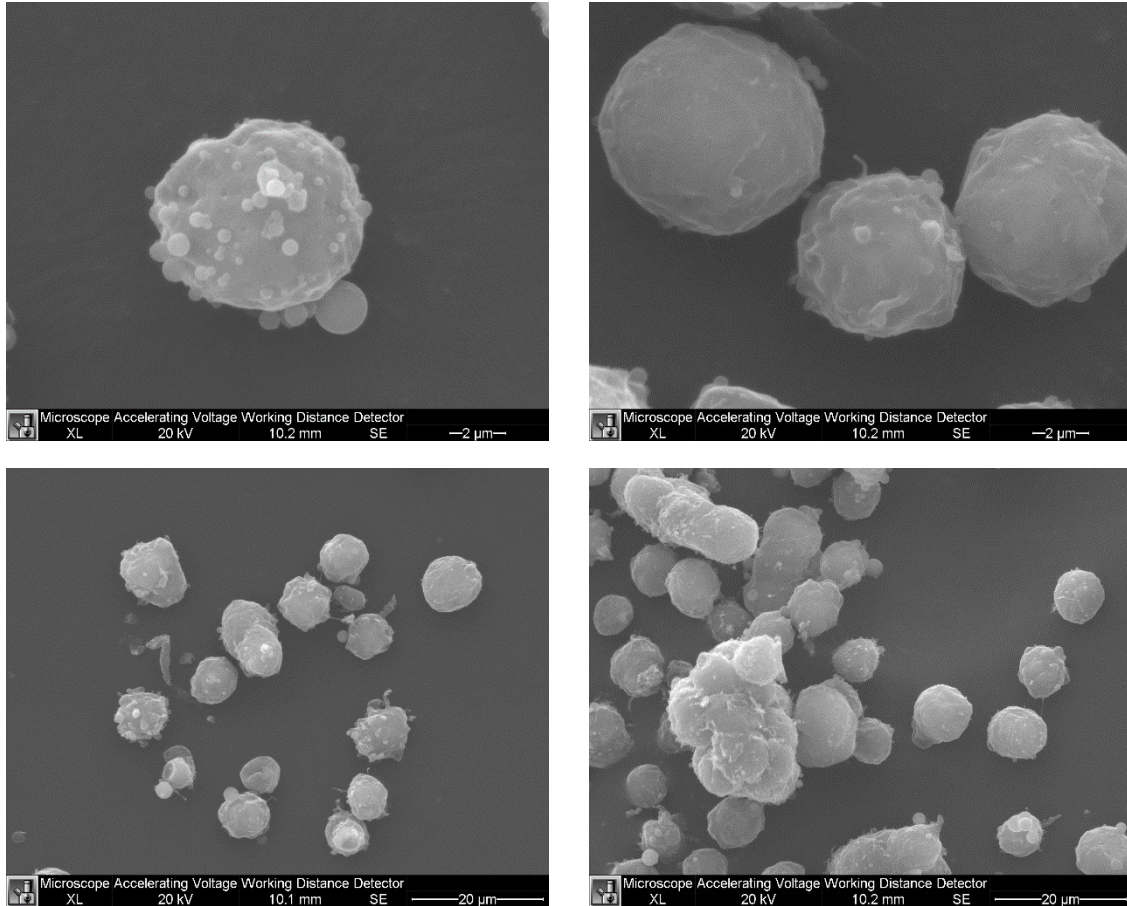


Figure 7. 0.1: SEM imaging of non-treated SH-SY5Y neuroblastoma cells.

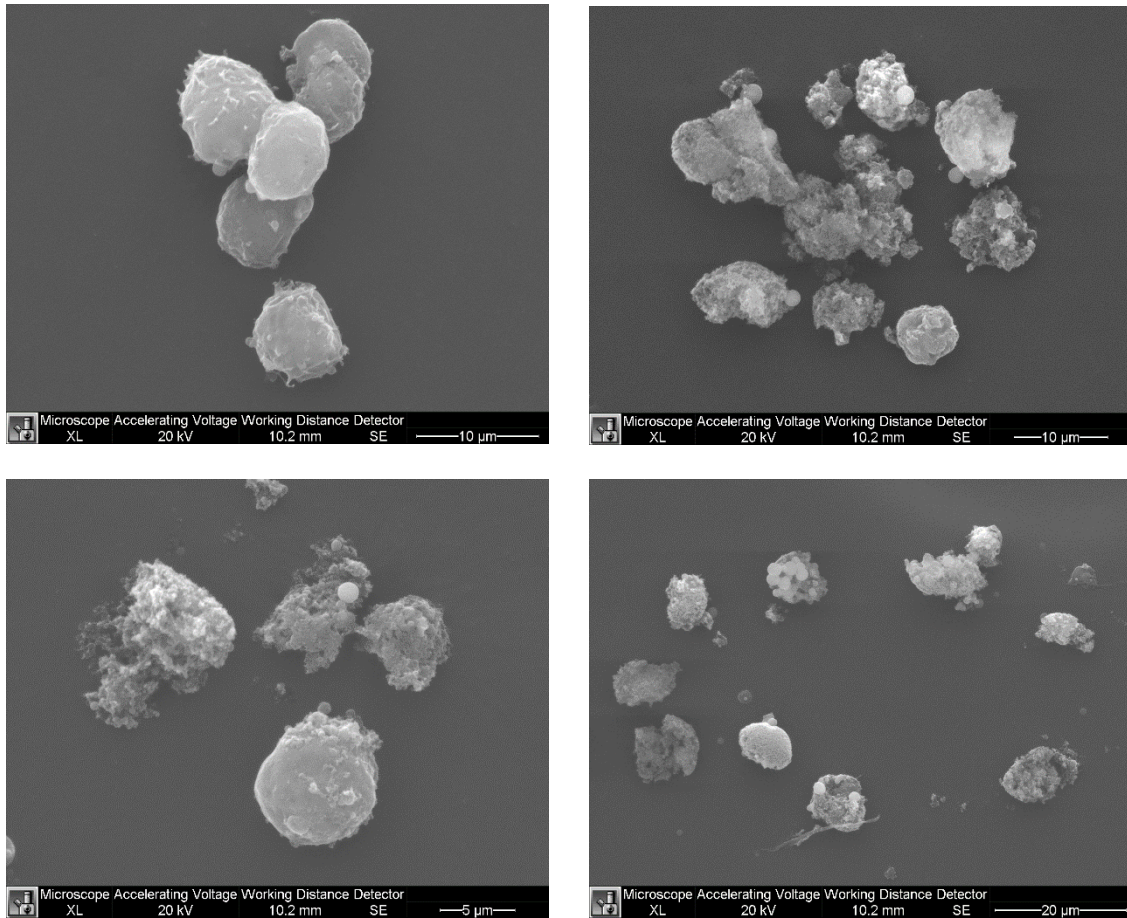


Figure 7.0.2: SEM imaging of staurosporine-treated SH-SY5Y neuroblastoma cells.

Figure 7.0.3 and Figure 7.0.4 shows the TEM imaging of non-treated SH-SY5Y neuroblastoma cells and staurosporine-treated SH-SY5Y neuroblastoma cells, respectively.

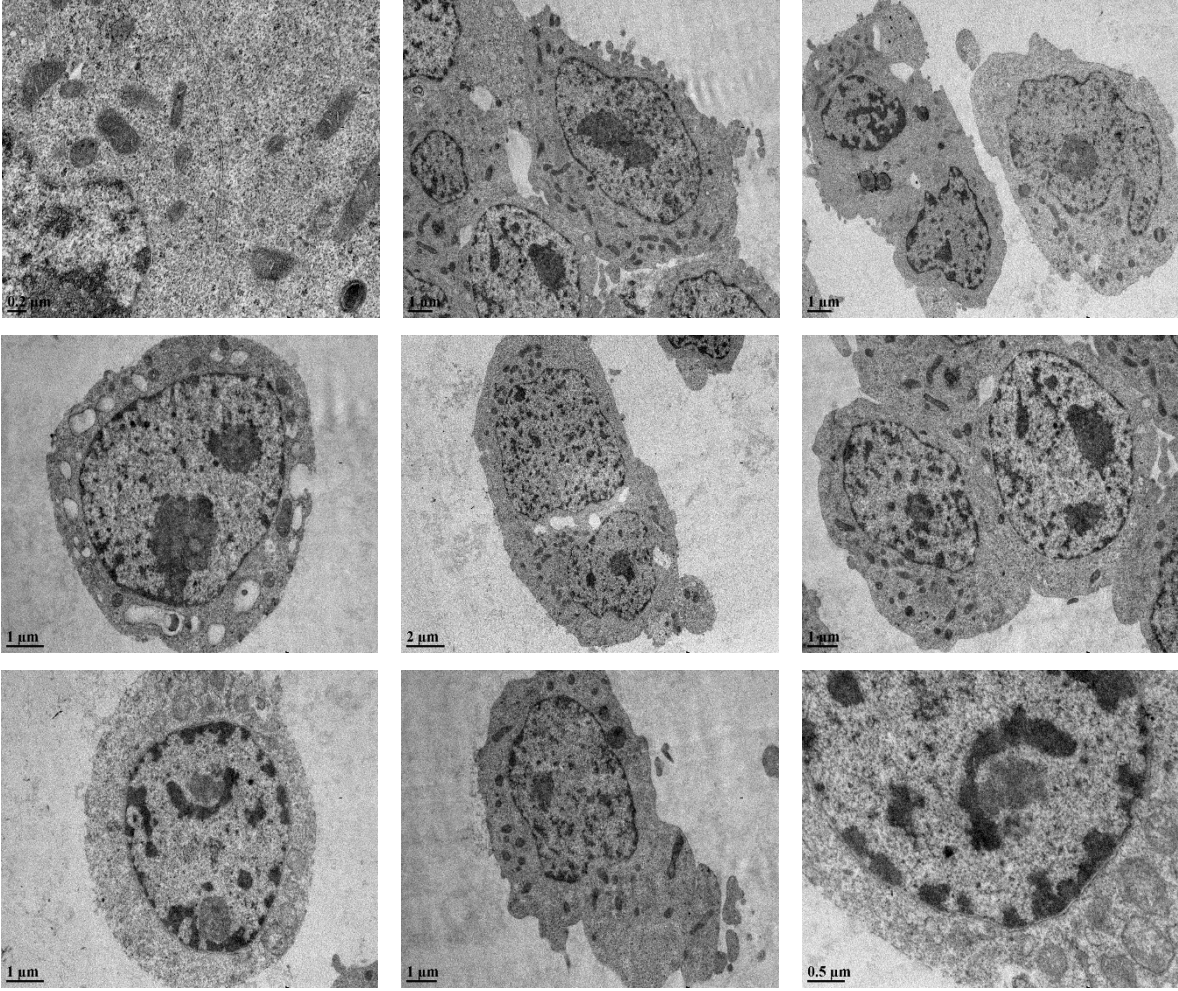


Figure 7.0.3: TEM imaging of non-treated SH-SY5Y neuroblastoma cells.

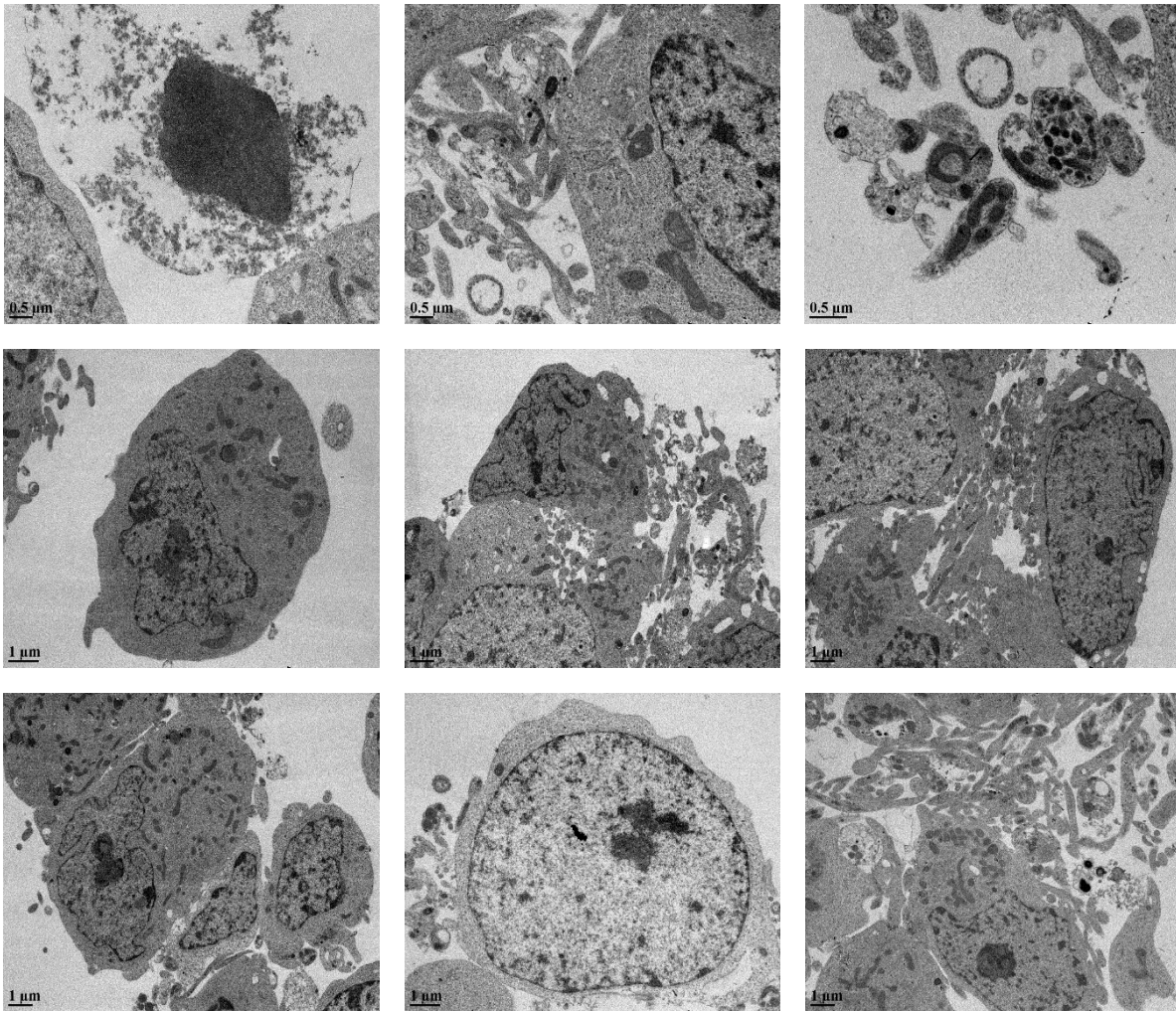


Figure 7.0.4: TEM imaging of staurosporine-treated SH-SY5Y neuroblastoma cells.

A.4 Flow chart of collecting data from CCD camera until data analysis

Figure 7. 0.5 briefly described the main procedure after scattering pattern obtained from CCD camera. Some frames satisfy the intensity threshold in step two like Figure 7. 0.6 (A) shows, which are considered as good frames, while other frames also satisfy the intensity threshold like Figure 7. 0.6 (B) shows but cannot be used for further analysis. As a result, a manually selection step is required like step three describes. However, if large quantities of data are required for analysis, manually selection is not practical. A fully automatic selection system is required in this case.

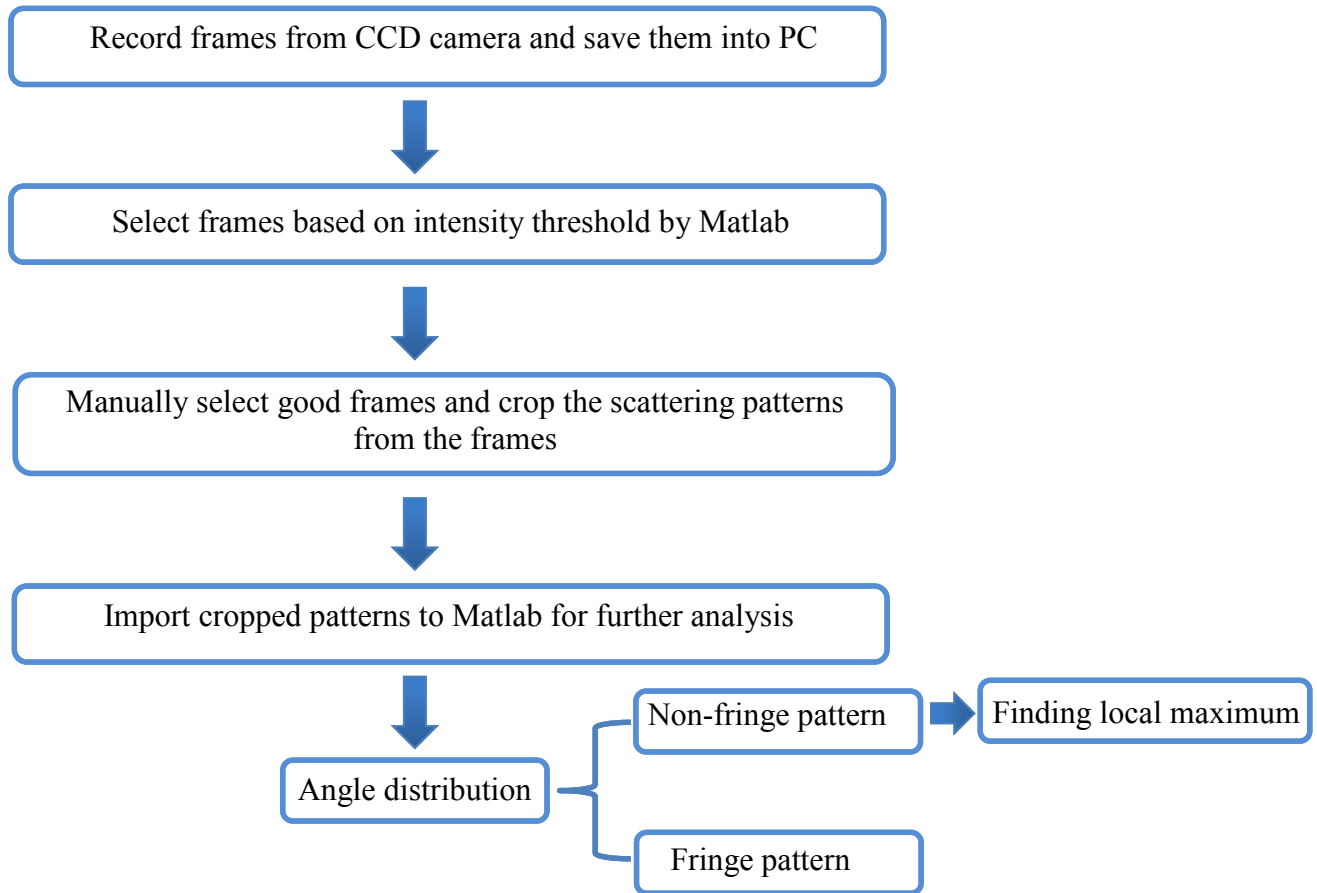


Figure 7. 0.5: Flow chart of procedure after data collected from CCD camera.

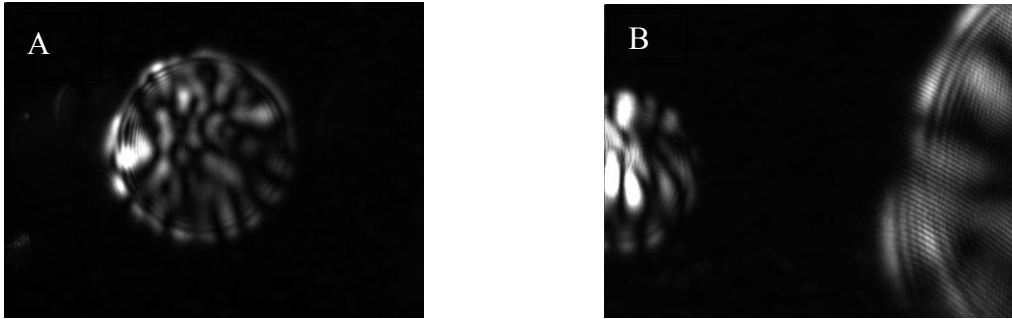


Figure 7. 0.6: A is an example of good frame after filtered by intensity, B is an example of useless frame after filtered by intensity.

A.5 Preparation procedure of non-treated and treated SH-SY5Y

SH-SY5Y cells were first received from the American Type Culture Collection (ATCC, Manassas, Va, USA) and cultured using a 1:1 mixture of Eagle's Minimum Essential Medium supplemented with F12 Medium containing 10% v/v fetal bovine serum and penicillin/streptomycin mixture. Cultures were seeded at 20% cell density and then allowed to grow for approximately 48 h until they had reached 70% confluence of adherent cells. At this point, staurosporine was added to a final concentration of 5 mM to make it as treated SH-SY5Y cell group, while PBS added to no staurosporine control to make it as non-treated SH-SY5Y cell group. Both groups were allowed to incubate for 48 h. Cells were fixed with 10% p-formaldehyde for 15 minutes. A sample of cells from each of the two samples (\pm 5 mM staurosporine) were then counted using a hemocytometer to determine cell density present for each.